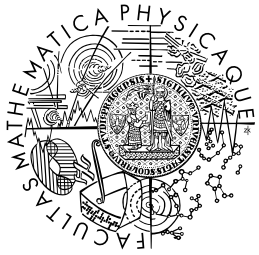

FACULTY
OF MATHEMATICS
AND PHYSICS
Charles University

MASTER THESIS

Bc. Marek Kuchař

Quantum statistics and coherence of photons emitted by optically modulated electron beams

Institute of Theoretical Physics

Supervisor of the master thesis: doc. RNDr. Martin Kozák, Ph.D.

Study programme: Theoretical Physics

Study branch: FTFP

Prague 2024

I declare that I carried out this master thesis independently, and only with the cited sources, literature and other professional sources. It has not been used to obtain another or the same degree.

I understand that my work relates to the rights and obligations under the Act No. 121/2000 Sb., the Copyright Act, as amended, in particular the fact that the Charles University has the right to conclude a license agreement on the use of this work as a school work pursuant to Section 60 subsection 1 of the Copyright Act.

In ..... date ....

Author's signature

I am very grateful to my supervisor, doc. RNDr. Martin Kozák, Ph.D. for his time, insightful guidance and patience, but mostly for allowing me to work on interesting theoretical concepts with experimental applications, because it has taught me a great deal about what I want to focus on in the future.

A special thanks also belongs to all the wonderful people in my life, who have always showed me a great deal of support and encouragement.

Název práce: Kvantová statistika a koherence fotonů emitovaných opticky modulovanými elektronovými svazky

Autor: Bc. Marek Kuchař

Ústav: Ústav teoretické fyziky

Vedoucí: doc. RNDr. Martin Kozák, Ph.D., Katedra chemické fyziky a optiky

Abstrakt: Interakce vysoce energetických elektronů s látkou je využívána ke studiu a zobrazování struktury materiálů v elektronové mikroskopii a difrakci. Jednou z forem této interakce je emise fotonu díky vazbě elektromagnetického pole elektronu s polarizací látky v jeho blízkosti, jedná se o jev tzv. katodoluminiscence. Nedávné teoretické práce předpovídají, že by mohlo být možné optickou koherenci přenesenou do elektronové vlnové funkce pomocí modulace skrze optická pole následně pozorovat v koherenčních vlastnostech emitovaných fotonů. V této práci se zabýváme rozšířením současně používaného teoretického formalismu pro studium tohoto efektu s cílem hlubšího porozumění díky studiu různých režimů optické modulace elektronového svazku. V první části popisujeme důležité aspekty interakce elektronů s látkou vyplývající z klasické elektrodynamiky a v druhé části systematicky budujeme kvantově elektrodynamický formalismus pro studium statistiky emitovaných fotonů. Pomocí numerických simulací pak na základě analytických výsledků diskutujeme očekávanou závislost jejich míry koherence na relevantních fyzikálních parametrech.

Klíčová slova: Kvantová elektrodynamika elektron-fotonová interakce koherence koherentní katodoluminiscence

Title: Quantum statistics and coherence of photons emitted by optically modulated electron beams

Author: Bc. Marek Kuchař

Institute: Institute of Theoretical Physics

Supervisor: doc. RNDr. Martin Kozák, Ph.D., Department of Chemical Physics and Optics

Abstract: The interaction of swift electrons with matter is used to study and image the structure of materials in the field of electron microscopy and diffraction. One particular form of this interaction is the emission of a photon due to the coupling of the electron's electromagnetic field with the polarization of the material in its vicinity, a phenomenon called cathodoluminescence. Recent theoretical works predict that it might be possible to observe the optical coherence imprinted upon the electron wavefunction by modulation through optical fields in the coherence properties of the emitted photons. In this thesis, we extend the theoretical formalism currently used to study this effect in order to gain a deeper understanding by studying different regimes of optical modulation of the electron beam. In the first chapter of this thesis, we discuss important aspects of electron-matter interaction arising from classical electrodynamics, and in the second chapter, we systematically construct a quantum electrodynamic formalism for studying the statistical properties of emitted photons. By using simple numerical simulations, we then visualize the expected dependence of their degree of coherence on relevant physical parameters based on derived analytical results.

Keywords: Quantum electrodynamics electron-photon interaction coherence coherent cathodoluminescence

Contents

Introduction

Electron microscopy is currently among the best options for imaging both localized and nonlocalized modes in various materials with sub-nanometer spatial detail and sub-eV energy resolution. There are different variations of experiments conducted in the field of electron microscopy, but the interests of this thesis lie in the case of swift electron interactions with nanoscopic samples. When an ultrafast electron beam strikes a target, a multitude of different phenomena can be measured, for instance secondary electron emission (SEE) or electron energy-loss spectrum (EELS). The latter uses the fact that electrons themselves are a source of electromagnetic field that generates a response from the material when located in proximity of the studied sample. The created induced field then acts as a stopping force on the electron and the measured energy-loss spectrum allows us to analyze the excitation spectrum of our sample. An interesting subset of all electron energy-losses are those that lead to the excitation and subsequent emission of radiative modes in samples, which consequently add an asymptotical component of the induced field, the so called coherent cathodoluminiscence (CL). In this thesis, a particular focus will be given to the theoretical analysis of various properties of coherent CL from classical and quantum viewpoint. In the quantum picture, this means to determine the statistics of photons contained within the medium-assisted electromagnetic field, consequently enabling us to describe the spectrum of specific modes within our sample. Recent works [1], [2] also point out that due to modern methods of electron wavefunction modulation (in both spatial and temporal domain), we might observe a considerable level of correlation between the coherence properties of photons emitted by the sample and the modulating photons, by which the incident electron beam has been shaped. Such an effect would suggest a measurable transfer of optical coherence by free electrons that could be then utilized in a wide range of experiments. The main goal of this thesis is to theoretically describe the interaction of modulated electron beams with sample modes and to extend the formalism by which the transfer of optical coherence is currently studied, in order to enable the possibility of examining the behaviour of this quantity in different regimes of electron beam modulation.

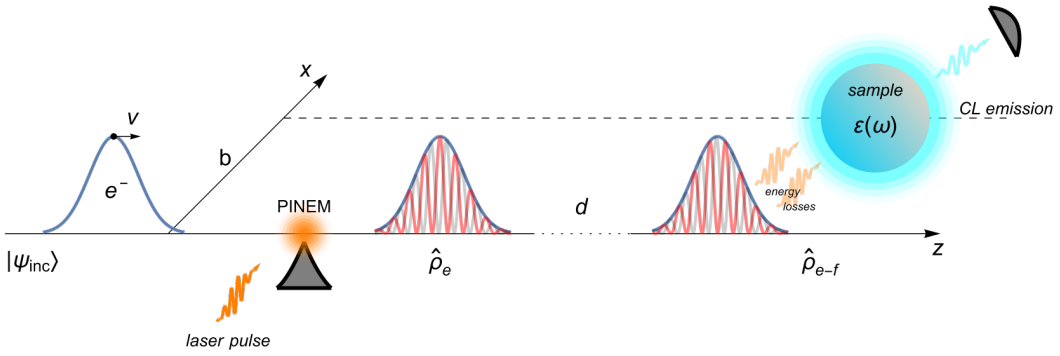

Figure 1: Schematic representation of the interaction of a modulated electron beam with optical sample modes theoretically examined within this thesis.

Figure 1 represents a schematic outline of this thesis. We begin by considering an initial electron wavepacket moving along a straight-line trajectory and describe its modulation by a photon-induced electromagnetic near-field created through external illumination of a nanoscopic structure with a modulating laser pulse. This method of shaping the electron beam will be primarily employed because of its reciprocity with respect to the subsequent interaction with radiative sample modes. The modulated electron beam is then generally described by a density operator, the specific form of which depends on the modulation regime and, consequently, on the properties of the laser pulse. The electron's statistical ensemble then freely propagates over a distance significantly greater than the modulating region, resulting in periodic acceleration and deceleration of its specific components. This leads to temporal lensing and the creation of energy sidebands corresponding to the absorption or emission of photons from the electromagnetic near-field. We will then study the quantum interaction of such an electron beam with an electromagnetic field mediated by a dielectric sample. This endeavor will require us to adapt the formalism of macroscopic quantum electrodynamics (QED) to describe the electron-field system and the post-interaction statistics of emitted photons. Once we have established a comprehensible theoretical framework, we will quantify the optical coherence carried by the electron beam from the modulating laser field to the medium-assisted electromagnetic field.

1. Relevant quantities from classical electrodynamics

In this chapter, we will discuss important concepts, quantities and formalisms applied in classical electrodynamics and describe the form, in which they may be used in QED calculations. This will involve discussing the methods, by which we may quantify the rate of electron energy-loss events and their characterization and the description of very simple dielectric functions that model material response with emphasis on the means to ensure their consistency with causality. These approaches will be then utilized in order to solve a problem with rather simple geometry in a fully analytical manner with the inclusion of relativistic effects. At the beginning however, we need to specify the electromagnetic properties of a moving electron.

1.1 Electromagnetic field of a non-accelerated point charge

It will prove useful to restrict ourselves to the description of swift electrons interacting with sample modes of low excitation energies, the reason for which is that we may then use the so called non-recoil approximation where an electron is considered to be moving with constant velocity along a straight line and interacting linearly with the individual modes. However, we have to determine the electromagnetic field set up by such an electron first in order to understand its capabilities as a probe into the excitation spectrum of our sample. It is necessary to mention that throughout this thesis, it will also be assumed that the electron interacts with homogeneous media described by the frequency dependent dielectric function $\varepsilon(\omega)$, relating c_0, the speed of light in vacuum and $c(\omega)$, the frequency dependent speed of light inside the medium. Later, we will briefly comment upon the derivation of two simple homogeneous dielectric functions used in various practical calculations.

Let's consider an electron moving with constant velocity $\mathbf{v} = v\mathbf{e_z}$, where $\mathbf{e_z}$ denotes unity vector along z-axis. Therefore, it is advantageous to split the position vector as $\mathbf{r} = (\mathbf{R}, z)$, where $\mathbf{R} = (x, y)$, in order to adapt to the symmetry of motion. Crucial tool for handling the calculations seen below is the Fourier transform between $(\mathbf{r}, t)$ and $(\mathbf{q}, \omega)$, where $\mathbf{q}$ denotes a wave vector, which will be defined as

$$\phi(\mathbf{r}, t) = \frac{1}{(2\pi)^2} \int d^3\mathbf{q} \int d\omega \, \tilde{\phi}(\mathbf{q}, \omega) e^{i\mathbf{q}\cdot\mathbf{r} - i\omega t} \,. \tag{1.1}$$

To determine the electron's electromagnetic field, we will start from the wave equations for scalar and vector potential, ϕ and $\mathbf{A}$ respectively

$$\begin{aligned} -\Box\phi(\mathbf{r}, t) &= \frac{\rho(\mathbf{r}, t)}{\varepsilon_t} \,, \\ -\Box\mathbf{A}(\mathbf{r}, t) &= \frac{\mathbf{j}(\mathbf{r}, t)}{\epsilon_0 c_0^2} \,, \end{aligned} \tag{1.2}$$

where $\Box = \Delta - \frac{1}{c^2}\frac{\partial^2}{\partial t^2}$ (Δ is the Laplacian operator), ρ is the free charge density, $\mathbf{j}$ denotes free current density, ε_0 is the permittivity of free space and $\varepsilon_t = \varepsilon(\omega)\,\varepsilon_0$ the total permittivity of the medium[1]. Applying Fourier transform (1.1) to the set of equations (1.2) yields algebraic equations for Fourier components

$$\begin{aligned}\left(q^2 - \varepsilon(\omega)k^2(\omega)\right)\tilde{\phi}(\mathbf{q},\,\omega) &= \frac{\tilde{\rho}(\mathbf{q},\,\omega)}{\varepsilon(\omega)\varepsilon_0}\,,\\ \left(q^2 - \varepsilon(\omega)k^2(\omega)\right)\tilde{\mathbf{A}}(\mathbf{q},\,\omega) &= \frac{\tilde{\mathbf{j}}(\mathbf{q},\,\omega)}{c_0^2\varepsilon_0}\,,\end{aligned} \tag{1.3}$$

where $k^2(\omega) = \omega^2/c_0^2$. The charge density of an electron moving along a straight-line trajectory can be written as $\rho(\mathbf{r},\,t) = -e\delta^{(3)}(\mathbf{r} - \mathbf{v}t)$, where e denotes the elementary charge and $\delta^{(3)}(\cdot)$ is the 3D Dirac delta function. Therefore, the inverse Fourier transform results in

$$\tilde{\rho}(\mathbf{q},\,\omega) = -\frac{e}{(2\pi)^2}\int d^3\mathbf{r}\int dt\;\delta^{(3)}(\mathbf{r} - \mathbf{v}t)e^{-i\mathbf{q}\cdot\mathbf{r}+i\omega t} = -\frac{e}{2\pi}\delta(\omega - \mathbf{q}\cdot\mathbf{v})\,,$$

where we only canceled the integration over $\mathbf{r}$ thanks to the delta function and then carried out the integral over t resulting in $2\pi\delta(\omega - \mathbf{q}\cdot\mathbf{v})$. Since current density of a single electron can be written as $\mathbf{j} = \mathbf{v}\rho$, it also holds (within the non-recoil approximation) that $\tilde{\mathbf{j}} = \mathbf{v}\tilde{\rho}$. The standard expression for electric field $\mathbf{E}$ in terms of potentials $\mathbf{E} = -\nabla\phi - \partial_t\mathbf{A}$ gives us the frequency dependent Fourier components as

$$\begin{aligned}\mathbf{E}(\mathbf{r},\,\omega) &= \frac{-i}{(2\pi)^{\frac{3}{2}}}\int d^3\mathbf{q}\,\left(\mathbf{q}\,\tilde{\phi}(\mathbf{q},\omega) - \omega\tilde{\mathbf{A}}(\mathbf{q},\omega)\right)e^{i\mathbf{q}\cdot\mathbf{r}} =\\ &= \frac{ie}{\varepsilon_0(2\pi)^{\frac{5}{2}}}\int d^3\mathbf{q}\,\frac{\frac{\mathbf{q}}{\varepsilon} - k\frac{\mathbf{v}}{c_0}}{q^2 - \varepsilon k^2}e^{i\mathbf{q}\cdot\mathbf{r}}\delta(\omega - \mathbf{q}\cdot\mathbf{v})\,,\end{aligned} \tag{1.4}$$

where we only made use of equations (1.3) and substituted for $\tilde{\rho}$ and $\tilde{\mathbf{j}}$.

Since $\mathbf{v}$ is assumed to be along the z-axis, the integral (1.4) can be carried out in cylindrical coordinates by transforming it to the form

$$\begin{aligned}\mathbf{E}(\mathbf{r},\,\omega) = \frac{ie}{\varepsilon_0(2\pi)^{\frac{5}{2}}}\int_{-\infty}^{\infty}dq_z\int_0^{\infty}dq_\perp\,q_\perp\int_{-\pi}^{\pi}d\varphi\\ \frac{\frac{1}{\epsilon}(q_\perp\cos\varphi,\;q_\perp\sin\varphi,\;q_z) - \frac{kv}{c_0}(0,0,1)}{q_\perp^2 + q_z^2 - \varepsilon k^2}e^{i(\mathbf{q}_\perp\cdot\mathbf{R}+q_z z)}\delta(\omega - q_z v)\,.\end{aligned} \tag{1.5}$$

Integration over q_z is trivial due to the delta function. Before we proceed, let us evaluate arising factors

$$\begin{aligned}\left(\frac{\omega}{v}\right)^2 - \varepsilon k^2 = \frac{\omega^2}{v^2}\left(1 - \varepsilon\frac{v^2}{c_0^2}\right) = \left(\frac{\omega}{\gamma_\varepsilon v}\right)^2\,,\\ \frac{\omega}{\varepsilon v} - \frac{kv}{c_0} = \frac{\omega}{\varepsilon v}\left(1 - \varepsilon\frac{v^2}{c_0^2}\right) = \frac{\omega}{\gamma_\varepsilon^2\varepsilon v}\,,\end{aligned}$$

where γ_ε denotes the frequency dependent Lorentz factor related to the electron moving inside a sample described by the dielectric function $\varepsilon(\omega)$.

[1]We assume the magnetic properties of the medium to be negligible, therefore its permeability $\mu_t \approx \mu_0$.

The integration over φ in (1.5) can be done by converting to polar coordinates for $\mathbf{R} = R(\cos\psi,\, \sin\psi)$, which leads to the remaining exponential becoming $\exp(iq_\perp R\cos(\varphi-\psi))$ and the integral taking form

$$\mathbf{E}(\mathbf{r},\,\omega) = \frac{ie}{\varepsilon(\omega)\varepsilon_0(2\pi)^{\frac{5}{2}}} e^{\frac{iz\omega}{v}} \int_0^\infty dq_\perp\, q_\perp^2 \int_{-\pi}^{\pi} d\varphi \\ \frac{(\cos\left[\varphi+\psi\right],\, \sin\left[\varphi+\psi\right],\, \frac{\omega}{\gamma_\varepsilon^2 v q_\perp})}{q_\perp^2 + \left(\frac{\omega}{\gamma_\varepsilon v}\right)^2} e^{iq_\perp R\cos\varphi}\,.$$

We then utilize the integral representation of ordinary Bessel functions [3]

$$J_n(z) = \frac{i^{-n}}{\pi}\int_0^\pi d\theta e^{iz\cos\theta}\cos(n\theta)\,,\ n\in\mathbb{Z}\,,$$

which can be directly observed in our integral if we expand the cosine and sine of $(\varphi+\psi)$, omit terms odd in φ, since their integration results in zero and limit the boundaries of integration to $\langle 0,\,\pi\rangle$ for even terms. The last integration over $q_\perp$ then leads immediately to modified Bessel functions through their relation to the ordinary Bessel functions [3]

$$K_n(z) = \frac{1}{z^n}\int_0^\infty dt \frac{t^{n+1}J_n(t)}{t^2+z^2}$$

and the final result for the frequency component of the electron's electric field then becomes

$$\mathbf{E}(\mathbf{r},\,\omega) = \frac{e\omega\exp(i\frac{z\omega}{v})}{\varepsilon_0(2\pi)^{\frac{3}{2}}\varepsilon(\omega)\gamma_\varepsilon v^2}\left[-K_1\left(\frac{\omega R}{\gamma_\varepsilon v}\right)\mathbf{e_R} + \frac{i}{\gamma_\varepsilon}K_0\left(\frac{\omega R}{\gamma_\varepsilon v}\right)\mathbf{e_z}\right]\,, \tag{1.6}$$

where $\mathbf{e_R}$ is a unit radial vector perpendicular to the z-axis. By comparing with other literature (e.g. [4]), we recognize that this is indeed the correct[2] expression for the field component set up by a non-accelerated electron in a homogeneous medium. By calculating the curl of (1.6), we find the associated magnetic field component

$$\mathbf{B}(\mathbf{r},\,\omega) = -\frac{e\omega\exp(i\frac{z\omega}{v})}{\varepsilon_0(2\pi)^{\frac{3}{2}}\varepsilon(\omega)\gamma_\varepsilon v c_0^2}K_1\left(\frac{\omega R}{\gamma_\varepsilon v}\right)\mathbf{e}_\varphi\,, \tag{1.7}$$

where $\mathbf{e}_\varphi$ is the azimuthal unit vector.

If we analyze the discovered electromagnetic field, we can make a few key observations about its effect on samples with which it interacts. First, we mention the asymptotics [3]

$$K_0(z) \xrightarrow{z\to 0} -\ln z\,,\\ K_m(z) \xrightarrow{z\to 0} \frac{\Gamma(m)}{2}\left(\frac{z}{2}\right)^{-m}\,,\ m>0\,,\\ K_m(z) \xrightarrow{z\to\infty} \sqrt{\frac{\pi}{2z}}e^{-z}\,,\ m\geq 0\,,$$

[2]Except for multiplication by a constant stemming from using SI instead of Gaussian units and a different definition of the Fourier transform.

from which we see that the field diverges at $R \to 0$ and thus we can expect a significant interaction contrast over small regions close to the electron's trajectory. Additionally, the field exponentially decays at large R for $v < c(\omega)$ ($\gamma_\varepsilon \in \mathbb{R}$) and therefore exhibits evanescent behaviour. However, for $v > c(\omega)$ we have an oscillating field decaying as $1/\sqrt{R}$, so the electron actually emits electromagnetic waves known as Cherenkov radiation[3] (CR). This property means that an electron can be regarded as a source of radiation permitting the study of momentum-energy space regions outside the light cone. Moreover, it means that fast electrons can also excite nondipolar modes in small particles, which would be difficult to resolve using external light instead [4].

1.2 Semi-classical EELS and CL

Evanescent character of the electron's field is beneficial in the investigation of localized excitations, which enables EELS experiments to achieve nanometer spatial resolution. Similar types of spectroscopies were used to discover and characterize collective excitations of conduction electrons, also known as plasmons. Additionally, localized plasmons have the ability to radiatively decay and therefore create a component of the induced field that carries energy which was transmitted from the electron, thus contributing to CL.

Theoretical analysis of both EELS and CL involves the definition of so-called probabilities $\Gamma(\omega)$, which in classical description represent an artificial quantization using $\hbar$ as a semiclassical prescription to convert the energy loss (or energy emission) into a probability [4], [5]. The true quantum nature of these quantities will be discussed later, for now we shall show how even classical description of both the electromagnetic field and the interacting bodies (probe and sample) can lead to complex analytical results with practical applications.

1.2.1 EELS probability

The energy loss of a swift electron on a straight-line trajectory $\mathbf{r}(t)$ with constant velocity $\mathbf{v}$ is obtained from integrating the stopping force proportional to the induced field $\mathbf{E}_{ind}(\mathbf{r}(t),\, t)$

$$\Delta E = e \int dt\, \mathbf{v} \cdot \mathbf{E}_{ind}(\mathbf{r}(t),\, t)\,, \tag{1.8}$$

where the sign has been changed in order to have $\Delta E > 0$. By rewriting $\mathbf{E}_{ind}(\mathbf{r}(t),\, t)$ as a real part of its Fourier decomposition in frequency domain, we can define the mentioned EELS probability

$$\Gamma_{\mathrm{EELS}}(\omega) = \sqrt{\frac{2}{\pi}} \frac{e}{\hbar\omega} \int dt\, \Re\{\mathbf{v} \cdot \mathbf{E}_{ind}(\mathbf{r}(t),\, \omega) e^{-i\omega t}\}\,, \tag{1.9}$$

which enables us to write

$$\Delta E = \int_0^\infty d\omega\, \hbar\omega \Gamma_{\mathrm{EELS}}(\omega)\,. \tag{1.10}$$

[3] In the rest of this thesis, we will be only discussing fields in vacuum and we therefore return to the notation $c \equiv c_0$.

Using this definition, we can see that the normalization of $\Gamma_{\mathrm{EELS}}(\omega)$ is such that its integral over $\omega \in \langle 0, \infty \rangle$ represents the total loss probability and (1.10) the average energy loss. It is also often convenient, especially in nonhomogeneous media, to express the EELS probability in terms of the electromagnetic Green tensor $\boldsymbol{G}(\mathbf{r}, \mathbf{r}', \omega)$, defined by the equation

$$\nabla \times \nabla \times \boldsymbol{G}(\mathbf{r}, \mathbf{r}', \omega) - \frac{\omega^2}{c^2} \varepsilon(\mathbf{r}, \omega) \boldsymbol{G}(\mathbf{r}, \mathbf{r}', \omega) = \delta^{(3)}(\mathbf{r} - \mathbf{r}') \mathbb{1} \,, \tag{1.11}$$

which is related to the total electric field as

$$\mathbf{E}(\mathbf{r}, \omega) = \frac{i\omega}{\varepsilon_0 c^2} \int d^3\mathbf{r}' \, \boldsymbol{G}(\mathbf{r}, \mathbf{r}', \omega) \cdot \mathbf{j}(\mathbf{r}', \omega) \,,$$

but we shall discuss this later in the quantum picture. As was previously mentioned however, our primary interest at this point does not concern all energy losses, but mainly those that stem from coupling of the electron's electromagnetic field to sample modes capable of radiative decay resulting in CL, because we wish to describe the detectable radiation spectrum.

1.2.2 CL probability

Cathodoluminiscence offers a method for characterizing nanostructures with virtually no sample damage and is commonly used to study the electronic bands of insulators and doped semiconductors. It is important to classify the sources of CL emission in accordance with their degree of coherence relative to the external field. There is a multitude of mechanisms of coherent CL, the most known of which are Cherenkov radiation, diffraction radiation and transition radiation [4]. What we observe as CL is actually an interference between all of the coherent sources and this is a consequence of the fact that the quantum-mechanical state of the sample after the emission returns to the same as before the interaction (all the energy transferred from the electron has radiated away). On the other hand, the incoherent part of CL bears a resemblance to photoluminescence, where the sample is first excited but decays inelastically, either to an intermediate state or via nonradiative decay, where in both cases the final state differs from the initial ground state and the eventual radiation is not coherent with respect to the external field.

The definition of Γ_{CL} is similar to the case of EELS, but instead of energy loss we start with a total radiated energy obtained by integrating the flux of the Poynting vector over a large sphere

$$E_{\mathrm{rad}} = \lim_{r \to \infty} \int dt \, r^2 \int_{\mathbb{S}_2} d\Omega \, \mathbf{e}_r \cdot [\mathbf{E}(\mathbf{r}, t) \times \mathbf{H}(\mathbf{r}, t)] \,, \tag{1.12}$$

where $\int_{\mathbb{S}_2} d\Omega = \int_0^\pi d\vartheta \, \sin\vartheta \int_{-\pi}^{\pi} d\varphi$, $\mathbf{e}_r$ is a unit radial vector from the origin and $\mu_0 \mathbf{H} = \mathbf{B}$. Decomposing both $\mathbf{E}$ and $\mathbf{H}$ into their frequency components ω and ω', respectively and then carrying out the integral over t resulting in $2\pi\delta(\omega + \omega')$, leads to the definition

$$\Gamma_{\mathrm{CL}}(\omega, \Omega) = \lim_{r \to \infty} \frac{2r^2}{\hbar\omega} \Re\{\mathbf{e}_r \cdot [\mathbf{E}(\mathbf{r}, \omega) \times \mathbf{H}(\mathbf{r}, -\omega)]\} \,, \tag{1.13}$$

which represents the solid angle and frequency resolved CL probability[4]. Integrating over all solid angles gives us the total probability for emission of a photon with frequency ω, $\Gamma_{\mathrm{CL}}(\omega) = \int_{\mathbb{S}_2} d\Omega\, \Gamma_{\mathrm{CL}}(\omega, \Omega)$ and in terms of this quantity, the final result then reads

$$E_{\mathrm{rad}} = \int_0^\infty d\omega\, \hbar\omega \Gamma_{\mathrm{CL}}(\omega)\,. \tag{1.14}$$

1.3 Elementary causal homogeneous dielectric functions

Before we proceed and determine the classical EELS and CL probabilities for a particular geometry, we will briefly discuss two simple dielectric functions that are applicable for the description of certain materials with surprisingly good results.

1.3.1 Drude and Lindhard models

Shortly after the discovery of electrons, Paul Drude developed a model providing a simple description of the optical properties of solids. Its applicability is mainly limited to metals, but it showed satisfying results even in the case of heavily doped semiconductors [6]. The derivation is very straightforward, the conduction electrons are influenced by external field $\mathbf{E}(t)$ and their oscillations are assumed to be damped due to collisions that occur with a characteristic frequency η and the equation of motion can therefore be written as

$$m^*\ddot{\mathbf{r}} + m^*\eta\dot{\mathbf{r}} = -e\mathbf{E}(t)\,,$$

where $\mathbf{r}$ is the average electron displacement and m^* denotes the electron effective mass incorporating band structure of the material. Applying Fourier transform to this equation then yields

$$\mathbf{r}(\omega) = \frac{e\mathbf{E}(\omega)}{m^*\omega(\omega + i\eta)}\,.$$

Assuming n to be the number density of electrons, we can easily evaluate macroscopic polarization

$$\mathbf{P}(\omega) = -ne\mathbf{r}(\omega) = -\frac{ne^2}{m^*\omega(\omega + i\eta)}\mathbf{E}(\omega)\,,$$

from which we can immediately extract the dielectric function as

$$\varepsilon_D(\omega) = 1 - \frac{\omega_p^2}{\omega(\omega + i\eta)}\,, \tag{1.15}$$

where $\omega_p = \sqrt{ne^2/(m^*\varepsilon_0)}$ is the bulk plasma frequency of free electron gas. Such a dielectric function has been used to accurately describe the properties of aluminium for instance, where [4] $\hbar\eta \approx 0.6\,\mathrm{eV}$ and $\hbar\omega_p \approx 15.8\,\mathrm{eV}$, which is in good agreement with the value of 15 eV obtained from EELS measurements. A slight

[4] In literature, it is also being referred to as the number of photons emitted per incoming electron, per unit of solid angle of emission and per unit of photon frequency range.

modification to (1.15) is to change the 1 to an unknown parameter ε_∞, which then accounts for the net contribution from the positive ion cores present in the metal. Even with this modification, we can see that the Drude model fails to describe very small frequencies, where the imaginary part of dielectric function tends to infinity, which is an unphysical behaviour.

A better model for the behaviour of electron gas was derived by Lindhard in 1954. It is based on quantum mechanical calculations of the effects of electric field screening by electrons in a solid and uses the first-order perturbation theory while utilizing the random phase approximation. The resulting dielectric function can be written as [7]

$$\varepsilon_L(\mathbf{q},\,\omega) = 1 - V_\mathbf{q} \sum_\mathbf{k} \frac{f_{\mathbf{k}-\mathbf{q}} - f_\mathbf{k}}{\hbar(\omega + i\delta) + E_{\mathbf{k}-\mathbf{q}} - E_\mathbf{k}}\,,$$

where $V_\mathbf{q} = V_{\text{eff}}(\mathbf{q}) - V_{\text{ind}}(\mathbf{q})$, $f_\mathbf{k}$ is the Fermi-Dirac distribution function for electrons in thermodynamic equilibrium, $E_\mathbf{k}$ is the energy level of wavevector $\mathbf{k}$, δ is a positive infinitesimal constant and the sum runs over all possible $\mathbf{k}$ in an assumed quantization volume. An explicit analytical expression for the Lindhard dielectric function can be determined either at zero temperature or at high temperatures in the long wavelength limit $\mathbf{q} \to 0$, where we get [6]

$$\varepsilon_L(\omega) = 1 - \frac{\omega_p^2}{(\omega + i\eta)^2}\,. \tag{1.16}$$

Dielectric functions (1.15) and (1.16) behave similarly at high frequencies, but there is obviously a major difference at $\omega \to 0$, namely (1.16) no longer diverges. However, it has been shown [8] that it is not consistent with conservation of the number of electrons in the metal. Different approaches towards obtaining various dielectric functions for specific materials can be found in literature (see e.g. the appendix of [4]), but for our purposes it will suffice to consider the simplest Drude dielectric function (1.15) and pay special attention to the case of $\omega \to 0$ in numerical calculations if neccessary.

1.3.2 Kramers-Kronig relations

We have very briefly summarized the derivation of two homogeneous dielectric functions, but we have not yet ensured that they are consistent with relativistic description. The causality of any linear response function leads to the Kramers-Kronig relations, which bind the real and imaginary part of said function. A simple derivation of these relations for $\varepsilon(\omega) = \varepsilon_R(\omega) + i\varepsilon_I(\omega)$, where ε_R denotes the real and ε_I the imaginary part of $\varepsilon(\omega)$, can be found in [9] and we will shortly comment on it.

If we begin from a linear relation between electric field and electric displacement field, $\mathbf{D}(\mathbf{r},\,\omega) = \varepsilon_0\varepsilon(\omega)\mathbf{E}(\mathbf{r},\,\omega)$ and apply Fourier transform, we arrive to

$$\mathbf{D}(\mathbf{r},\,t) = \varepsilon_0 \left[\mathbf{E}(\mathbf{r},\,t) + \int_{-\infty}^{\infty} d\tau G(\tau)\mathbf{E}(\mathbf{r},\,t-\tau)\right]\,,\ \text{where}$$
$$G(\tau) = \frac{1}{2\pi}\int_{-\infty}^{\infty} d\omega(\varepsilon(\omega) - 1)e^{-i\omega\tau}\,.$$

However, it would be against our understanding of causality if $\mathbf{D}(\mathbf{r}, t)$ was influenced by future electric field $\mathbf{E}(\mathbf{r}, t')$, $t' > t$. Therefore, in order to preserve a spatially-local causal relation between $\mathbf{D}$ and $\mathbf{E}$, it must hold that $G(\tau) = 0$ for $\tau < 0$, which yields an inverse relation

$$\varepsilon(\omega) = 1 + \int_0^\infty d\tau G(\tau) e^{i\omega\tau} \,.$$

This expression, along with reasonable physical assumptions for $G(\tau)$ and the fact that $G(\tau)$ is real (it connects real fields $\mathbf{E}(\mathbf{r}, t)$ and $\mathbf{D}(\mathbf{r}, t)$) leads us to the conclusion that $\varepsilon(\omega)$ is analytic in the upper half-plane as a function of complex ω. We can therefore invoke Cauchy's theorem to relate the real and imaginary part of ε on the real axis,

$$\varepsilon(z) = 1 + \frac{1}{2\pi i} \oint_C d\omega' \frac{\varepsilon(\omega') - 1}{\omega' - z} \,,$$

where the contour C is chosen to consist of the real axis and a large semicircle at infinity in the upper half-plane. A suitable expansion (shown in [9]) demonstrates that there is no contribution from the semicircle and by relating the real and imaginary parts of the remaining result (and utilizing the parity of $\varepsilon(\omega)$), we get the known Kramers-Kronig relations for homogeneous dielectric function

$$\begin{aligned} \varepsilon_R(\omega) &= 1 + \frac{2}{\pi} \mathcal{P} \int_0^\infty d\omega' \frac{\omega' \varepsilon_I(\omega')}{\omega'^2 - \omega^2} \,, \\ \varepsilon_I(\omega) &= -\frac{2\omega}{\pi} \mathcal{P} \int_0^\infty d\omega' \frac{\varepsilon_R(\omega') - 1}{\omega'^2 - \omega^2} \,, \end{aligned} \tag{1.17}$$

where $\mathcal{P}$ represents Cauchy principal value integral. These relations are applied in practise when one empirically models the absorption properties of a certain material and arrives to an explicit expression for $\varepsilon_I(\omega)$. They can then use (1.17) to calculate a causality ensuring $\varepsilon_R(\omega)$ from the first relation. If we were to separate the imaginary parts of (1.15), (1.16) and apply this method, we would see that the real parts are in order and therefore these dielectric functions are in fact consistent with a proper causality preserving theory.

1.4 Analytical relativistic solution of a single dielectric sphere

In this section, we will use the classical formalism for calculating CL and EELS probabilities to solve the case of a single dielectric sphere analytically with the inclusion of retardation effects associated with full relativistic description of the interaction. We will be mainly focusing on the CL probability, in order to emphasize the shape of expected induced radiative field, but the result for EELS probability will also be presented, because it will play a crucial role in the subsequent quantum calculations. The result for this geometry has been derived [10] by expanding the retarded Green function in free space, but we will use a slightly different approach and show that it is possible to reach the same result by working directly with the already determined external field set up by a non-accelerated electron (1.6), as well as provide all the details of the underlying calculations. Obtained results will then be used further in the quantum picture.

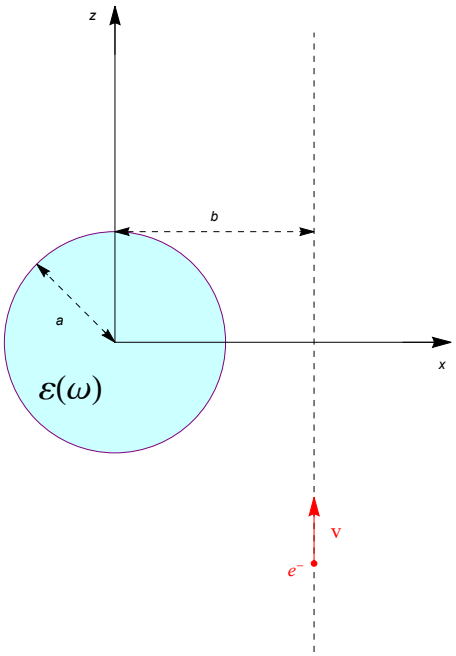

Figure 1.1: A simple diagram depicting assumed geometry of the analytically solved CL problem.

The geometry of our problem is summarized on figure 1.1. Suppose we have a dielectric sphere of radius a placed in the origin and described by the homogeneous dielectric function $\varepsilon(\omega)$ and an electron moving in vacuum along a straight-line trajectory $\mathbf{r}(t) = b\mathbf{e}_x + vt\mathbf{e}_z$ outside the sphere ($b > a$) with constant velocity v. We already know that the external electromagnetic field set up by the electron corresponds to the translated field $\mathbf{E}(\mathbf{r} - b\mathbf{e}_x, \omega)$, expressed from (1.6). The task is then to evaluate the CL probability (1.13). The mathematical analysis of (1.6) has also concluded that it falls of exponentially in vacuum, therefore it will not contribute to radiation and fields $\mathbf{E}$, $\mathbf{H}$ in (1.13) can be replaced by only the radiative components of induced fields $\mathbf{E}_{\text{ind}}$, $\mathbf{H}_{\text{ind}}$.

The starting point for finding the induced field is the dyadic identity [11]

$$\mathbb{1} = \nabla\frac{1}{\Delta}\nabla + \mathbf{L}\frac{1}{\mathbf{L}^2}\mathbf{L} - (\nabla\times\mathbf{L})\,\frac{1}{\mathbf{L}^2\Delta}(\mathbf{L}\times\nabla)\,,$$

where $\mathbf{L} = -i\mathbf{r}\times\nabla$ is the orbital momentum operator. This identity allows us to express the electric field in terms of 3 scalar functions, which are called longitudinal, magnetic and electric,

$$\mathbf{E} = \nabla\psi^L + \mathbf{L}\psi^M - \frac{i}{k}\nabla\times\mathbf{L}\psi^E\,.$$

In accordance with the dyadic identity, they are determined as

$$\begin{aligned}
\psi^L &= \frac{1}{\Delta}\nabla\cdot\mathbf{E}\,,\\
\psi^M &= \frac{1}{\mathbf{L}^2}\mathbf{L}\cdot\mathbf{E}\,,\\
\psi^E &= \frac{-ik}{\mathbf{L}^2\Delta}(\mathbf{L}\times\nabla)\cdot\mathbf{E}\,.
\end{aligned}$$

By recalling (1.3), we see that in a vacuum free of charges and currents it holds that $(\Delta+k^2)\mathbf{E}=0$ and since Δ commutes with both ∇ and $\mathbf{L}$, the same equation must be true for each of the individual ψ. With this knowledge, we can also evaluate magnetizing field from $\nabla\times\mathbf{E}=\frac{i\omega}{\varepsilon_0 c^2}\mathbf{H}$ as

$$\mathbf{H}=-\varepsilon_0 c\left(\frac{i}{k}\nabla\times\mathbf{L}\psi^M+\mathbf{L}\psi^E\right), \tag{1.18}$$

where we have utilized that $\nabla\times(\nabla\times\mathbf{L})=-\mathbf{L}\Delta$, which is easily provable by evaluation of individual components in Cartesian coordinates. Additionally, the analysis done in [11] shows that the contribution of ψ^L describes an instant propagation and it must cancel with the contribution of $1/\Delta$ present in the prescription for ψ^E. The situation can therefore be considerably simplified by setting $\psi^L=0$ and rewriting $1/\Delta=-1/k^2$ in the definition of ψ^E. These adjustments then lead to a new decomposition[5]

$$\begin{aligned}\mathbf{E}&=\mathbf{L}\psi^M-\frac{i}{k}\nabla\times\mathbf{L}\psi^E,\\ \psi^M&=\frac{1}{\mathbf{L}^2}\mathbf{L}\cdot\mathbf{E},\\ \psi^E&=\frac{i}{k\mathbf{L}^2}(\mathbf{L}\times\nabla)\cdot\mathbf{E}.\end{aligned} \tag{1.19}$$

Our task of finding the electric field $\mathbf{E}=\mathbf{E}_{\text{ext}}+\mathbf{E}_{\text{ind}}$, of which we know that $\lim_{r\to\infty}$ keeps only the induced component, therefore requires us to solve the scalar Helmholtz equation $(\Delta+k^2)\psi=0$ in the outter region, its analogy with $k^2\to\varepsilon(\omega)k^2$ inside the sphere and apply geometrically appropriate boundary conditions to match these solutions. We will briefly summarize the derivation of such conditions, but the comprehensive mathematical reasoning can be found in [11], [12].

Directly from Maxwell equations, one can immediately conclude that $\mathbf{E}_T$, $\mathbf{B}_T$, $\varepsilon\mathbf{E}_N$, $\mathbf{B}_N$ must be continuous at $r=a$ where the indices T and N denote field components tangential and normal to the sphere. The continuity of $\mathbf{E}_T$ at $r=a$ implies the same for $\mathbf{L}\cdot\mathbf{E}$ and therefore ψ^M. The second term of $\mathbf{E}$ will have a continuous tangential component if $\mathbf{r}\times(\nabla\times\mathbf{L}\psi^E)$ is continuous, which after some manipulation implies the continuity of $(1+r\frac{\partial}{\partial r})\psi^E$. The same procedure is then applied to $\mathbf{B}_T$, which leads to continuity of $\varepsilon\psi^E$ and $(1+r\frac{\partial}{\partial r})\psi^M$ as well. It is then shown that these 4 conditions are sufficient also for continuous $\varepsilon\mathbf{E}_N$ and $\mathbf{B}_N$, therefore the functions ψ^E and ψ^M can be completely determined.

Having described the boundary conditions for ψ at $r=a$ we now turn to prescribing suitable multipole expansions in vacuum for ψ^{E_e}, ψ^{M_e}, ψ^{E_i}, ψ^{M_i}, where the subscripts e and i denote either external or induced part. We know that the external field set up by an electron cannot give rise to any radiation and since the electron's trajectory is always external to the sphere, a divergent behaviour

[5]The equation (1.18) retains its form, we just need to apply the new expression for ψ^E.

at $r \to 0$ should not occur, therefore the only suitable multipole expansion[6] is

$$\begin{aligned} \psi^{E_e}(\mathbf{r}) &= \sum_{l=1}^{\infty} \sum_{m=-l}^{l} i^l j_l(kr) Y_{lm}(\vartheta, \varphi) \psi_{lm}^{E_e} , \\ \psi^{M_e}(\mathbf{r}) &= \sum_{l=1}^{\infty} \sum_{m=-l}^{l} i^l j_l(kr) Y_{lm}(\vartheta, \varphi) \psi_{lm}^{M_e} , \end{aligned} \tag{1.20}$$

where j_l are the spherical Bessel functions and Y_{lm} are scalar spherical harmonics. Multipole expansion of the induced component is then simply based on the fact that a general electromagnetic field is the combination of incoming and outgoing waves [11] represented by spherical Hankel functions $h_l^{(-)}(kr)$ and $h_l^{(+)}(kr)$, respectively and since our induced field is produced by the sources within a finite sphere, the field outside it has to be composed of only the outgoing components, therefore it holds that

$$\begin{aligned} \psi^{E_i}(\mathbf{r}) &= \sum_{l=1}^{\infty} \sum_{m=-l}^{l} i^l h_l^{(+)}(kr) Y_{lm}(\vartheta, \varphi) \psi_{lm}^{E_i} , \\ \psi^{M_i}(\mathbf{r}) &= \sum_{l=1}^{\infty} \sum_{m=-l}^{l} i^l h_l^{(+)}(kr) Y_{lm}(\vartheta, \varphi) \psi_{lm}^{M_i} . \end{aligned} \tag{1.21}$$

By combining these multipole expansions with the boundary conditions at $r = a$ that were mentioned above, we conclude the most important result

$$\begin{aligned} \psi_{lm}^{E_i} &= t_l^E \psi_{lm}^{E_e} , \\ \psi_{lm}^{M_i} &= t_l^M \psi_{lm}^{M_e} , \end{aligned} \tag{1.22}$$

where (details in [10], [12])

$$\begin{aligned} t_l^E &= \frac{-j_l(\rho_>)\left[\rho_< j_l(\rho_<)\right]' + \varepsilon \left[\rho_> j_l(\rho_>)\right]' j_l(\rho_<)}{h_l^{(+)}(\rho_>)\left[\rho_< j_l(\rho_<)\right]' - \varepsilon \left[\rho_> h_l^{(+)}(\rho_>)\right]' j_l(\rho_<)} , \\ t_l^M &= \frac{-j_l(\rho_>)\rho_< j_l'(\rho_<) + \rho_> j_l'(\rho_>) j_l(\rho_<)}{h_l^{(+)}(\rho_>)\rho_< j_l'(\rho_<) - \rho_> \left[h_l^{(+)}(\rho_>)\right]' j_l(\rho_<)} , \end{aligned} \tag{1.23}$$

with the notation $\rho_> = ka$, $\rho_< = ka\sqrt{\varepsilon}$ (positive imaginary part is applied) and the prime denoting differentiation with respect to $\rho_>$ or $\rho_<$. This result means that the components of external and induced field are related by a scattering matrix, much like in the partial-wave scattering analysis of finite-range potential in quantum mechanics. The scattering matrix elements t_l^E and t_l^M, which are independent of m due to spherical symmetry of the scattering body, are even more commonly being derived in terms of phase shifts δ_l.

The significance of the result (1.22) is clear, based on boundary conditions stemming directly from Maxwell equations and multipole expansions that were unambiguous due to the physical properties (no radiation or $r \to 0$ divergence in the external field and only outgoing spherical waves in the induced field), we have acquired a direct way to calculate the total electromagnetic field in our geometry

[6] It can be seen from (1.19) that $l = 0$ waves do not contribute to the electromagnetic field.

depicted on figure 1.1. It is also worth mentioning that zeros of denominators in (1.23) directly describe the modes characteristic for homogeneous spheres.

So far, we have mainly summarized the technique for finding the electromagnetic field in the presence of a dielectric sphere, but now we provide a very straightforward approach towards determining the expansion coefficients $\psi_{lm}^{E_e}$ and $\psi_{lm}^{M_e}$, because it turns out that we do not require the definition and multipole expansion of a retarded Green function like in [10], but we may directly utilize the translated external field (1.6), since the associated integrals are reducible to a single known integral of the modified Bessel functions.

As was already mentioned above, the external field set up by an electron is simply the field (1.6) translated to be centered at $b\mathbf{e}_x$ instead of the origin, therefore

$$\mathbf{E}_{\text{ext}}(\mathbf{r},\,\omega) = \frac{e\omega\exp(i\frac{z\omega}{v})}{\varepsilon_0(2\pi)^{\frac{3}{2}}\gamma v^2}\left[-K_1\left(\frac{\omega\sqrt{(x-b)^2+y^2}}{\gamma v}\right)\frac{(x-b)\mathbf{e}_x+y\mathbf{e}_y}{\sqrt{(x-b)^2+y^2}} + \frac{i}{\gamma}K_0\left(\frac{\omega\sqrt{(x-b)^2+y^2}}{\gamma v}\right)\mathbf{e}_z\right]. \tag{1.24}$$

We first turn our attention to ψ^{E_e}, in case of which the equation (1.19) shows that we need to first determine $(\mathbf{L}\times\nabla)\cdot\mathbf{E}_{\text{ext}}$. By rewriting the acting differential operator into Cartesian coordinates, it is simple to explicitly show the identity $\mathbf{L}\times\nabla = -i\left[(\mathbf{r}\cdot\nabla)\nabla - \mathbf{r}\Delta\right]$. Since $\nabla\cdot\mathbf{E}_{\text{ext}}$ vanishes outside the electron's trajectory and $(\Delta+k^2)\mathbf{E}_{\text{ext}} = 0$, we can directly write

$$(\mathbf{L}\times\nabla)\cdot\mathbf{E}_{\text{ext}}(\mathbf{r},\,\omega) = \frac{e\omega^3\exp(i\frac{z\omega}{v})}{\varepsilon_0(2\pi)^{\frac{3}{2}}\gamma^2c^2v^2}\left[i\gamma K_1\left(\frac{\omega\sqrt{(x-b)^2+y^2}}{\gamma v}\right)\frac{x(x-b)+y^2}{\sqrt{(x-b)^2+y^2}} + zK_0\left(\frac{\omega\sqrt{(x-b)^2+y^2}}{\gamma v}\right)\right]. \tag{1.25}$$

By also applying $\mathbf{L}^2$ to the definition of ψ^E in (1.19), rewriting the left-hand side according to (1.20) and utilizing $\mathbf{L}^2Y_{lm} = l(l+1)Y_{lm}$, we get the equation

$$\sum_{l=1}^{\infty}\sum_{m=-l}^{l} i^l l(l+1)j_l(kr)Y_{lm}(\vartheta,\,\varphi)\psi_{lm}^{E_e} = \frac{i}{k}(\mathbf{L}\times\nabla)\cdot\mathbf{E}_{\text{ext}}\,. \tag{1.26}$$

Spherical harmonics Y_{lm} obey the orthogonality relations

$$\int_{-\pi}^{\pi}d\varphi\int_0^{\pi}d\vartheta\sin\vartheta\,Y_{lm}(\vartheta,\,\varphi)Y_{l'm'}^*(\vartheta,\,\varphi) = \delta_{ll'}\delta_{mm'}$$

and therefore multiplying the equation (1.26) by $Y_{l'm'}^*$ and integrating over $\mathbb{S}_2$ gives us

$$\psi_{lm}^{E_e} = \frac{i^{1-l}}{k\,l(l+1)j_l(kr)}\int_{\mathbb{S}_2}d\Omega\,Y_{lm}^*(\vartheta,\,\varphi)(\mathbf{L}\times\nabla)\cdot\mathbf{E}_{\text{ext}}\,. \tag{1.27}$$

To evaluate this integral, we recall that

$$Y_{lm}(\vartheta,\,\varphi) = \sqrt{\frac{2l+1}{4\pi}\frac{(l-m)!}{(l+m)!}}P_l^m(\cos\vartheta)e^{im\varphi}\,,$$

where P_l^m are the associated Legendre polynomials with the Condon-Shortley phase $(-1)^m$ included. First, we carry out the integral over φ in (1.27), for which we will use the integral representations [3]

$$\begin{aligned} K_m(z) &= \frac{1}{2}\left(\frac{z}{2}\right)^m \int_0^\infty \frac{dt}{t^{m+1}} \exp\left(t - \frac{z^2}{4t}\right), \\ I_m(z) &= \frac{1}{\pi}\int_0^\pi e^{z\cos\varphi}\cos(m\varphi) \end{aligned} \tag{1.28}$$

and a known integral [13]

$$\int_0^\infty \frac{dt}{t}\exp\left(-\frac{t}{2} - \frac{a^2+b^2}{2t}\right) I_m\left(\frac{ab}{t}\right) = 2I_m(a)K_m(b)\,, \quad 0 < a < b\,. \tag{1.29}$$

Integration over φ of the second term in (1.25) reduces (by omitting all φ independent functions) to evaluation of

$$\int_{-\pi}^{\pi} d\varphi e^{-im\varphi} K_0(\sqrt{A^2+B^2-2AB\cos\varphi})\,,$$

where $A = \omega R/(\gamma v)$ and $B = \omega b/(\gamma v)$. We can take only $\cos(m\varphi)$ from the exponential, limit integration to $\langle 0,\, \pi\rangle$, rewrite K_0 according to (1.28), discover that terms dependent on φ integrate to form $\pi I_m\left(\frac{AB}{2t}\right)$ and the remaining integration then leads us directly to $2\pi I_m(A)K_m(B)$ through (1.29).

Evaluating the integral over φ of the first term in (1.25) requires slightly more complicated manipulation, therefore we will comment it a bit more thoroughly. The integral in question reduces to

$$\begin{aligned} &\int_{-\pi}^{\pi} d\varphi e^{-im\varphi} K_1(\sqrt{A^2+B^2-2AB\cos\varphi})\frac{A^2 - AB\cos\varphi}{\sqrt{A^2+B^2-2AB\cos\varphi}} = \\ &\int_0^\pi d\varphi\cos(m\varphi)(A^2 - AB\cos\varphi)\int_0^\infty \frac{dt}{2t^2}\exp\left(t - \frac{A^2+B^2-2AB\cos\varphi}{4t}\right) = \\ &\frac{\pi}{2}\int_0^\infty \frac{dt}{t^2} e^{t-\frac{A^2+B^2}{4t}}\left[A^2 I_m\left(\frac{AB}{2t}\right) - \frac{AB}{2}\left(I_{m+1}\left(\frac{AB}{2t}\right) + I_{m-1}\left(\frac{AB}{2t}\right)\right)\right], \end{aligned}$$

where the first equality stems from the integral representation of K_1 and the second one is simply the consequence of the representation of I_m after using the identity $\cos(m\varphi)\cos\varphi = 1/2(\cos[(m+1)\varphi] + \cos[(m-1)\varphi])$. We will use a trick to bring the integral to a form, in which we can utilize (1.29). First, it can be found [3] that $I_{m+1}(z) + I_{m-1}(z) = 2I'_m(z)$ and therefore

$$\begin{aligned} &A^2 I_m\left(\frac{AB}{2t}\right) - \frac{AB}{2}\left(I_{m+1}\left(\frac{AB}{2t}\right) + I_{m-1}\left(\frac{AB}{2t}\right)\right) = \\ &A^2 I_m\left(\frac{AB}{2t}\right) - 2At\frac{\partial}{\partial A} I_m\left(\frac{AB}{2t}\right) = -2Ate^{\frac{A^2}{4t}}\frac{\partial}{\partial A}\left[e^{-\frac{A^2}{4t}} I_m\left(\frac{AB}{2t}\right)\right]. \end{aligned}$$

This manipulation quite miraculously allows us to bring the partial derivative with respect to A out of the integral since dependence on A in the exponential is first canceled and then reintroduced. It also reduces dt/t^2 to dt/t, which is exactly what we required in order to apply (1.29). The integral then results in $-2\pi A I'_m(A)K_m(B)$.

With the integration over φ completed, we return to (1.27), which can now be written in full form as

$$\psi_{lm}^{E_e} = \frac{i^{1-l}\sqrt{\frac{2l+1}{8\pi^2}\frac{(l-m)!}{(l+m)!}}}{k\,l(l+1)j_l(kr)}\frac{e\omega^3 K_m\left(\frac{\omega b}{\gamma v}\right)}{\varepsilon_0\gamma^2c^2v^2}\int_0^\pi d\vartheta\sin\vartheta\, e^{i\frac{z\omega}{v}}P_l^m(\cos\vartheta) \left[zI_m\left(\frac{\omega R}{\gamma v}\right) - i\gamma R I_m'\left(\frac{\omega R}{\gamma v}\right)\right], \tag{1.30}$$

where there is also ϑ dependence through $z = r\cos\vartheta$ and $R = r\sin\vartheta$. The right-hand side of (1.30) is independent of r and therefore the left-hand side must be as well and to make use of this fact, we will now substitute I_m and the exponential for their expansions around $r = 0$, where it is known that $j_l(kr) \to (kr)^l/(2l+1)!!$. After we plug in the expansions, the integral that we need to evaluate becomes[7]

$$\sum_{j=m}^{\infty}\sum_{n=j}^{\infty}\frac{i^{n-j}\left(\frac{\omega}{v}\right)^n(2\gamma)^{-j}}{(n-j)!\left(\frac{j-m}{2}\right)!\left(\frac{j+m}{2}\right)!}\left[r^{n+1}\mathcal{I}^{lm}_{j,\,n+1-j} - ij\gamma^2\frac{v}{\omega}r^n\mathcal{I}^{lm}_{j,\,n-j}\right],$$

where the first sum runs only over even $j-m$ and

$$\mathcal{I}^{lm}_{j,\,n-j} = \int_{-1}^{1} du(1-u^2)^{\frac{j}{2}}u^{n-j}P_l^m(u)\,. \tag{1.31}$$

By examining (1.31) and realizing the orthogonality relations held by P_l^m [3], we can conclude that $\mathcal{I}^{lm}_{j,\,n-j}$ is equal to zero if conditions $j \geq m$ and $n < l$ are true, therefore only terms with $n \geq l$ survive, which is very convenient since the limit $r \to 0$ then cancels all contributions of $r^n\mathcal{I}^{lm}_{j,\,n-j}$ with $n > l$. Therefore the sum over n reduces only to $n = l$ and since our expansion permitted only $(n-j) \geq 0$ in the first place, the sum over j is then bound to even values of $j-m$ from all the remaining $j \in \{m,\, m+1,\, \ldots,\, l\}$. After elementary manipulations of the sums and constants, we then arrive to the final closed result for multipole expansion coefficients

$$\psi_{lm}^{E_e} = \frac{(2l+1)!!}{l(l+1)}\sqrt{\frac{2l+1}{8\pi^2}\frac{(l-m)!}{(l+m)!}}\frac{e\omega K_m\left(\frac{\omega b}{\gamma v}\right)}{\varepsilon_0\gamma^2c^2\beta^{l+1}}\left[\sum_{j=m}^{l-1}\frac{\mathcal{I}^{lm}_{j,\,l-j}(l+j\beta^2\gamma^2)}{(l-j)!\left(\frac{j-m}{2}\right)!\left(\frac{j+m}{2}\right)!(2i\gamma)^j} + [(l-m+1) \bmod 2]\,\frac{l\gamma^2\mathcal{I}^{lm}_{l,\,0}}{\left(\frac{l-m}{2}\right)!\left(\frac{l+m}{2}\right)!(2i\gamma)^l}\right], \tag{1.32}$$

where $\beta = v/c$ and the last term is present in the result only if $l-m$ is divisible by 2, since the sum over j is still restricted to even $j-m$. It is clear that an efficient evaluation of these coefficients depends on our approach to the determination of integrals (1.31). Our best option is to use a natural reccurence relation

$$(l-m)\mathcal{I}^{lm}_{j_1j_2} = (2l-1)\mathcal{I}^{l-1,\,m}_{j_1,\,j_2+1} - (l+m-1)\mathcal{I}^{l-2,\,m}_{j_1j_2}\,,$$

which stems directly from the properties of P_l^m and we may find various starting values for this reccurence in [13]. Although the result (1.32) is in a form different

[7] $I_m(x) = \sum_{k=m}^{\infty}(x/2)^k/\left[\frac{k-m}{2}!\frac{k+m}{2}!\right]$ and the sum runs over even $k-m$ values.

from the one in [10], an extensive numerical analysis showed that the results for expansion coefficients are proportional with a constant factor $e/(4\pi\sqrt{2\pi}\varepsilon_0)$, which stems from the difference of used units as well as a different definition of the Fourier transform.

Having covered the derivation of $\psi_{lm}^{E_e}$, we will now quickly skim through an analogous procedure for the derivation of $\psi_{lm}^{M_e}$. From (1.19), we proceed to evaluate

$$\mathbf{L}\cdot\mathbf{E}_{\mathrm{ext}} = -i(\mathbf{r}\times\nabla)\cdot\mathbf{E}_{\mathrm{ext}} = -i\mathbf{r}\cdot(\nabla\times\mathbf{E}_{\mathrm{ext}}) = \omega\mathbf{r}\cdot\mathbf{B}_{\mathrm{ext}}\,,$$

where $\mathbf{B}_{\mathrm{ext}}$ refers to the translated field (1.7) ($\mathbf{r}\to\mathbf{r}-b\mathbf{e}_x$)[8] and therefore

$$\mathbf{L}\cdot\mathbf{E}_{\mathrm{ext}} = \frac{e\omega^2 b\exp(i\frac{z\omega}{v})}{\varepsilon_0(2\pi)^{\frac{3}{2}}\gamma v c^2}K_1\left(\frac{\omega\sqrt{(x-b)^2+y^2}}{\gamma v}\right)\frac{y}{\sqrt{(x-b)^2+y^2}}\,.$$

We then need to again multiply this quantity by Y_{lm}^* and integrate over $\int_{\mathbb{S}_2}d\Omega$. The integral over φ dependent parts reduces to

$$\int_{-\pi}^{\pi}d\varphi e^{-im\varphi}K_1(\sqrt{A^2+B^2-2AB\cos\varphi})\frac{A\sin\varphi}{\sqrt{A^2+B^2-2AB\cos\varphi}}\,,$$

which can be evaluated by similar techniques as before, the result of which is $-\frac{2\pi i m}{B}I_m(A)K_m(B)$. The integration over ϑ is then carried out in the same way as in the previous case, utilizing the expansion of $\exp(iz\omega/v)$, $I_m\left(\frac{\omega R}{\gamma v}\right)$ and then applying the limit $r\to 0$, which cancels most of the $r^n\mathcal{I}^{lm}_{j,n-j}$ contributions. The final result for expansion coefficients of ψ^{M_e} then takes form

$$\psi_{lm}^{M_e} = \frac{m(2l+1)!!}{il(l+1)}\sqrt{\frac{2l+1}{8\pi^2}\frac{(l-m)!}{(l+m)!}}\frac{e\omega K_m\left(\frac{\omega b}{\gamma v}\right)}{\varepsilon_0 c^2\beta^l}\left[\sum_{j=m}^{l}\frac{\mathcal{I}^{lm}_{j,l-j}(2i\gamma)^{-j}}{(l-j)!\left(\frac{j-m}{2}\right)!\left(\frac{j+m}{2}\right)!}\right]\,. \tag{1.33}$$

This expression has again been compared with the result provided in [10] and the proportionality with identical constant multiplier has been verified.

We have therefore acquired an analytical result for $\mathbf{E}_{\mathrm{ind}}$, one just needs to combine (1.32), (1.33) with (1.22), (1.23) and plug it into (1.21), but as we will now show, there is a rather straightforward way to write the probability (1.13) in terms of $\psi_{lm}^{E_i}$ and $\psi_{lm}^{M_i}$. As we know, for an electron moving in vacuum, the external field vanishes in $r\to\infty$ and then

$$\Gamma_{\mathrm{CL}}(\omega) = \int_{\mathbb{S}_2}d\Omega\lim_{r\to\infty}\frac{2r^2}{\hbar\omega}\Re\{\mathbf{e}_r\cdot[\mathbf{E}_{\mathrm{ind}}(\mathbf{r},\,\omega)\times\mathbf{H}^*_{\mathrm{ind}}(\mathbf{r},\omega)]\}\,. \tag{1.34}$$

In the limit $r\to\infty$, we may replace $h_l^{(+)}(kr)$ by its asymptotics and therefore acquire

$$\psi^{E_i}(\mathbf{r}) = \sum_{l=1}^{\infty}\sum_{m=-l}^{l}\frac{e^{ikr}}{kr}Y_{lm}(\vartheta,\,\varphi)\psi_{lm}^{E_i}\,,$$
$$\psi^{M_i}(\mathbf{r}) = \sum_{l=1}^{\infty}\sum_{m=-l}^{l}\frac{e^{ikr}}{kr}Y_{lm}(\vartheta,\,\varphi)\psi_{lm}^{M_i}\,.$$

[8] This translation then makes $\mathbf{e}_\varphi\to\frac{(x-b)\mathbf{e}_y-y\mathbf{e}_x}{\sqrt{(x-b)^2+y^2}}$

It also proves useful to write the following operators in spherical coordinates

$$\begin{aligned}
\nabla &= \mathbf{e}_r \frac{\partial}{\partial r} + \mathbf{e}_\vartheta \frac{1}{r}\frac{\partial}{\partial \vartheta} + \mathbf{e}_\varphi \frac{1}{r\sin\vartheta}\frac{\partial}{\partial \varphi}\,, \\
\mathbf{L} &= -i\left(\mathbf{e}_\varphi \frac{\partial}{\partial \vartheta} - \mathbf{e}_\vartheta \frac{1}{\sin\vartheta}\frac{\partial}{\partial \varphi}\right), \\
\Delta &= \frac{1}{r}\frac{\partial^2}{\partial r^2} r - \frac{1}{r^2}\mathbf{L}^2\,, \\
\nabla \times \mathbf{L} &= -i\left[\mathbf{r}\Delta - \nabla\left(1 + r\frac{\partial}{\partial r}\right)\right],
\end{aligned}$$

because we can then simply evaluate

$$\begin{aligned}
\mathbf{L}\left(\frac{e^{ikr}}{kr}Y_{lm}\right) &= -i\frac{e^{ikr}}{kr}\left(\mathbf{e}_\varphi Y_{lm,\vartheta} - \mathbf{e}_\vartheta \frac{im}{\sin\vartheta}Y_{lm}\right), \\
\mathbf{L}\times\nabla\left(\frac{e^{ikr}}{kr}Y_{lm}\right) &= i\mathbf{e}_r \frac{l(l+1)}{kr^2}e^{ikr}Y_{lm} - \frac{e^{ikr}}{r}\left(\mathbf{e}_\vartheta Y_{lm,\vartheta} + \mathbf{e}_\varphi \frac{im}{\sin\vartheta}Y_{lm}\right),
\end{aligned}$$

where $Y_{lm,\vartheta}$ denotes $\frac{\partial}{\partial\vartheta}Y_{lm}$. By plugging these results in (1.18) and (1.19), we get

$$\begin{aligned}
&\int_{\mathbb{S}_2} d\Omega \lim_{r\to\infty} r^2 \Re\{\mathbf{e}_r \cdot [\mathbf{E}_{\mathrm{ind}}(\mathbf{r},\,\omega)\times\mathbf{H}^*_{\mathrm{ind}}(\mathbf{r},\omega)]\} = \\
&-\varepsilon_0 c\int_{\mathbb{S}_2} d\Omega \lim_{r\to\infty} r^2 \mathbf{e}_r \cdot \Re\left\{\left[\mathbf{L}\psi^{M_i} - \frac{i}{k}\nabla\times\mathbf{L}\psi^{E_i}\right]\times\left[\frac{i}{k}\nabla\times\mathbf{L}\psi^{M_i} + \mathbf{L}\psi^{E_i}\right]^*\right\} = \\
&\frac{\varepsilon_0 c}{k^2}\sum_{lm,\,l'm'}\int_{\mathbb{S}_2} d\Omega\,\Re\left\{\left[\left(Y_{lm,\vartheta}Y^*_{lm,\vartheta} + \frac{mm'}{\sin^2\vartheta}Y_{lm}Y^*_{l'm'}\right)(\psi^{E_i}_{lm}\psi^{*E_i}_{l'm'} + \psi^{M_i}_{lm}\psi^{*M_i}_{l'm'})\right.\right. \\
&\left.\left. + \,i\left(\frac{m}{\sin\vartheta}Y_{lm}Y^*_{l'm',\vartheta} + \frac{m'}{\sin\vartheta}Y_{lm,\vartheta}Y^*_{l'm'}\right)(\psi^{M_i}_{lm}\psi^{*E_i}_{l'm'} - \psi^{E_i}_{lm}\psi^{*M_i}_{l'm'})\right]\right\}.
\end{aligned}$$

The first equality is simply the consequence of definitions, but the second equality is the result of a quite extensive algebraic manipulation, which is however very straightforward, we just need to plug in the asymptotic multipole expansion, substitute for the acting of operators mentioned above and then evaluate the products of unit vectors in spherical coordinates. It turns out that the pair of large parentheses containing spherical harmonics each represent a different scalar product of vector spherical harmonics, for which there are known integral identities [14]

$$\begin{aligned}
\int_{\mathbb{S}_2} d\Omega\left(\frac{mm'Y_{lm}Y^*_{l'm'}}{\sin^2\vartheta} + Y_{lm,\vartheta}Y^*_{l'm',\vartheta}\right) &= l(l+1)\delta_{ll'}\delta_{mm'}\,, \\
\int_{\mathbb{S}_2} d\Omega\left(\frac{m'Y_{lm,\vartheta}Y^*_{l'm'}}{\sin\vartheta} + \frac{mY_{lm}Y^*_{l'm',\vartheta}}{\sin\vartheta}\right) &= 0\,.
\end{aligned}$$

We can therefore write the complete result for $\Gamma_{\mathrm{CL}}(\omega)$ as

$$\Gamma_{\mathrm{CL}}(\omega) = \frac{2\varepsilon_0}{\hbar k^3}\sum_{l=1}^{\infty}\sum_{m=-l}^{l} l(l+1)\left(\left|\psi^{E_i}_{lm}\right|^2 + \left|\psi^{M_i}_{lm}\right|^2\right),$$

but to gain a better understanding of the dependence of this result on individual physical parameters, we will recast it into a more transparent form. By recalling

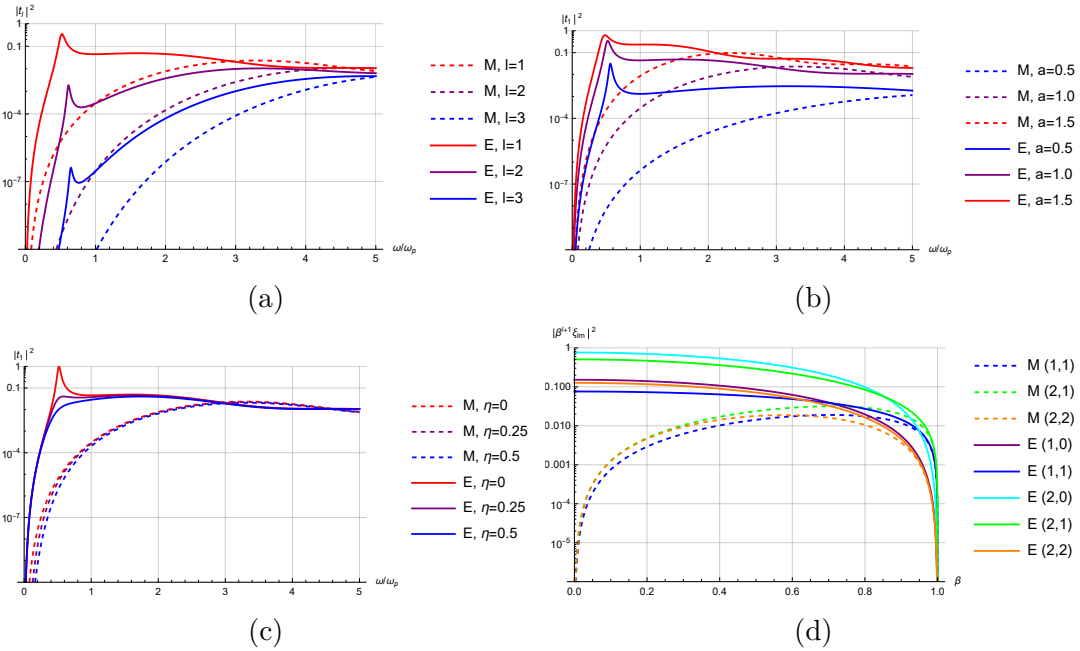

Figure 1.2: Dependency of the scattering matrix elements $|t_l|^2$ on photon frequency for different values of (a) the multipole order l, (b) the radius of our dielectric sphere a, (c) the electron gas damping frequency η. Plots (a) and (b) are evaluated for $\eta = 0.04\,\omega_p$ (valid for aluminium), plots (a) and (c) consider the radius $a = 1.0\,c/\omega_p$. (d) shows the dependence of decomposition coefficients $|\beta^{l+1}\xi_{lm}|^2$ (see (1.35)) on β for a few values of l, m.

(1.22) and (1.23), we realize that dependence on the sphere's radius and dielectric function is included through $|t_l^E|^2$ and $|t_l^M|^2$. By looking at (1.32) and (1.33), it becomes apparent that by factoring out $e\omega K_m\left(\frac{\omega b}{\gamma v}\right)/(\varepsilon_0 c^2)$, we will be left with expansion coefficients dependent only on β. A suitable form of the result is then

$$\begin{aligned}
\Gamma_{\mathrm{CL}}(\omega) &= \frac{4\pi\alpha}{\omega}\sum_{l=1}^{\infty}\sum_{m=-l}^{l} K_m^2\left(\frac{\omega b}{\gamma v}\right)\left[\left|t_l^E\xi_{lm}^E\right|^2 + \left|t_l^M\xi_{lm}^M\right|^2\right], \\
\xi_{lm}^M &= \frac{m(2l+1)!!}{i\beta^l\sqrt{l(l+1)}}\sqrt{\frac{2l+1}{4\pi^2}\frac{(l-m)!}{(l+m)!}}\left[\sum_{j=m}^{l}\frac{\mathcal{I}_{j,l-j}^{lm}(2i\gamma)^{-j}}{(l-j)!\left(\frac{j-m}{2}\right)!\left(\frac{j+m}{2}\right)!}\right], \\
\xi_{lm}^E &= \frac{(2l+1)!!}{\gamma^2\beta^{l+1}\sqrt{l(l+1)}}\sqrt{\frac{2l+1}{4\pi^2}\frac{(l-m)!}{(l+m)!}}\left[\sum_{j=m}^{l-1}\frac{\mathcal{I}_{j,l-j}^{lm}(l+j\beta^2\gamma^2)}{(l-j)!\left(\frac{j-m}{2}\right)!\left(\frac{j+m}{2}\right)!(2i\gamma)^j}\right. \\
&\qquad \left. + [(l-m+1) \bmod 2]\,\frac{l\gamma^2\mathcal{I}_{l,0}^{lm}}{\left(\frac{l-m}{2}\right)!\left(\frac{l+m}{2}\right)!(2i\gamma)^l}\right],
\end{aligned} \tag{1.35}$$

where $\alpha \approx 1/137$ is the fine-structure constant.

Due to the properties of associated Legendre polynomials [3], we know that for both types of expansion coefficients, it holds that $|\xi_{lm}| = |\xi_{l,-m}|$ and the explicit expression also tells us that $\xi_{l0}^M = 0$. Figure 1.2 shows some of the key dependancies of both t_l and ξ_{lm} on physical parameters, where the numerical

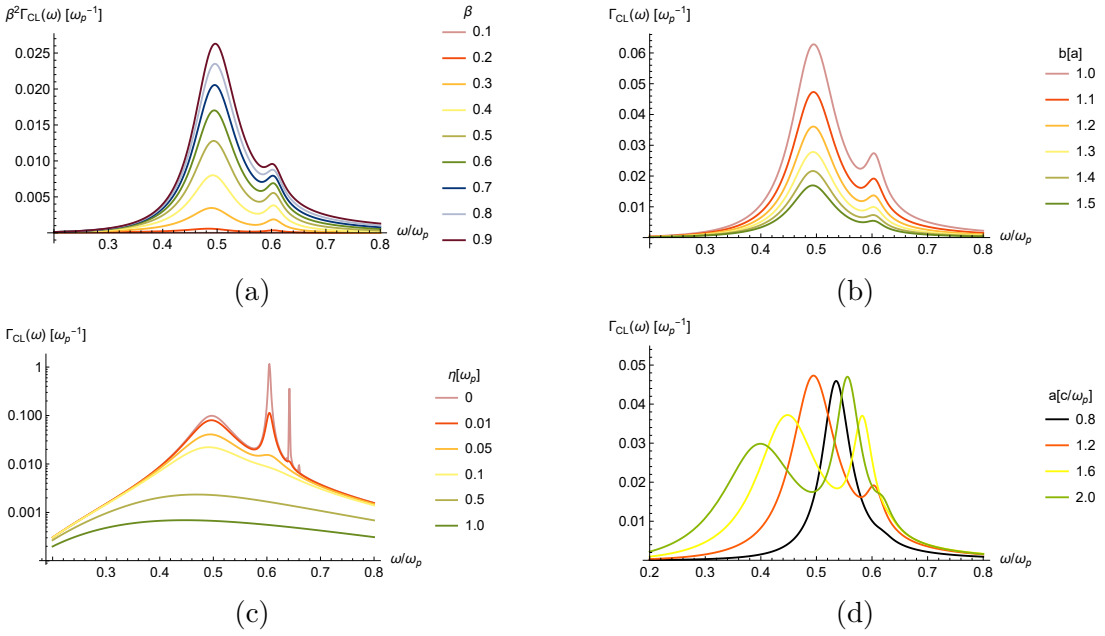

Figure 1.3: Dependency of the full CL probability $\Gamma_{\mathrm{CL}}(\omega)$, given by (1.35), on photon frequency for different values of (a) the ratio β of electron's velocity to c, (b) the impact parameter b of the trajectory, (c) the electron gas damping frequency η, (d) the dielectric sphere's radius a. Plots (a), (b), (c) consider the sphere's radius $a = 1.2\, c/\omega_p$, plots (a),(b) and (d) are evaluated for $\eta = 0.04\,\omega_p$. Plots (a), (c), (d) represent a situation with impact parameter $b = 1.1a$ and (b), (c), (d) assume $\beta = 0.6$.

values of η are in proportion to ω_p and the radius in proportion to c/ω_p[9]. We can see that the scattering matrix elements rapidly decrease with rising l in the small frequency region, where the $l = 1$ wave is dominant. It is also clear that $|t_l|^2$ increase with the sphere's radius and decrease with larger damping frequency η, which means that the sample absorbs more energy that is not then radiated away. From the dependence of $|\beta^{l+1}\xi_{lm}|^2$, we observe that they tend to larger values with larger l, but this growth will be effectively suppressed by $|t_l|^2$ in the region, where ω/ω_p is small[10]. We should also note that despite there being an apparent divergence of $|\xi_{lm}|^2$ with $\beta \to 0$, it will never be an issue in context of the full expression (1.35), since we know that $K_m(z)$ exponentially vanishes for large z and $\frac{\omega b}{\gamma v} \propto \beta^{-1}$ for $\beta \to 0$.

Figure 1.3 visualizes the behaviour of analytical result (1.35) with respect to different physical parameters. We can tell from the graphs that lesser impact parameter b significantly increases the probability of emission. The dependence on β is slightly more complex, because our result includes retardation effects. Figure 1.3a shows that the behaviour of $\beta^2\Gamma_{\mathrm{CL}}(\omega)$ is increasing with β, but if we were to evaluate the probability on its own, we would see that it increases up until $\beta \approx 0.4 - 0.5$, depending on the heights of individual peaks, which correspond to the sphere's eigenfrequencies [10], and then it decreases. Radius a

[9]For the experimentally determined value $\hbar\omega_p \approx 15\,\mathrm{eV}$ in case of aluminium, $c/\omega_p \approx 13.165\,\mathrm{nm}$.

[10]Large frequencies are then being suppressed by the modified Bessel functions.

of the dielectric sphere determines the modes that the sphere is able to contain and it therefore influences the number and positions of peaks. Lastly, we see that the dependence on η appears quite irregular, because the extreme value $\eta = 0$ means that the sample is unable to absorb any energy and the entire electron energy loss is converted into radiation, which creates additional peaks that would otherwise not contribute to radiation.

The last note concerning this particular analytical solution is that if we were to use the determined induced field to evaluate the probability $\Gamma_{\mathrm{EELS}}(\omega)$ (see (1.9)) for any event, in which the electron loses energy and not just those resulting in radiation, we would find a very similar result [10]

$$\Gamma_{\mathrm{EELS}}(\omega) = \frac{4\pi\alpha}{\omega} \sum_{l=1}^{\infty} \sum_{m=-l}^{l} K_m^2 \left(\frac{\omega b}{\gamma v}\right) \left[\Im\{t_l^E\} \left|\xi_{lm}^E\right|^2 + \Im\{t_l^M\} \left|\xi_{lm}^M\right|^2\right] , \qquad (1.36)$$

where $\Im\{\cdot\}$ denotes imaginary part. It can then be shown from (1.23) that $\left|t_l^{E,\,M}\right|^2 \leq \Im\{t_l^{E,\,M}\}$ and they are equal for strictly real-valued dielectric functions. This is consistent with the underlying fact that CL events are a subset of all electron energy losses, but they coincide if the specific dielectric medium is not able to absorb any energy.

1.5 Classical-Quantum equivalence of EELS probabilities

The presented classical formalism for calculating electron energy losses and their consequent contributions to CL is still currently widely used, because there exists an intuitive correspondence with results obtained by approaches involving second quantization of plasmon excitations.

The validity of classically determined probabilities manifests itself, if we modify the relation for $\Gamma_{\mathrm{EELS}}(\omega)$ in order to express it solely in terms of the electromagnetic Green tensor, satisfying (1.11). The induced electric field, which is present in (1.9), can be written as

$$\mathbf{E}_{\mathrm{ind}}(\mathbf{r},\,\omega) = \frac{i\omega}{\varepsilon_0 c^2} \int d^3\mathbf{r}' \, \left[\boldsymbol{G}(\mathbf{r},\,\mathbf{r}',\,\omega) - \boldsymbol{G}^0(\mathbf{r},\,\mathbf{r}',\,\omega)\right] \cdot \mathbf{j}(\mathbf{r}',\,\omega) \,,$$

where $\boldsymbol{G}^0$ is the solution to (1.11) in case of an infinite vacuum. Frequency dependent charge density of an electron moving in a straight line with constant velocity along the z-axis can be written as $\rho(\mathbf{r},\,\omega) = \frac{-e}{v\sqrt{2\pi}} \exp(iz\omega/v)\delta^{(2)}(\mathbf{R}-\mathbf{R}_0)$, where $\mathbf{R}_0 = (x_0,\,y_0)$ are the electron coordinates in xy-plane. With current density $\mathbf{j}$ being equal to $\mathbf{v}\rho$, we can evaluate (1.9) as

$$\Gamma_{\mathrm{EELS}}(\mathbf{R}_0,\omega) = \frac{4\alpha}{c} \iint dz dz' \Re\left\{i\left[G_{zz}^0(\mathbf{R}_0,z,z',\omega) - G_{zz}(\mathbf{R}_0,z,z',\omega)\right] e^{i\frac{\omega}{v}(z'-z)}\right\},$$

where the $\mathbf{R}_0$ dependence enters through both $\mathbf{r}$ and $\mathbf{r}'$ and we used the notation $G_{zz} = \mathbf{e}_z \cdot \boldsymbol{G} \cdot \mathbf{e}_z$. This relation can be simplified by entirely omitting G_{zz}^0, since it is known that the electromagnetic field set up by an electron in vacuum cannot lead to any energy losses due to a kinematical mismatch between electrons and

photons in free space [15]. By also utilizing the reciprocity theorem [9], which states that $\boldsymbol{G}(\mathbf{r},\, \mathbf{r}',\, \omega) = \boldsymbol{G}^T(\mathbf{r}',\, \mathbf{r},\, \omega)$, we can then identify the correct real part and get the desired result

$$\Gamma_{\mathrm{EELS}}(\mathbf{R}_0, \omega) = \frac{4\alpha}{c} \iint dz dz' \Im \left\{ G_{zz}(\mathbf{R}_0,\, z, z', \omega) \right\} \cos\left[\frac{\omega}{v}(z - z') \right] . \tag{1.37}$$

Various works (e.g. [4], [5], [16], [17]) have studied the formation of images in EELS experiments from a QED viewpoint and here we only summarize the relevant results connected to discussed probabilities, but the entirety of the next chapter will be dedicated towards the application of QED formalism in presence of dielectric media.

The state of current experimental setups allows us to consider each electron as a coherent superposition of plane waves with a narrow focus ($\approx 1\,\mathrm{nm}$) of the wavefunction in perpendicular direction. We may therefore describe an incident energetic electron with a wavefunction

$$\psi_{\mathrm{inc}}(\mathbf{r}) = \frac{1}{\sqrt{L}} e^{ikz} \psi_{\perp}(\mathbf{R}) \,,$$

where $\hbar k$ is the momentum along electron's trajectory, L is a quantization length in the same direction and $\psi_{\perp}(\mathbf{R})$ is a wavefunction in the perpendicular plane, which is assumed to remain unchanged after the interaction due to the slow motion in xy-plane and available experimental techniques. In the works mentioned, it is shown that under these assumptions, while adopting the non-recoil approximation, a minimal coupling interaction Hamiltonian between the electron and a quantized photon field, consisting of electric-field eigenfunctions (satisfying homogeneous form of (1.11), see [17]) and using Fermi's golden rule to evaluate the probability that an electron creates a photon in a specific state, we then arrive to the expression

$$\Gamma_{\mathrm{EELS}}(\omega) = \int d^2\mathbf{R}\, |\psi_{\perp}(\mathbf{R})|^2\, \Gamma_{\mathrm{EELS}}(\mathbf{R}, \omega) \,, \tag{1.38}$$

with $\Gamma_{\mathrm{EELS}}(\mathbf{R}, \omega)$ being given by (1.37). This important result validates the classical formalism including retardation effects in approaches, where all the inelastic losses are collected. The analytical result derived in the previous section can therefore be utilized in the following chapter if we average it over the perpendicular probability profile of an incident electron wavefunction. We will also discover that (1.38) will serve as an effective coupling coefficient between electrons and a quantized electromagnetic field, when we study the coherence transfer from modulating fields to the electromagnetic field, which is the result of coherent cathodoluminiscence.

2. Quantum description of the interaction of modulated electron beams with optical sample modes

In this chapter, we will build upon the insight acquired from classical electron-sample interactions and describe the problem within the formalism of second quantization. This will entail an extensive discussion of EM field quantization in the presence of absorbing and dispersing bodies, as well as the description of the process of electron beam modulation through interaction with quantum light. Once we acquire these tools, we will proceed to describe the interaction of a modulated electron with optical sample modes by adapting a minimal coupling Hamiltonian. The post-interaction state of our system will then serve as the foundation for analyzing the coherence properties present in the generated EM field.

2.1 PINEM-modulated electron beams

Photon-induced near-field electron microscopy (PINEM) is a technique, in which external photons are used to impulsively heat or excite a sample in order to follow its nonequlibrium state evolution in real time [15]. The result of light scattering from the surface of a nanostructure is the formation of a confined nanoscale electromagnetic near-field, which contains photons with altered dispersion relations and eliminates the energy-momentum mismatch that is present in vacuum and kinematically forbids the net absorption/emission of photons by electrons. The result is an energy exchange in tens of electronvolts, which is then resolved in energy spectra and enables both spatial and temporal imaging.

An interesting effect of this procedure is its application in dynamical manipulation of the electron wavefunction by utilizing a conveniently prepared electromagnetic near-field. The subsequent propagation of an electron beam beyond the PINEM region leads to a modulated wavepacket resembling the structure of a frequency comb made up of different sidebands related to the number of photons absorbed/emitted by the electron. The purpose of this section will be to derive the expression for such a modulated electron state by adopting a simplified second-quantization scheme resulting from a reduction of the Dirac equation to an effective form of the Schrödinger equation, which is an approach applied in [18], [19].

The Dirac equation describing an electron's interaction with a nonclassical electromagnetic field reads

$$\left[mc^2\beta + c\vec{\alpha}\cdot(\mathbf{p}+e\mathbf{A}) - e\phi\right]\Psi = i\hbar\frac{\partial\Psi}{\partial t}\,, \tag{2.1}$$

where m is the electron's rest mass, Ψ is the four-component electron spinor, $\mathbf{p} = -i\hbar\nabla$, $\mathbf{A}$ and ϕ are operators corresponding to vector and scalar potential respectively and β, $\vec{\alpha}$ are represented through 2×2 identity $\mathbb{1}$ and Dirac matrices

$\vec{\sigma}$ as

$$\beta = \begin{pmatrix} \mathbb{1} & 0 \\ 0 & -\mathbb{1} \end{pmatrix}, \quad \vec{\alpha} = \begin{pmatrix} 0 & \vec{\sigma} \\ \vec{\sigma} & 0 \end{pmatrix}.$$

By neglecting processes involving electron-positron pair creation [19], we may expand Ψ in terms of plane-waves of momenta $\hbar\mathbf{k}$ and positive relativistic energies $E_k = c\sqrt{m^2c^2 + \hbar^2k^2}$ located within a quantization volume V as

$$\begin{aligned} \Psi(\mathbf{r},\, t) &= \frac{1}{\sqrt{V}} \sum_{\mathbf{k}} \psi_{\mathbf{k}} \exp\left[i\left(\mathbf{k}\cdot\mathbf{r} - \frac{E_k t}{\hbar}\right)\right] \Psi_{\mathbf{k}}\,, \\ \Psi_{\mathbf{k}} &= A_k \begin{pmatrix} \mathbf{s} \\ B_k(\mathbf{k}\cdot\vec{\sigma})\,\mathbf{s} \end{pmatrix}, \end{aligned} \tag{2.2}$$

where $A_k = \sqrt{(E_k + mc^2)/(2E_k)}$, $B_k = \hbar c/(E_k + mc^2)$ and $\mathbf{s}$ is a two-component unit spin vector. By elementary calculations[1], one can show that (2.2) satisfies (2.1) in the absence of $\mathbf{A}$ and ϕ, therefore we can replace $(mc^2\beta + c\vec{\alpha}\cdot\mathbf{p})$ by E_k when plugging this expansion in (2.1).

Experimental results [15] justify the assumption that the incident electron forms a wavepacket which is narrowly focused around a central value $\mathbf{k}_0$ and we may then approximate $E_k \approx E_0 + (\hbar^2c^2/E_0)\,\mathbf{k}_0\cdot(\mathbf{k} - \mathbf{k_0})$, where $E_0 \equiv E_{k_0}$. Due to the form of our expansion (2.2), we may also substitute $\mathbf{k} \to -i\nabla$ within this expression. We will further assume the conservation of initial four-component spinor $\Psi_{\mathbf{k}} \approx \Psi_{\mathbf{k_0}}$ and hence the electron's spin $\mathbf{s}$ itself, because the non-recoil approximation concludes that replacing $\mathbf{k}$ by $\mathbf{k}_0$ in $\Psi_{\mathbf{k}}$ results in only a negligible error [19].

Relativistic expressions $\hbar\mathbf{k}_0 = m\gamma\mathbf{v}$ and $E_0 = mc^2\gamma$ lead to the electron velocity vector (assumed to be constant within the non-recoil approximation) $\mathbf{v} = \hbar c^2\mathbf{k}_0/E_0$. By elementary manipulations, it is also very straightforward to see that spinors $\Psi_{\mathbf{k}}$ satisfy the relations $\Psi^\dagger_{\mathbf{k}}\Psi_{\mathbf{k}} = 1$ and $\Psi^\dagger_{\mathbf{k}}\vec{\alpha}\Psi_{\mathbf{k}} = \hbar c\mathbf{k}/E_k$. If we then multiply (2.1) by $\Psi^\dagger_{\mathbf{k}_0}$ from the left and put all of the above together, we recast (2.1) into an effective Schrödinger equation for the scalar spinor amplitude $\psi(\mathbf{r},\, t)$, expressed by the expansion (2.2) when omitting $\Psi_{\mathbf{k}} \approx \Psi_{\mathbf{k}_0}$, which takes the form

$$\left[E_0 - \hbar\mathbf{v}\cdot(i\nabla + \mathbf{k}_0) + e\mathbf{v}\cdot\mathbf{A} - e\phi\right]\psi(\mathbf{r},\, t) = i\hbar\frac{\partial\psi(\mathbf{r},\, t)}{\partial t}\,. \tag{2.3}$$

It is important to note that despite the form of this equation, it fully incorporates relativistic kinematics through E_0 and $\hbar\mathbf{k}_0$.

Since we assume a tightly focused electron beam, which means that the overlap of the electron wavefunction and any charges within the light-scattering sample is negligible, we can work in the radiation gauge [20] with $\phi = 0$ and therefore $\mathbf{E} = -\partial\mathbf{A}/\partial t$. The operator $\mathbf{A}$ can[2] then be written as

$$\mathbf{A} = \sum_j -\frac{i}{\omega_j}\left[\boldsymbol{\mathcal{E}}_j(\mathbf{r})\hat{a}_j - \boldsymbol{\mathcal{E}}^*_j(\mathbf{r})\hat{a}^\dagger_j\right], \tag{2.4}$$

[1] Only the identity $(\mathbf{k}\cdot\vec{\sigma})^2 = k^2\mathbb{1}$ is required.

[2] An extensive description of the EM field quantization will be the topic of the following section, now we just adapt the expressions from [20].

where $\boldsymbol{\mathcal{E}}_j(\mathbf{r})$ denotes electric-field eigenfunction associated to the optical bosonic mode (contained by the electromagnetic near-field) with frequency ω_j and creation and annihilation operators, $\hat{a}_j^\dagger$ and $\hat{a}_j$ respectively. However, we will consider a simplification, in which the sample response is modeled to be dominated by a single bosonic optical mode at frequency ω_0 corresponding to an electric-field distribution $\boldsymbol{\mathcal{E}}_0(\mathbf{r})$. This approximation then allows, after accounting for the energy stored within the single optical mode, for the formulation of (2.3) as

$$\begin{aligned} i\hbar\frac{\partial|\psi(\mathbf{r},\,t)\rangle}{\partial t} &= (\hat{H}_0+\hat{H}_I)|\psi(\mathbf{r},\,t)\rangle, \quad \text{with} \\ \hat{H}_0 &= \hbar\omega_0\hat{a}_0^\dagger\hat{a}_0 + E_0 - \hbar\mathbf{v}\cdot(i\nabla+\mathbf{k}_0)\,, \\ \hat{H}_I &= -\frac{ie}{\omega_0}\mathbf{v}\cdot\left[\boldsymbol{\mathcal{E}}_0(\mathbf{r})\hat{a}_0 - \boldsymbol{\mathcal{E}}_0^*(\mathbf{r})\hat{a}_0^\dagger\right]\,, \end{aligned} \tag{2.5}$$

where $|\psi(\mathbf{r},\,t)\rangle$ is a state describing both the electron and the optical mode contained by the sample. We will consider an initial electron wavefunction of the form

$$\psi_{\text{inc}}(\mathbf{r},\,t) = e^{i\left(\mathbf{k_0}\cdot\mathbf{r}-\frac{E_0 t}{\hbar}\right)}\phi_{\text{inc}}(\mathbf{r}-\mathbf{v}t)\,,$$

with $\phi_{\text{inc}}(\mathbf{r}-\mathbf{v}t)$ being a slowly varying function of the moving frame coordinate $\mathbf{r}-\mathbf{v}t$ (its derivatives may be neglected). This initial condition and the assumption that $\mathbf{v}=v\mathbf{e}_z$ permit us to find that the solution to (2.5) can be written as

$$|\psi(\mathbf{r},\,t)\rangle = \psi_{\text{inc}}(\mathbf{r},\,t)\sum_{l=-\infty}^{\infty}\sum_{n=0}^{\infty}e^{i\omega_0[l(z/v-t)-nt]}f_l^n(\mathbf{r})|n\rangle\,, \tag{2.6}$$

where $|n\rangle$ denotes the Fock state with n excitations contained by the bosonic optical mode, the sum over l corresponds to the sum over electron energy sidebands associated with l energy quanta being absorbed by the electron ($l<0$ then denotes electron energy loss) and $f_l^n(\mathbf{r})$ are the amplitudes for such states. By inserting (2.6) into (2.5) and neglecting $\partial\phi_{\text{inc}}/\partial\mathbf{r}'$, we see that (2.6) is in fact a solution, provided that the equations

$$\frac{\partial f_l^n(\mathbf{r})}{\partial z} = \sqrt{n}\,g^*(\mathbf{r})f_{l+1}^{n-1}(\mathbf{r}) - \sqrt{n+1}\,g(\mathbf{r})f_{l-1}^{n+1}(\mathbf{r})\,, \tag{2.7}$$

with $g(\mathbf{r}) = e/(\hbar\omega_0)\exp\left[-i(\omega_0 z/v)\right]\mathcal{E}_{0z}(\mathbf{r})$, are satisfied. An important consequence of (2.7) is that $n+l$ is conserved during the interaction, which means that each initial population p_n of state $|n\rangle$ can be treated separately. The dependence of f_l^n on perpendicular coordinates $\mathbf{R}=(x,\,y)$ stems from $\mathcal{E}_{0z}$ and even though it plays a crucial role in the determination of orbital momentum transfer and could be used to calculate electron beam aberrations, we will neglect it altogether, since the detailed form of $\mathcal{E}_{0z}$ will not influence the asymptotic electron wavefunction, if those effects contribution is negligible[3].

Since we are interested only in the electron spectrum far beyond the PINEM region, it is convenient to initiate $f_l^n(-\infty)=\sqrt{p_n}\,\delta_{l0}$, the interpretation of which is that before the interaction, the electron has not yet absorbed/emitted any photons ($l=0$) and $|n\rangle$ has been populated with the probability p_n. After the interaction, the probability that the electron changed its energy by $l\hbar\omega_0$ then

[3]For a more detailed discussion, we may refer to [15], [18], [19].

reduces to $P_l = \sum_{n=\max\{0,-l\}}^{\infty} |f_l^n(\infty)|^2$. Equation (2.7) is (after disregarding the **R**-dependence) equivalent to the Schrödinger equation for a classically driven quantum harmonic oscillator and an exact solution is therefore obtainable (solutions can be found in [18], [19]) in a closed form

$$f_l^n(z) = \sqrt{p_{n+l}} e^{i\chi(z)} \sqrt{n!(n+l)!} (-\beta_0(z))^l e^{-\frac{|\beta_0(z)|^2}{2}} \sum_{n'=\max\{0,-l\}}^{n} \frac{(-|\beta_0(z)|^2)^{n'}}{n'!(n'+l)!(n-n')!}\,, \tag{2.8}$$

where χ is a global phase irrelevant to the electron spectrum and β_0 is a dimensionless coupling coefficient defined as $\beta_0(z) = \int_{-\infty}^{z} g(z')dz'$. Since the field $\mathcal{E}_{0z}$ is assumed to have evanescent character, we are permitted to separate the spatial scale on which PINEM modulation takes place and use $f_l^n \equiv f_l^n(\infty)$ within (2.6).

Probability P_l that the electron underwent a net exchange of l photons is therefore only dependent on the initial population p_n of the optical mode excitations and a coupling coefficient $\beta_0 \equiv \beta_0(\infty)$. We may consider various statistics for p_n (e.g. a pure Fock state or thermal excitations [19]), but we are interested in excitations that result from coherent external illumination. In such conditions, it can be shown[4] [21] that the initial populations follow a Poissonian distribution $p_n = e^{-\mu}\mu^n/n!$, where $\mu = \sum_{n=0}^{\infty} n p_n$ is the mean number of excitations. Figure 2.1 depicts the dependence of electron sideband populations P_l (or occupancy probabilities), for different μ, on the coupling parameter β_0. It can be seen from the spectra that for lower μ, the electron energy losses prevail, since the electron cannot possibly absorb more photons than there are stored within the bosonic optical mode. With increasing μ, the spectra are progressively more and more symmetrical.

To extract only information about the electron states from (2.6), we can trace out degrees of freedom related to the bosonic excitation from a pure joint-state density matrix

$$\langle \mathbf{r}|\hat{\rho}_e(t)|\mathbf{r}'\rangle = \sum_{n=0}^{\infty} \langle n|\psi(\mathbf{r},\, t)\rangle\langle\psi(\mathbf{r}',\, t)|n\rangle = \sum_{n=0}^{\infty} \psi_n(\mathbf{r},\, t)\psi_n^*(\mathbf{r}',\, t)\,, \tag{2.9}$$

where $\hat{\rho}_e(t)$ is the time-dependent electron density operator and

$$\psi_n(\mathbf{r},\, t) = \phi_{\mathrm{inc}}(\mathbf{r} - \mathbf{v}t) \sum_{l=-\infty}^{\infty} \exp\left[iz\left(k_0 + \frac{l\omega_0}{v}\right) - \frac{it}{\hbar}(E_0 + l\hbar\omega_0)\right] f_l^n\,.$$

It is worthwhile to note that $\hat{\rho}_e(t)$ admits the form of a pure-state density operator, if we assume a general smooth optical mode population strongly peaked around $\mu \gg 1$ and consider only $|l| \ll n$, after which one can separate the dependence of f_l^n. This subsequently allows for complete splitting of light and electron degrees of freedom and transforms (2.6) into (for details, see [18])

$$|\psi(\mathbf{r},\, t)\rangle = \left[\sum_{n=0}^{\infty} \sqrt{p_n} e^{-in\omega_0 t}|n\rangle\right] \left[\psi_{\mathrm{inc}}(\mathbf{r},\, t) \sum_{l=-\infty}^{\infty} e^{i(\chi+\varphi_l(z-vt))} J_l(2\sqrt{\mu}|\beta_0|)\right]\,,$$

where $\varphi_l(z - vt) = l\mathrm{Arg}\{-\beta_0\} + l\omega_0(z/v - t)$. Tracing of the joint-state density operator in this form results in a pure-state electron density matrix with the

[4] This result stems from the average occupation number of a Fock state $|n\rangle$ in a single-frequency quantum harmonic oscillator described by a coherent state.

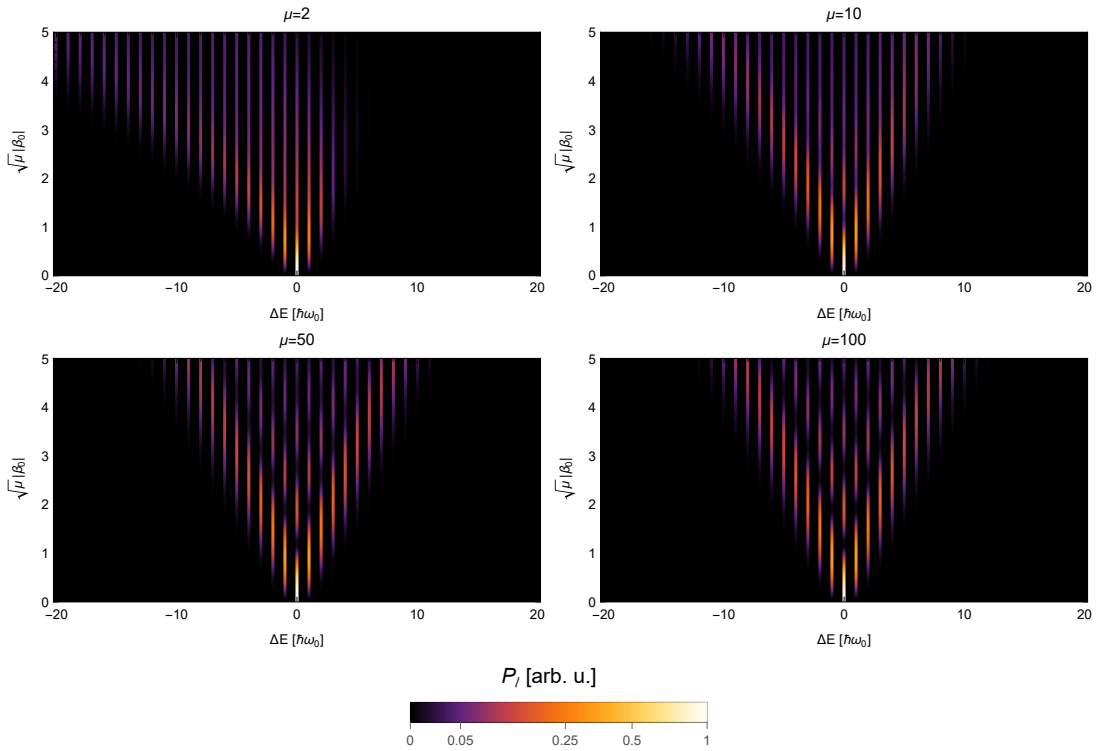

Figure 2.1: Dependencies of asymptotic electron energy spectra after the PINEM modulation described by an interaction of a single bosonic optical mode with the incident electron. The optical mode of frequency ω_0 is assumed to be initially populated due to coherent external illumination, resulting in Poissonian distribution of Fock states with a mean value μ, and its coupling with the electron is described through a dimensionless parameter β_0.

state being represented by the wavefunction contained in the second brackets, which is a well-known expression for a PINEM modulated electron calculated with classical light [15].

However, we believe that a keener insight into the transfer of optical coherence might be obtained, if we work with the entire electron density matrix. We will therefore attempt to formulate a theoretical framework for its calculation that would allow us to retain the impurity of electron state, in order to describe an interaction regime with a finite number of optical excitations performing the modulation. In this regime, we should be able to distinguish between an initial population resulting from coherent external illumination and a pure Fock state $|\mu\rangle$, which the limit presented above ultimately erases[5]. But first, we need to cover the procedure of electromagnetic field quantization in the presence of macroscopic media.

[5]We will also be able to examine other initial populations, e.g. thermal excitations created by chaotic illumination.

2.2 Overview of QED formalism in linearly responding media

Quantization of the free electromagnetic field was first formulated by Heisenberg, Jordan and Born in 1926. The theory of QED predicted a fluctuating vacuum field existing even in the absence of any sources and the well-estabilished formalism permitted the study of a vast range of light-matter interactions. However, the standard quantization procedure needed to be altered in order to include absorbing and dispersing bodies, which was achieved through quantization schemes for medium-assisted electromagnetic fields. In this section, we will point out the most important aspects of this alteration in comparison with the standard procedure.

Quantization of the electromagnetic field in vacuum is standardly done in one of two ways, either through a postulated Lagrangian satisfying relativistic covariance or by mode expansion of a general solution to the Maxwell equations. The latter is considerably more transparent (in its connection to classical theory) and a procedure starting with Maxwell equations is usually utilized also in the formulation of macroscopic QED. We will therefore comment on this approach.

2.2.1 Quantization procedure in vacuum

In vacuum, the Coulomb gauge comes also with zero scalar potential and therefore the homogeneous wave equation $\Box\mathbf{A}(\mathbf{r},\,t) = 0$ for the vector potential $\mathbf{A}$ encompasses all information on both electric and magnetic field. The solutions to this equation permit separation of variables through mode decomposition

$$\mathbf{A}(\mathbf{r},\,t) = \sum_{\kappa} \mathbf{A}_\kappa(\mathbf{r}) u_\kappa(t)\,,$$

where the sum turns into an integral for mode continuum. The modes $\mathbf{A}_\kappa(\mathbf{r})$ are therefore determined as eigenfunctions to the Hermitian operator $-\Delta$ corresponding to eigenvalues conveniently parametrized as ω_κ^2/c^2. As a consequence, they form a complete orthogonal basis, albeit in only a distributional sense. The individual solutions can be written in a form of plane waves

$$\mathbf{A}_\kappa(\mathbf{r}) = \mathcal{N}_\kappa \mathbf{e}_\alpha(\mathbf{k}_\kappa) e^{i\mathbf{k}_\kappa\cdot\mathbf{r}}\,,$$

where wavevectors obey dispersion relations $k_\kappa^2 = \omega_\kappa^2/c^2$ and allow for two orthogonal polarizations satisfying $\mathbf{e}_\alpha(\mathbf{k}_\kappa)\cdot\mathbf{e}^*_{\alpha'}(\mathbf{k}_\kappa) = \delta_{\alpha\alpha'}$ and $\mathbf{e}_\alpha(\mathbf{k}_\kappa)\cdot\mathbf{k}_\kappa = 0$, which are the consequences of imposed gauge. The orthogonality and completeness of $\mathbf{A}_\kappa$ can be summarized as

$$\begin{aligned}
\int d^3\mathbf{r}\, \mathbf{A}_\kappa(\mathbf{r})\cdot\mathbf{A}^*_{\kappa'}(\mathbf{r}) &= (2\pi)^3 \mathcal{N}_\kappa^2 \delta^{(3)}(\mathbf{k}_\kappa - \mathbf{k}_{\kappa'})\delta_{\alpha\alpha'}\,,\\
\sum_\kappa \mathbf{A}_\kappa(\mathbf{r})\otimes\mathbf{A}^*_\kappa(\mathbf{r}') &= \sum_\kappa \mathcal{N}_\kappa^2 \mathbf{e}_\alpha(\mathbf{k}_\kappa)\otimes\mathbf{e}^*_\alpha(\mathbf{k}_\kappa)\, e^{i\mathbf{k}_\kappa\cdot(\mathbf{r}-\mathbf{r}')}\,.
\end{aligned}$$

The mode decomposition in infinite vacuum therefore means $\sum_\kappa \to \sum_{\alpha=1}^2 \int d^3\mathbf{k}$ and a suitable normalization is $\mathcal{N}_\mathbf{k} = (2\pi)^{-3/2}$, which changes the right-hand side of the second condition to $\boldsymbol{\delta}^\perp(\mathbf{r}-\mathbf{r}') \equiv \delta^{(3)}(\mathbf{r}-\mathbf{r}')\mathbb{1}^\perp$, with $\mathbb{1}^\perp$ being identity on a space spanned by polarization vectors. The time-dependent functions $u_\kappa(t)$

satisfy classical equations for linear harmonic oscillators with frequencies ω_κ and are therefore expressed as

$$u_\kappa(t) = e^{\pm i\omega_\kappa t} u_\kappa(0) \equiv e^{\pm i\omega_\kappa t} u_\kappa \,.$$

By further imposing the conditions $u_{\mathbf{k}\alpha}(t) = u^*_{-\mathbf{k}\alpha}(t)$ and[6] $\mathbf{e}_\alpha(-\mathbf{k}) = \mathbf{e}^*_\alpha(\mathbf{k})$, we can write the decomposition of real vector potential

$$\mathbf{A}(\mathbf{r},\, t) = \sum_{\alpha=1}^{2} \int \frac{d^3\mathbf{k}}{(2\pi)^{\frac{3}{2}}} \left[\mathbf{e}_\alpha(\mathbf{k}) u_{\mathbf{k}\alpha} e^{i(\mathbf{k}\cdot\mathbf{r}-\omega t)} + \mathbf{e}^*_\alpha(\mathbf{k}) u^*_{\mathbf{k}\alpha} e^{-i(\mathbf{k}\cdot\mathbf{r}-\omega t)} \right] . \tag{2.10}$$

The vector potential can then be used to write the field's Hamiltonian

$$\begin{aligned} H =& \frac{1}{2} \int d^3\mathbf{r} \left[\varepsilon_0 \mathbf{E}^2(\mathbf{r},\, t) + \frac{1}{\mu_0} \mathbf{B}^2(\mathbf{r},\, t) \right] = \\ & \frac{1}{2} \int d^3\mathbf{r} \left[\varepsilon_0 \left(\frac{\partial \mathbf{A}(\mathbf{r},\, t)}{\partial t} \right)^2 + \frac{1}{\mu_0} (\nabla \times \mathbf{A}(\mathbf{r},\, t))^2 \right] = \\ & 2\varepsilon_0 \sum_{\alpha=1}^{2} \int d^3\mathbf{k}\, \omega^2 |u_{\mathbf{k}\alpha}|^2 \,, \end{aligned}$$

where we just substituted from (2.10), integrated over $d^3\mathbf{r}$, which ultimately cancelled time-dependence, and utilized the identities $\mathbf{e}_\alpha(\mathbf{k}) \cdot \mathbf{e}^*_{\alpha'}(\mathbf{k}) = \delta_{\alpha\alpha'}$ and $(\mathbf{k} \times \mathbf{e}_\alpha(\mathbf{k})) \cdot (\mathbf{k} \times \mathbf{e}^*_{\alpha'}(\mathbf{k}) = k^2 \mathbf{e}_\alpha(\mathbf{k}) \cdot \mathbf{e}^*_{\alpha'}(\mathbf{k})$. By further defining

$$\begin{aligned} q_{\mathbf{k}\alpha} &= \sqrt{\varepsilon_0} (u_{\mathbf{k}\alpha} + u^*_{\mathbf{k}\alpha}) \,, \\ p_{\mathbf{k}\alpha} &= -i\omega \sqrt{\varepsilon_0} (u_{\mathbf{k}\alpha} - u^*_{\mathbf{k}\alpha}) \,, \end{aligned}$$

we turn the Hamiltonian of the classical electromagnetic field into the familiar form

$$H = \frac{1}{2} \sum_{\alpha=1}^{2} \int d^3\mathbf{k} (p^2_{\mathbf{k}\alpha} + \omega^2 q^2_{\mathbf{k}\alpha}) \,, \tag{2.11}$$

which represents an infinite set of uncoupled harmonic oscillators. The functions $q_{\mathbf{k}\alpha}$, $p_{\mathbf{k}\alpha}$ can be therefore treated as canonical coordinates and momenta, respectively. In the context of classical mechanics, they then obey the Poisson bracket relation

$$\{q_{\mathbf{k}\alpha},\, p_{\mathbf{k}'\alpha'}\} = \delta^{(3)}(\mathbf{k} - \mathbf{k}') \delta_{\alpha\alpha'} \,,$$

which is the cornerstone for performing quantization and formulating canonical commutators

$$q_{\mathbf{k}\alpha} \to \hat{q}_{\mathbf{k}\alpha} \,, \quad p_{\mathbf{k}\alpha} \to \hat{p}_{\mathbf{k}\alpha} \,, \quad [\hat{q}_{\mathbf{k}\alpha},\, \hat{p}_{\mathbf{k}'\alpha'}] = i\hbar \delta^{(3)}(\mathbf{k} - \mathbf{k}') \delta_{\alpha\alpha'} \,.$$

We then circle back to complex functions resembling the former mode amplitudes and define operators

$$\hat{a}_\alpha(\mathbf{k}) = \sqrt{\frac{\omega}{2\hbar}} \left(\hat{q}_{\mathbf{k}\alpha} + \frac{i}{\omega} \hat{p}_{\mathbf{k}\alpha} \right) \,, \quad \hat{a}^\dagger_\alpha(\mathbf{k}) = \sqrt{\frac{\omega}{2\hbar}} \left(\hat{q}_{\mathbf{k}\alpha} - \frac{i}{\omega} \hat{p}_{\mathbf{k}\alpha} \right) \,, \tag{2.12}$$

[6] Complex valued polarization vectors are permitted in order to also include circular polarization.

for which the following commutation relations arise

$$[\hat{a}_\alpha(\mathbf{k}),\, \hat{a}_{\alpha'}(\mathbf{k}')] = \left[\hat{a}^\dagger_\alpha(\mathbf{k}),\, \hat{a}^\dagger_{\alpha'}(\mathbf{k}')\right] = 0\,, \quad \left[\hat{a}_\alpha(\mathbf{k}),\, \hat{a}^\dagger_{\alpha'}(\mathbf{k}')\right] = \delta^{(3)}(\mathbf{k}-\mathbf{k}')\delta_{\alpha\alpha'}\,. \tag{2.13}$$

By tracing back the quantization procedure to (2.10) and estabilishing a connection between $\hat{a}$, $\hat{a}^\dagger$ and u, u^*, we can now write the operator for vector potential $\hat{\mathbf{A}}$ in the Schrödinger picture as

$$\hat{\mathbf{A}}(\mathbf{r}) = \sum_{\alpha=1}^{2} \int \frac{d^3\mathbf{k}}{(2\pi)^{\frac{3}{2}}} \sqrt{\frac{\hbar}{2\varepsilon_0\omega}} \left[\mathbf{e}_\alpha(\mathbf{k})\hat{a}_\alpha(\mathbf{k})e^{i\mathbf{k}\cdot\mathbf{r}} + \mathbf{e}^*_\alpha(\mathbf{k})\hat{a}^\dagger_\alpha(\mathbf{k})e^{-i\mathbf{k}\cdot\mathbf{r}}\right]\,. \tag{2.14}$$

This plane-wave expansion represents a special case of a general mode expansion

$$\hat{\mathbf{A}}(\mathbf{r}) = \sum_\kappa \left[\mathbf{A}_\kappa(\mathbf{r})\hat{a}_\kappa + \mathbf{A}^*_\kappa(\mathbf{r})\hat{a}^\dagger_\kappa\right]\,, \tag{2.15}$$

with a sole non-zero commutator $\left[\hat{a}_\kappa,\, \hat{a}^\dagger_{\kappa'}\right] = \delta_{\kappa\kappa'}$. Various problems of different geometries might encourage other specific forms of this general decomposition, e.g. an expansion of $\mathbf{A}(\mathbf{r})$ into spherical or cylindrical Bessel functions. Their common feature is the familiar Hamiltonian operator

$$\hat{H} = \sum_\kappa \hbar\omega_\kappa \left(\hat{a}^\dagger_\kappa\hat{a}_\kappa + \frac{1}{2}\right)\,,$$

which one can derive from (2.11) by using (2.12) and (2.13) for the plane-wave expansion.

The expansion (2.15) enables us to also determine the electric and magnetic field operators

$$\hat{\mathbf{E}}(\mathbf{r}) = i\sum_\kappa \omega_\kappa \left[\mathbf{A}_\kappa(\mathbf{r})\hat{a}_\kappa - \mathbf{A}^*_\kappa(\mathbf{r})\hat{a}^\dagger_\kappa\right]\,,$$
$$\hat{\mathbf{B}}(\mathbf{r}) = \sum_\kappa \left[\nabla\times\mathbf{A}_\kappa(\mathbf{r})\hat{a}_\kappa + \nabla\times\mathbf{A}^*_\kappa(\mathbf{r})\hat{a}^\dagger_\kappa\right]\,.$$

By combining these expressions, we can evaluate

$$\left[\hat{\mathbf{E}}(\mathbf{r}), \hat{\mathbf{B}}(\mathbf{r}')\right] = i\sum_\kappa \omega_\kappa \left\{\mathbf{A}_\kappa(\mathbf{r})\otimes[\nabla'\times\mathbf{A}^*_\kappa(\mathbf{r}')] + \mathbf{A}^*_\kappa(\mathbf{r})\otimes[\nabla'\times\mathbf{A}_\kappa(\mathbf{r}')]\right\}\,,$$

where we have only utilized the commutators of $\hat{a}$, $\hat{a}^\dagger$ and used notation ∇' in order to emphasize its acting on $\mathbf{r}'$ coordinates. The operator $(\nabla'\times)$ can be therefore taken out of the expansion and by plugging in the plane-wave decomposition (2.14) along with the completeness of $\mathbf{A}_\kappa(\mathbf{r})$ basis (discussed earlier in this section), we arrive at the fundamental (equal-time) commutation relation for the electromagnetic field operators

$$\left[\hat{\mathbf{E}}(\mathbf{r}), \hat{\mathbf{B}}(\mathbf{r}')\right] = -\frac{i\hbar}{\varepsilon_0}\nabla\times\boldsymbol{\delta}^\perp(\mathbf{r}-\mathbf{r}')\,, \tag{2.16}$$

where the change of sign results from $\nabla'\times\boldsymbol{\delta}^\perp(\mathbf{r}-\mathbf{r}') = -\nabla\times\boldsymbol{\delta}^\perp(\mathbf{r}-\mathbf{r}')$.

This particular commutator is the reason for such a prolonged discussion of a long-known quantization scheme. It reveals the bosonic nature of excitations,

photons, within the electromagnetic field and shows the mutual algebraic properties of electric and magnetic field operators. However, operators $\hat{\mathbf{E}}$ and $\hat{\mathbf{B}}$ describe only the electromagnetic degrees of freedom and when one wants to formulate a theory with medium-assisted fields, it requires the usage of electric displacement field ($\hat{\mathbf{D}}$) and magnetizing field ($\hat{\mathbf{H}}$). In free space, their connection to $\hat{\mathbf{E}}$ and $\hat{\mathbf{B}}$ is trivial, but in general, they contain both electromagnetic and matter degrees of freedom. Nevertheless, we will see that in the context of macroscopic QED, one can proceed with the quantization scheme in a way that ultimately satisfies (2.16), which is regarded as the fundamental building block for such a theory.

2.2.2 Quantization of medium-assisted EM field

In the formulation of macroscopic QED, we will mostly rely on general results and widely used procedures, examples of which can be found in [22], [23]. Some of the highly technical results will be just commented upon, since the main goal is to understand the conceptual differences from the vacuum QED. Significant attention will be paid to media described by local and isotropic dielectric functions, because we ultimately want to address the situation analytically solved in the first chapter. It is also worth noting that a naive attempt at quantization through plane-wave mode expansion, like in the vacuum case, fails. The reason is that simply changing $\mathbf{k} \to \sqrt{\varepsilon(\omega)}\mathbf{k}$ erases the completeness and orthogonality of the plane-wave basis, since refractive index is a complex-valued quantity in a general absorbing medium and the corresponding plane-waves are ultimately damped and therefore cannot be used.

One of the correct ways is to start from constitutive relations

$$\mathbf{D}(\mathbf{r},\, t) = \varepsilon_0 \mathbf{E}(\mathbf{r},\, t) + \mathbf{P}(\mathbf{r},\, t)\,, \quad \mathbf{H}(\mathbf{r},\, t) = \frac{1}{\mu_0}\mathbf{B}(\mathbf{r},\, t) - \mathbf{M}(\mathbf{r},\, t)\,,$$

where $\mathbf{P}(\mathbf{r},\, t)$ denotes the polarization field and $\mathbf{M}(\mathbf{r},\, t)$ the magnetization field. If we assume the medium response to be linear and local, we can write the most general expressions relating the fields, while retaining causality and following the linear fluctuation-dissipation theorem [22] as

$$\begin{aligned}
\mathbf{P}(\mathbf{r},\, t) &= \varepsilon_0 \int_0^\infty d\tau \chi_e(\mathbf{r},\, \tau)\mathbf{E}(\mathbf{r},\, t-\tau) + \mathbf{P}_N(\mathbf{r},\, t)\,, \\
\mathbf{M}(\mathbf{r},\, t) &= \frac{1}{\mu_0}\int_0^\infty d\tau \chi_m(\mathbf{r},\, \tau)\mathbf{B}(\mathbf{r},\, t-\tau) + \mathbf{M}_N(\mathbf{r},\, t)\,,
\end{aligned}$$

with $\chi_e(\mathbf{r},\, t)$, $\chi_m(\mathbf{r},\, t)$ denoting electric and magnetic susceptibilities, respectively and $\mathbf{P}_N(\mathbf{r},\, t)$, $\mathbf{M}_N(\mathbf{r},\, t)$ representing noise polarization and magnetization resulting from absorption, respectively.

These noise responses are the consequence of the fluctuation-dissipation theorem which states that the linear response of a given system to an external perturbation is expressed in terms of fluctuation properties of the system in equilibrium. This theorem is usually formulated in the form of a stochastic equation describing fluctuations by adding a Langevin noise term, which in our context is due to absorption itself. To put it very bluntly, Langevin noise sources, introduced above by $\mathbf{P}_N$, $\mathbf{M}_N$, can be understood as bridges between the classical and quantum

regimes in macroscopic systems in a sense that they effectively incorporate quantum fluctuations into the classical equations of motion and they represent the stochastic forces arising from the quantum nature of the electromagnetic field. They are therefore ensuring consistency between descriptions and accounting for dissipation processes in materials.

If we limit further discussion to media without inherent magnetic response ($\chi_m = 0$) and reintroduce the dielectric function

$$\varepsilon(\mathbf{r},\,\omega) = 1 + \int_0^\infty d\tau \chi_e(\mathbf{r},\,\tau) e^{i\omega\tau}\,,$$

we can write down the macroscopic Maxwell equations

$$\begin{aligned} \nabla \cdot \mathbf{B}(\mathbf{r},\,\omega) &= 0\,, \\ \nabla \times \mathbf{E}(\mathbf{r},\,\omega) &= i\omega \mathbf{B}(\mathbf{r},\,\omega)\,, \\ \varepsilon_0 \nabla \cdot [\varepsilon(\mathbf{r},\,\omega)\mathbf{E}(\mathbf{r},\,\omega)] &= \rho_N(\mathbf{r},\,\omega)\,, \\ \nabla \times \mathbf{B}(\mathbf{r},\,\omega) + \frac{i\omega}{c^2}\varepsilon(\mathbf{r},\,\omega)\mathbf{E}(\mathbf{r},\,\omega) &= \mu_0 \mathbf{j}_N(\mathbf{r},\,\omega)\,. \end{aligned} \tag{2.17}$$

By using notation

$$\begin{aligned} \rho_N(\mathbf{r},\,\omega) &= -\nabla \cdot \mathbf{P}_N(\mathbf{r},\,\omega)\,, \\ \mathbf{j}_N(\mathbf{r},\,\omega) &= -i\omega \mathbf{P}_N(\mathbf{r},\,\omega) + \nabla \times \mathbf{M}_N(\mathbf{r},\,\omega)\,, \end{aligned}$$

it is made clear that even though no free charges or currents have been put into consideration, the noise sources themselves act as a driving force for electromagnetic field in absorbing media and it is also evident that they obey the standard continuity equation.

In a more general case concerning nonisotropic media with $\chi_m \neq 0$, we would combine the analogies of the second and fourth equation in (2.17) and write down

$$\begin{aligned} &\nabla \times \nabla \times \mathbf{E}(\mathbf{r},\,\omega) - \frac{\omega^2}{c^2}\mathbf{E}(\mathbf{r},\,\omega) = i\omega\mu_0 \mathbf{j}(\mathbf{r},\,\omega)\,, \quad \text{with} \\ &\mathbf{j}(\mathbf{r},\,\omega) = \mathbf{j}_N(\mathbf{r},\,\omega) + \int d^3\mathbf{r}'\, \boldsymbol{Q}(\mathbf{r},\mathbf{r}',\omega)\cdot \mathbf{E}(\mathbf{r}',\,\omega)\,, \end{aligned}$$

where $\boldsymbol{Q}(\mathbf{r},\mathbf{r}',\omega)$ denotes the general complex conductivity tensor and its real part $\boldsymbol{\sigma}(\mathbf{r},\mathbf{r}',\omega) \equiv \Re\{\boldsymbol{Q}(\mathbf{r},\mathbf{r}',\omega)\}$ describes the dissipation of electromagnetic energy. This can be simply seen from the equations (2.17) for media under consideration, where the mentioned tensors simplify to

$$\begin{aligned} \boldsymbol{Q}(\mathbf{r},\mathbf{r}',\omega) &= -i\omega\varepsilon_0(\varepsilon(\mathbf{r}',\,\omega) - 1)\delta^{(3)}(\mathbf{r}-\mathbf{r}')\mathbb{1}\,, \\ \boldsymbol{\sigma}(\mathbf{r},\mathbf{r}',\omega) &= \omega\varepsilon_0 \Im\{\varepsilon(\mathbf{r}',\,\omega)\}\,\delta^{(3)}(\mathbf{r}-\mathbf{r}')\mathbb{1}\,. \end{aligned} \tag{2.18}$$

The entire system (2.17) can therefore be reduced into

$$\nabla \times \nabla \times \mathbf{E}(\mathbf{r},\,\omega) - \frac{\omega^2}{c^2}\varepsilon(\mathbf{r},\,\omega)\mathbf{E}(\mathbf{r},\,\omega) = i\omega\mu_0 \mathbf{j}_N(\mathbf{r},\,\omega)$$

and we can understand $\mathbf{B}$ to be defined through the second Maxwell equation in (2.17) and ρ_N to be determined by $\mathbf{j}_N$ due to the continuity equation. If we recall

the electromagnetic Green tensor $\boldsymbol{G}(\mathbf{r},\,\mathbf{r}',\,\omega)$, defined by (1.11), we see that the electric field can be uniquely calculated solely from the noise current as

$$\mathbf{E}(\mathbf{r},\,\omega) = i\mu_0\omega \int d^3\mathbf{r}\, \boldsymbol{G}(\mathbf{r},\,\mathbf{r}',\,\omega)\cdot\mathbf{j}_N(\mathbf{r}',\,\omega)\,.$$

This expression is crucial, when it comes to quantization, since we know that the electromagnetic Green tensor encompasses the structure of Maxwell equations as well as all the information on geometry and macroscopic response properties of considered dielectrics. In order to quantize the theory, the noise current itself will be therefore regarded as an operator and then

$$\begin{aligned}\hat{\mathbf{E}}(\mathbf{r},\,\omega) &= i\mu_0\omega \int d^3\mathbf{r}'\, \boldsymbol{G}(\mathbf{r},\,\mathbf{r}',\,\omega)\cdot\hat{\mathbf{j}}_N(\mathbf{r}',\,\omega)\,,\\ \hat{\mathbf{B}}(\mathbf{r},\,\omega) &= \mu_0\nabla\times\int d^3\mathbf{r}'\, \boldsymbol{G}(\mathbf{r},\,\mathbf{r}',\,\omega)\cdot\hat{\mathbf{j}}_N(\mathbf{r}',\,\omega)\,.\end{aligned} \tag{2.19}$$

This approach is quite intuitive, since as we commented earlier, the noise sources originate from quantum fluctuations related to dissipation. There is still the question of prescribing suitable commutators for $\hat{\mathbf{j}}_N$ and it is done in a way that consequently ensures the validity of (2.16). First, we write the total electromagnetic field operators in the Schrödinger picure as

$$\begin{aligned}\hat{\mathbf{E}}(\mathbf{r}) &= \int_0^\infty d\omega\, \hat{\mathbf{E}}(\mathbf{r},\,\omega) + \text{H.c.}\,,\\ \hat{\mathbf{B}}(\mathbf{r}) &= \int_0^\infty d\omega\, \hat{\mathbf{B}}(\mathbf{r},\,\omega) + \text{H.c.}\,,\end{aligned} \tag{2.20}$$

where H.c. denotes Hermitian conjugate.

By first postulating (motivated by creation and annihilation operators (2.13)) commutation relations

$$\left[\hat{\mathbf{j}}_N(\mathbf{r},\,\omega),\,\hat{\mathbf{j}}_N(\mathbf{r}',\,\omega')\right] = 0 = \left[\hat{\mathbf{j}}_N^\dagger(\mathbf{r},\,\omega),\,\hat{\mathbf{j}}_N^\dagger(\mathbf{r}',\,\omega')\right]\,,$$

we can simplify the fundamental equal-time commutator to assume the form [22]

$$\begin{aligned}&\left[\hat{\mathbf{E}}(\mathbf{r}),\,\hat{\mathbf{B}}(\mathbf{r}')\right] = -i\mu_0^2\int_0^\infty d\omega\,\omega\int_0^\infty d\omega'\int d^3\boldsymbol{\xi}\int d^3\boldsymbol{\xi}'\\ &\Big\{\boldsymbol{G}(\mathbf{r},\boldsymbol{\xi},\omega)\cdot\left[\hat{\mathbf{j}}_N(\boldsymbol{\xi},\,\omega),\,\hat{\mathbf{j}}_N^\dagger(\boldsymbol{\xi}',\,\omega')\right]\cdot\boldsymbol{G}^*(\boldsymbol{\xi}',\mathbf{r}',\omega')+\\ &\boldsymbol{G}^*(\mathbf{r},\boldsymbol{\xi},\omega)\cdot\left[\hat{\mathbf{j}}_N^\dagger(\boldsymbol{\xi},\,\omega),\,\hat{\mathbf{j}}_N(\boldsymbol{\xi}',\,\omega')\right]\cdot\boldsymbol{G}(\boldsymbol{\xi}',\mathbf{r}',\omega')\Big\}\times\overleftarrow{\nabla}'\,,\end{aligned}$$

with the left-arrow of $\overleftarrow{\nabla}'$ emphasizing its acting on $\mathbf{r}'$ from the right. This expression comes directly from definitions (2.19), (2.20) by recalling the reciprocity of $\boldsymbol{G}(\mathbf{r},\,\mathbf{r}',\,\omega)$. Prescription of the remaining commutator is motivated by a general integral identity satisfied by the electromagnetic Green tensor,

$$\mu_0\omega\int d^3\boldsymbol{\xi}\int d^3\boldsymbol{\xi}'\,\boldsymbol{G}(\mathbf{r},\boldsymbol{\xi},\omega)\cdot\boldsymbol{\sigma}(\boldsymbol{\xi},\boldsymbol{\xi}',\omega)\cdot\boldsymbol{G}^*(\boldsymbol{\xi}',\mathbf{r}',\omega) = \Im\{\boldsymbol{G}(\mathbf{r},\mathbf{r}',\omega)\}\,. \tag{2.21}$$

Detailed derivations of this identity can be found in [22], [23]. We can then see that by introducing[7] the last commutation relation as

[7]It should be noted that this relation is not just mathematically convenient. It could have been also derived solely from the fluctuation-dissipation theorem.

$$\left[\hat{\mathbf{j}}_N(\mathbf{r},\,\omega),\,\hat{\mathbf{j}}_N^\dagger(\mathbf{r}',\,\omega')\right] = \frac{\hbar\omega}{\pi}\delta(\omega-\omega')\boldsymbol{\sigma}(\mathbf{r},\,\mathbf{r}',\,\omega)\,, \tag{2.22}$$

the fundamental equal-time commutator reduces to

$$\left[\hat{\mathbf{E}}(\mathbf{r}),\,\hat{\mathbf{B}}(\mathbf{r}')\right] = \frac{\hbar\mu_0}{i\pi}\int_{-\infty}^{\infty} d\omega\,\omega\Im\{\boldsymbol{G}(\mathbf{r},\mathbf{r}',\omega)\}\times\overleftarrow{\nabla}'\,. \tag{2.23}$$

The remaining integration is then done in the complex ω-plane over a contour that includes an infinite semi-circle in the upper half-plane, where $\boldsymbol{G}$ is known to be analytical, and then the real axis with an infinitesimal semi-circular cutout around the origin, where the Green tensor is known to be singular [9]. Integration over the large semi-circle can be done quite simply, since (1.11) shows that for $\varepsilon(\mathbf{r},\,\omega)$ approaching 1 at $|\omega|\to\infty$, $\boldsymbol{G}\to-(c^2/\omega^2)\delta^{(3)}(\mathbf{r}-\mathbf{r}')\mathbb{1}$. Its contribution therefore turns (2.23) exactly into (2.16) after properly handling the constants. Contribution of the infinitesimal semi-circle has been proven [22] to result in a tensor related to purely longitudinal electromagnetic field, which was then shown (using the projection into longitudinal waves) to vanish after performing the subsequent curl. We can then see that commutator of the form (2.22) ultimately leads to the satisfaction of (2.16) and hence an approach consistent with the quantization scheme in vacuum.

If we turn back to our specific simplification of local and isotropic dielectrics, expressed by (2.18), we see that a simple renormalization of the form

$$\hat{\mathbf{j}}_N(\mathbf{r},\,\omega) = \sqrt{\frac{\hbar\varepsilon_0}{\pi}\Im\{\varepsilon(\mathbf{r},\,\omega)\}}\,\omega\,\hat{\mathbf{f}}(\mathbf{r},\,\omega)$$

can be performed. The vector field operators $\hat{\mathbf{f}}(\mathbf{r},\,\omega)$ then satisfies the familiar commutators of a bosonic creation and annihilation operators

$$\left[\hat{\mathbf{f}}(\mathbf{r},\,\omega),\,\hat{\mathbf{f}}^\dagger(\mathbf{r}',\,\omega')\right] = \delta^{(3)}(\mathbf{r}-\mathbf{r}')\delta(\omega-\omega')\mathbb{1} \tag{2.24}$$

and the electric field can be calculated as

$$\hat{\mathbf{E}}(\mathbf{r},\,\omega) = i\sqrt{\frac{\hbar}{\pi\varepsilon_0}}\frac{\omega^2}{c^2}\int d^3\mathbf{r}'\,\sqrt{\Im\{\varepsilon(\mathbf{r}',\,\omega)\}}\,\boldsymbol{G}(\mathbf{r},\,\mathbf{r}',\,\omega)\cdot\hat{\mathbf{f}}(\mathbf{r}',\,\omega)\,. \tag{2.25}$$

In order to finalize the quantization procedure, we need to ensure that in the Heisenberg picture, operators $\hat{\mathbf{f}}$, $\hat{\mathbf{f}}^\dagger$ evolve in time with Fourier exponential factors $e^{-i\omega t}$ and $e^{i\omega t}$ respectively. Time evolution of any operator $\hat{O}$ is described through the equation $-i\hbar\,\partial_t\hat{O}(t) = \left[\hat{H},\hat{O}(t)\right]$ and we therefore need to prescribe a Hamiltonian satisfying

$$\begin{aligned}\left[\hat{H},\,\hat{\mathbf{f}}(\mathbf{r},\,\omega)\right] &= -\hbar\omega\,\hat{\mathbf{f}}(\mathbf{r},\,\omega)\,,\\ \left[\hat{H},\,\hat{\mathbf{f}}^\dagger(\mathbf{r},\,\omega)\right] &= \hbar\omega\,\hat{\mathbf{f}}^\dagger(\mathbf{r},\,\omega)\,.\end{aligned}$$

These constraints, together with (2.24), show that we are looking for a quadratic Hamiltonian and an intuitive choice would be

$$\hat{H} = \int_0^\infty d\omega\,\hbar\omega\int d^3\mathbf{r}\,\hat{\mathbf{f}}^\dagger(\mathbf{r},\,\omega)\cdot\hat{\mathbf{f}}(\mathbf{r},\,\omega)\,. \tag{2.26}$$

We can verify that it is indeed the right Hamiltonian satisfying both constraints mentioned above and can be shown to be unique up to a constant [23].

The described procedure shows that the quantization of medium-assisted fields also leads to a set of creation and annihilation operators of a bosonic nature. The difference here is that $\hat{\mathbf{f}}$, $\hat{\mathbf{f}}^\dagger$ collectively excite not only the field, but also the dielectric matter (polaritons). Such an approach can then be used to describe light-matter interactions in macroscopic environments with the input being only an experimentally accessible linear-response function (permittivity or refractive index). We will now proceed, equipped with this formalism, to study the quantum nature of coherent CL.

2.3 Quantum statistics of CL photons

This section will be devoted to the theoretical study of statistical properties inherent to the quantum light, emitted as a consequence of an electron-sample interaction. We will first prescribe the initial state of our system consisting of the modulated electron and the medium-assisted EM field and solve its evolution by adapting a minimal coupling interaction Hamiltonian. The post-interaction state will be then utilized for the statistical description of emitted photons, leading towards a simple local quantity related to the coherence transfer mediated by the modulated electron beam.

2.3.1 Initial state of the system

We will assume that the approaching electron beam was prepared through a single-mode PINEM modulation, which was discussed in the beginning of this chapter. Such an electron is described by the mixed state density matrix (2.9). In the expression for individual states ψ_n, contained within the mixture, we can recognize the energies $E_l = E_0 + l\hbar\omega_0$ and first-order expansions of wavevectors $k_l \approx k_0 + l\omega_0/v$ resulting from a net exchange of l photons. Since we assume the PINEM region to be at large distance from the CL emitting sample, we need to apply at least a second order correction from the full relativistic wavevector expression

$$\hbar k_l = \sqrt{\frac{E_l^2}{c^2} - m_e^2 c^2} \approx \hbar k_0 + \frac{l\hbar\omega_0}{v} - \frac{2\pi\hbar l^2}{z_T},$$

which is the result of an expansion at $l\hbar\omega_0/E_0 \ll 1$ and $z_T = 4\pi m_e v^3\gamma^3/(\hbar\omega_0^2)$ is the Talbot distance [18]. To gain perspective, for $\beta = 0.6$ electrons (127.75 keV) and $\hbar\omega_0 = 2.5\,\mathrm{eV}$, one obtains $z_T \approx 86\,\mathrm{mm}$, which is a large distance with respect to the range of evanescent PINEM fields.

Furthermore, we assumed in the first section of this chapter that the incident electron's spatial profile could be divided into

$$\phi_{\mathrm{inc}}(\mathbf{r} - \mathbf{v}t) = \phi_\perp(\mathbf{R})\phi_\parallel(z - vt)$$

and that $\phi_\perp$ described a narrowly focused beam centered at $\mathbf{R}_0$, which remained unchanged[8] throughout the modulation. This assumption will allow us to treat

[8]The term "unchanged" does not imply that the electron beam remains focused on its own,

perpendicular degrees of freedom separately and consider the modulated electron wavefunctions

$$\langle \mathbf{r}|\psi_n(t)\rangle = \langle \mathbf{R}|\phi_\perp\rangle\langle z|\tilde{\psi}_n(t)\rangle = \phi_\perp(\mathbf{R})\phi_\parallel(z-vt)\sum_{l=-\infty}^{\infty} f_l^n e^{i(k_l z - E_l t/\hbar)}\,.$$

In order to better manipulate with $|\tilde{\psi}_n(t)\rangle$ states, we will expand them in terms of plane waves as

$$\begin{aligned}|\tilde{\psi}_n(t)\rangle = \sum_k \langle k|\tilde{\psi}_n(t)\rangle|k\rangle = \frac{1}{\sqrt{L}}\sum_k\sum_{l=-\infty}^{\infty} f_l^n e^{-iE_l t/\hbar}\int dz\,\phi_\parallel(z-vt)e^{i(k_l-k)z}|k\rangle = \\ \frac{1}{\sqrt{L}}\sum_k\sum_{l=-\infty}^{\infty} f_l^n e^{-iE_l t/\hbar}e^{i(k_l-k)vt}\int dz'\,\phi_\parallel(z')e^{i(k_l-k)z'}|k\rangle \approx \\ \sum_{l=-\infty}^{\infty} f_l^n e^{-2\pi i l^2 vt/z_T - iE_l t/\hbar}|k_0 + l\omega_0/v\rangle\,,\end{aligned}$$

where the transition from the first to the second line is through a simple substitution $z' = z - vt$. However, the subsequent approximation involved disregarding the shape of longitudinal electron beam envelope by assuming $\phi_\parallel(z') = 1/\sqrt{L}$ as well as considering the interaction regions (in case of both PINEM and CL) to be smaller than the Talbot distance ($z' \ll z_T$). When substituting for the expansion of k_l, we can therefore use only the first-order within the integral.

In order to obtain an initial density operator for the description of an electron-sample interaction resulting in CL, we need to identify

$$\hat{\rho}_e(t_{\mathrm{CL}} \to -\infty) \equiv \hat{\rho}_e(t_{\mathrm{PINEM}} \to \infty)\,,$$

which means that we need to connect the future asymptotics of the PINEM modulation to the past asymptotics of the CL interaction. This can be done by replacing vt in the above expression for $|\tilde{\psi}_n(t)\rangle$ by d, the distance travelled from the PINEM region in the limit $t \to \infty$, therefore the approximate distance between the PINEM and CL samples. The initial state of our system, which consists of a modulated electron and a medium-assited electromagnetic field can be then described by a density operator

$$\begin{aligned}&\hat{\rho}_{e-f}^{\mathrm{inc}} \equiv \hat{\rho}_{e-f}(t\to-\infty) = \hat{\rho}_\perp \otimes \left[\hat{\rho}_\parallel \otimes \hat{\rho}_f\right]^{\mathrm{inc}}\,,\\ &\hat{\rho}_\perp = |\phi_\perp\rangle\langle\phi_\perp|\,,\quad \left[\hat{\rho}_\parallel \otimes \hat{\rho}_f\right]^{\mathrm{inc}} = \sum_{n=0}^{\infty}|\tilde{\psi}_n,0\rangle\langle\tilde{\psi}_n,0|\,,\\ &|\tilde{\psi}_n,0\rangle = \left(\sum_{l=-\infty}^{\infty} f_l^n e^{-2\pi i l^2 d/z_T - i\varphi_l}|k_0 + l\omega_0/v\rangle\right)\otimes|0\rangle_f\,,\end{aligned} \tag{2.27}$$

with $|0\rangle_f$ denoting the electromagnetic vacuum and $\varphi_l \equiv \lim_{t\to-\infty} E_l t/\hbar$ denoting a phase factor that will vanish when we transition to the interaction picture (see below). We can also verify that from the relation[9] $\sum_{n,l}|f_l^n|^2 = 1$, it can be seen that indeed $\mathrm{Tr}\,\hat{\rho}_\parallel = 1$, which is satisfied automatically for perpendicular electron degrees of freedom ($\hat{\rho}_\perp$) and also for the initial electromagnetic vacuum.

but we want to emphasize the fact that current experimental setups allow for refocusing in the perpendicular direction, while maintaining the longitudinal profile.

[9]This stems from the normalization of PINEM modulated electron states. A more detailed commentary can be found in [18].

2.3.2 S-operator derivation

To describe the evolution of (2.27), we need to formulate the Hamiltonian of our system. We have already commented upon the derivation of a free-electron Hamiltonian encompassing relativistic kinematics in the first section of this chapter. In the formalism of second quantization, we can rewrite the same expression as (see (2.5))

$$\hat{H}_0^{(e)} = \sum_{\mathbf{k}} \left[E_0 + \hbar \mathbf{v} \cdot (\mathbf{k} - \mathbf{k}_0)\right] \hat{c}_{\mathbf{k}}^{\dagger} \hat{c}_{\mathbf{k}} \,, \tag{2.28}$$

with $\hat{c}_{\mathbf{k}}^{\dagger}$, $\hat{c}_{\mathbf{k}}$ denoting fermionic creation and annihilation operators, respectively. The quantization of medium-assisted electromagnetic field was covered in the previous section and we therefore already know that the non-interacting EM field Hamiltonian $\hat{H}_0^{(f)}$ is given by (2.26).

The electron-field interaction Hamiltonian can be directly written through minimal coupling approach as [24]

$$\hat{H}_I = -\int d^3\mathbf{r}\, \hat{\mathbf{j}}(\mathbf{r}) \cdot \hat{\mathbf{A}}(\mathbf{r}) \,, \tag{2.29}$$

where $\hat{\mathbf{j}}(\mathbf{r})$ denotes the current density operator associated with an electron and $\hat{\mathbf{A}}(\mathbf{r})$ is the vector potential operator. In a gauge with zero scalar potential, we can immediately write $\hat{\mathbf{A}}(\mathbf{r})$ as

$$\begin{aligned} \hat{\mathbf{A}}(\mathbf{r}) &= \int_0^{\infty} d\omega\, \hat{\mathbf{A}}(\mathbf{r}, \omega) + \text{H.c.} \,, \\ \hat{\mathbf{A}}(\mathbf{r}, \omega) &= \sqrt{\frac{\hbar}{\pi\varepsilon_0}} \frac{\omega}{c^2} \int d^3\mathbf{r}' \sqrt{\Im\{\varepsilon(\mathbf{r}', \omega)\}}\, \boldsymbol{G}(\mathbf{r}, \mathbf{r}', \omega) \cdot \hat{\mathbf{f}}(\mathbf{r}', \omega) \,, \end{aligned} \tag{2.30}$$

which is a consequence of (2.20) and (2.25). The current density operator in non-recoil approximation can be determined as $\hat{\mathbf{j}}(\mathbf{r}) = -e\mathbf{v}\hat{\Psi}^{\dagger}(\mathbf{r})\hat{\Psi}(\mathbf{r})$, where $\hat{\Psi}^{\dagger}$, $\hat{\Psi}$ are electron field operators, which correspond to the coordinate representation of $\hat{c}_{\mathbf{k}}^{\dagger}$, $\hat{c}_{\mathbf{k}}$ and can therefore be written as $\hat{\Psi}(\mathbf{r}) = \sum_{\mathbf{k}} L^{-3/2} \exp(i\mathbf{k} \cdot \mathbf{r}) \hat{c}_{\mathbf{k}}$. We can then prescribe the current density operator as

$$\hat{\mathbf{j}}(\mathbf{r}) = -\frac{e\mathbf{v}}{L^3} \sum_{\mathbf{k},\,\mathbf{q}} e^{i\mathbf{q}\cdot\mathbf{r}}\, \hat{c}_{\mathbf{k}}^{\dagger} \hat{c}_{\mathbf{k}+\mathbf{q}} \,. \tag{2.31}$$

Time evolution of the proposed system turns out to be analytically solvable within the interaction picture, where states and operators satisfy

$$\begin{aligned} |\Psi^{(I)}(t)\rangle &= e^{i\hat{H}_0^{(S)} t/\hbar} |\Psi^{(S)}(t)\rangle \,, \\ \hat{A}^{(I)}(t) &= e^{i\hat{H}_0^{(S)} t/\hbar} \hat{A}^{(S)} e^{-i\hat{H}_0^{(S)} t/\hbar} \,, \end{aligned}$$

with superscripts S and I emphasizing the Schrödinger and interaction pictures[10], respectively. Time evolution in the interaction picture is then determined through the S-operator, which can be compactly written as

$$\hat{S}(t_f, t_i) = T \exp\left[-\frac{i}{\hbar} \int_{t_i}^{t_f} dt'\, \hat{H}_I(t')\right] \,, \tag{2.32}$$

[10]We will not need to distinguish between them by using indices, since in our case both non-interacting Hamiltonian and also $\hat{H}_I$ are time-independent, so $\hat{H}_I(t)$ will always imply interaction picture.

where T denotes time-ordering of the terms within the exponential Taylor series. Before we address the derivation of $\hat{H}_I(t)$, we should note that transition of the initial density operator (2.27) from Schrödinger to interaction picture only erases the phases φ_l, because it holds that

$$\hat{H}_0^{(e)}|\mathbf{k}_\perp, k_0 + l\omega_0/v\rangle = E_l|\mathbf{k}_\perp, k_0 + l\omega_0/v\rangle\,.$$

The calculation of interaction picture Hamiltonian $\hat{H}_I(t)$ requires us to evaluate

$$\hat{H}_I(t) = -\int d^3\mathbf{r}\,\left(e^{i\hat{H}_0 t/\hbar}\hat{\mathbf{j}}(\mathbf{r})e^{-i\hat{H}_0 t/\hbar}\right)\cdot\left(e^{i\hat{H}_0 t/\hbar}\hat{\mathbf{A}}(\mathbf{r})e^{-i\hat{H}_0 t/\hbar}\right)\,.$$

Obtaining $\hat{\mathbf{A}}(\mathbf{r},t)$ is very straightforward, because the non-interacting field Hamiltonian (the only part of $\hat{H}_0$, which does not commute with $\hat{\mathbf{A}}$) was constructed to ensure $\left[\hat{H}_0^{(f)}, \hat{\mathbf{f}}(\mathbf{r},\omega)\right] = -\hbar\omega\hat{\mathbf{f}}(\mathbf{r},\omega)$ and both $\hat{\mathbf{A}}(\mathbf{r},\,\omega)$ and its Hermitian conjugate are linear in $\hat{\mathbf{f}}$, $\hat{\mathbf{f}}^\dagger$, respectively. We can therefore conclude that

$$\hat{\mathbf{A}}(\mathbf{r},t) = \int_0^\infty d\omega\,\hat{\mathbf{A}}(\mathbf{r},\,\omega)e^{-i\omega t} + \text{H.c.} \tag{2.33}$$

In order to determine $\hat{\mathbf{j}}(\mathbf{r},t)$, we first need to recall the anticommutative relations satisfied by fermionic creation and annihilation operators

$$\{\hat{c}_\mathbf{k},\,\hat{c}_{\mathbf{k}'}\} = \left\{\hat{c}_\mathbf{k}^\dagger,\,\hat{c}_{\mathbf{k}'}^\dagger\right\} = 0\,,\quad \left\{\hat{c}_\mathbf{k},\,\hat{c}_{\mathbf{k}'}^\dagger\right\} = \delta_{\mathbf{k},\mathbf{k}'}\,,$$

where $\left\{\hat{A},\hat{B}\right\} = \hat{A}\hat{B}+\hat{B}\hat{A}$. These anticommutators can then be used to calculate the following commutative relation

$$\left[\hat{c}_{\mathbf{k}'}^\dagger\hat{c}_{\mathbf{k}'}, \hat{c}_\mathbf{k}^\dagger\hat{c}_{\mathbf{k}+\mathbf{q}}\right] = \hat{c}_\mathbf{k}^\dagger\hat{c}_{\mathbf{k}+\mathbf{q}}(\delta_{\mathbf{k},\mathbf{k}'} - \delta_{\mathbf{k}+\mathbf{q},\mathbf{k}'})\,,$$

which then gives us

$$\begin{aligned}\left[\hat{H}_0^{(e)},\,\hat{\mathbf{j}}(\mathbf{r})\right] &= -\frac{e\mathbf{V}}{L^3}\sum_{\mathbf{k}',\mathbf{k},\mathbf{q}} e^{i\mathbf{q}\cdot\mathbf{r}}\left(E_0 + \hbar\mathbf{v}\cdot(\mathbf{k}'-\mathbf{k}_0)\right)\left[\hat{c}_{\mathbf{k}'}^\dagger\hat{c}_{\mathbf{k}'}, \hat{c}_\mathbf{k}^\dagger\hat{c}_{\mathbf{k}+\mathbf{q}}\right]\\ &= -\frac{e\mathbf{V}}{L^3}\sum_{\mathbf{k},\,\mathbf{q}}(-\hbar\mathbf{v}\cdot\mathbf{q})e^{i\mathbf{q}\cdot\mathbf{r}}\,\hat{c}_\mathbf{k}^\dagger\hat{c}_{\mathbf{k}+\mathbf{q}}\,.\end{aligned}$$

The commutator with $\hat{H}_0^{(e)}$ therefore does not affect the operator structure within $\hat{\mathbf{j}}(\mathbf{r})$, but it just introduces a factor of $(-\hbar\mathbf{v}\cdot\mathbf{q})$. This allows us to conclude that

$$\hat{\mathbf{j}}(\mathbf{r},t) = -\frac{e\mathbf{V}}{L^3}\sum_{\mathbf{k},\,\mathbf{q}} e^{i\mathbf{q}\cdot(\mathbf{r}-\mathbf{v}t)}\,\hat{c}_\mathbf{k}^\dagger\hat{c}_{\mathbf{k}+\mathbf{q}}\,. \tag{2.34}$$

Now that we have $\hat{H}_I(t)$, it can be used to determine the S-operator (2.32). We will utilize a technique from [24] and discretize the time interval $\langle t_i,\,t_f\rangle$ into N segments with lengths $\Delta t = (t_f - t_i)/N$. If we denote the midpoint of each segment as $t_k = t_i + (k-1/2)\Delta t$, where $k \in \{1,\dots N\}$, we can directly apply time-ordering and rewrite

$$T\exp\left[-\frac{i}{\hbar}\int_{t_i}^{t_f} dt'\,\hat{H}_I(t')\right] = \lim_{N\to\infty} e^{-i\Delta t\hat{H}_I(t_N)}e^{-i\Delta t\hat{H}_I(t_{N-1})}\dots e^{-i\Delta t\hat{H}_I(t_1)}\,. \tag{2.35}$$

This particular approach works very well if $\left[\hat{H}_I(t), \hat{H}_I(t')\right]$ is just a time dependent multiple of $\hat{\mathbb{1}}$, which turns out to be true in our problem. It can be shown that $\left[\hat{\mathbf{j}}(\mathbf{r},t), \hat{\mathbf{j}}(\mathbf{r}',t')\right] = 0$, because

$$\frac{e^2 \mathbf{v}\otimes\mathbf{v}}{L^6} \sum_{\mathbf{k},\mathbf{q};\mathbf{k}',\mathbf{q}'} e^{i\mathbf{q}\cdot(\mathbf{r}-\mathbf{v}t)} e^{i\mathbf{q}'\cdot(\mathbf{r}'-\mathbf{v}t')} \left[\hat{c}^\dagger_{\mathbf{k}}\hat{c}_{\mathbf{k}+\mathbf{q}}, \hat{c}^\dagger_{\mathbf{k}'}\hat{c}_{\mathbf{k}'+\mathbf{q}'}\right] =$$
$$\frac{e^2 \mathbf{v}\otimes\mathbf{v}}{L^6} \sum_{\mathbf{k},\mathbf{q};\mathbf{k}',\mathbf{q}'} e^{i\mathbf{q}\cdot(\mathbf{r}-\mathbf{v}t)} e^{i\mathbf{q}'\cdot(\mathbf{r}'-\mathbf{v}t')} \left(\hat{c}^\dagger_{\mathbf{k}}\hat{c}_{\mathbf{k}'+\mathbf{q}'}\delta_{\mathbf{k}',\,\mathbf{k}+\mathbf{q}} - \hat{c}^\dagger_{\mathbf{k}'}\hat{c}_{\mathbf{k}+\mathbf{q}}\delta_{\mathbf{k},\,\mathbf{k}'+\mathbf{q}'}\right)$$

and after canceling one of the sums in each term, we can see the subtraction of two identical expressions (just by renaming $\mathbf{k} \leftrightarrow \mathbf{k}'$ in one of them). By recalling the expression (2.30) for $\hat{\mathbf{A}}(\mathbf{r},\,\omega)$, the integral identity (2.21) satisfied by electromagnetic Green tensor and the relation (2.18) held for considered media, we can derive

$$\left[\hat{\mathbf{A}}(\mathbf{r},t), \hat{\mathbf{A}}(\mathbf{r}',t')\right] = \int_0^\infty d\omega e^{-i\omega t} \int_0^\infty d\omega' e^{i\omega' t'} \left[\hat{\mathbf{A}}(\mathbf{r},\omega), \hat{\mathbf{A}}^\dagger(\mathbf{r}',\omega')\right] - \text{H.c.} =$$
$$\frac{2i\hbar}{\pi\varepsilon_0 c^2} \int_0^\infty d\omega \sin\left[\omega(t'-t)\right] \Im\{\boldsymbol{G}(\mathbf{r},\mathbf{r}',\omega)\}\,. \tag{2.36}$$

The very important consequence of this is that the commutator

$$\left[\hat{H}_I(t), \hat{H}_I(t')\right] =$$
$$\frac{2i\hbar}{\pi\varepsilon_0 c^2} \int d^3\mathbf{r} \int d^3\mathbf{r}' \int_0^\infty d\omega \sin\left[\omega(t'-t)\right] \hat{\mathbf{j}}(\mathbf{r},t) \cdot \Im\{\boldsymbol{G}(\mathbf{r},\mathbf{r}',\omega)\} \cdot \hat{\mathbf{j}}(\mathbf{r}',t') \tag{2.37}$$

acts only upon the electron degrees of freedom and even more crucially, since $\left[\hat{\mathbf{j}}(\mathbf{r},t), \hat{\mathbf{j}}(\mathbf{r}',t')\right] = 0$, it is indeed true that

$$\left[\hat{H}_I(t), \left[\hat{H}_I(t'), \hat{H}_I(t'')\right]\right] = 0\,. \tag{2.38}$$

We can now return to (2.35), because due to (2.38), it can[11] be rewritten as

$$\lim_{N\to\infty} \exp\left\{-\frac{i\Delta t}{\hbar}\sum_{j=1}^{N} \hat{H}_I(t_j) - \frac{\Delta t^2}{2\hbar^2} \sum_{1\le k<l\le N} \left[\hat{H}_I(t_l), \hat{H}_I(t_k)\right]\right\} =$$
$$\exp\left\{-\frac{i}{\hbar}\int_{t_i}^{t_f} dt \hat{H}_I(t) - \frac{1}{2\hbar^2}\int_{t_i}^{t_f} dt_1 \int_{t_i}^{t_f} dt_2 \Theta(t_1-t_2)\left[\hat{H}_I(t_1), \hat{H}_I(t_2)\right]\right\},$$

where we returned back to integration and applied time-ordering of the second term via the Heaviside theta function. Since our primary interest are going to be the statistical properties of field quantities after the electron leaves the interaction region, we will extend $t_i \to -\infty$ and $t_f \to \infty$ and write the S-operator in the following form

$$\begin{aligned}
\hat{S}(\infty,-\infty) &= e^{i\hat{\varphi}(\infty,-\infty)}\hat{U}(\infty,-\infty)\,,\\
\hat{U}(\infty,-\infty) &= \exp\left\{-\frac{i}{\hbar}\int_{-\infty}^{\infty} dt \hat{H}_I(t)\right\}\,,\\
\hat{\varphi}(\infty,-\infty) &= \frac{i}{2\hbar^2}\int_{-\infty}^{\infty} dt_1 \int_{-\infty}^{\infty} dt_2 \Theta(t_1-t_2)\left[\hat{H}_I(t_1), \hat{H}_I(t_2)\right]\,.
\end{aligned} \tag{2.39}$$

[11] Here, we utilized the BCH formula $\exp\left(\hat{X}\right)\exp\left(\hat{Y}\right) = \exp\left(\hat{X}+\hat{Y}+\left[\hat{X},\hat{Y}\right]/2\right)$, which is valid if $\left[\hat{X},\left[\hat{X},\hat{Y}\right]\right] = \left[\hat{Y},\left[\hat{X},\hat{Y}\right]\right] = 0$.

The exact expression for $\hat{\varphi}$ will not be necessary and it will suffice to realize its hermiticity[12] and the fact that it commutes with any operator describing a quantity related only to the electromagnetic field. The post-interaction expectation value of any such operator $\hat{F}$ can then be calculated as

$$\begin{aligned}\langle\hat{F}\rangle = \mathrm{Tr}\left(\hat{\rho}_{e-f}(\infty)\hat{F}\right) = \mathrm{Tr}\left(\hat{S}(\infty,-\infty)\hat{\rho}_{e-f}(-\infty)\hat{S}^{\dagger}(\infty,-\infty)\hat{F}\right) = \\ \mathrm{Tr}\left(\hat{\rho}_{e-f}(-\infty)\hat{U}^{\dagger}(\infty,-\infty)\hat{F}\hat{U}(\infty,-\infty)\right),\end{aligned} \tag{2.40}$$

where we also utilized the invariance of trace under circular shifts of the operators within it.

The derivation of $\hat{U}(\infty,-\infty)$ will be done in a way that takes into account the particular properties of (2.27), namely the electron motion with constant $\mathbf{v} = v\mathbf{e}_z$ and the separability of parallel and perpendicular degrees of freedom, with the latter being represented by a narrowly focused wavefunction $\phi_{\perp}(\mathbf{R})$. This justifies the separation of operators $\hat{c}_{\mathbf{k}} \approx \hat{c}_{\mathbf{k}_{\perp}}\hat{c}_{k_z}$ and the expansion $|\phi_{\perp}\rangle = \sum_{\mathbf{k}_{\perp}} \alpha_{\mathbf{k}_{\perp}}|\mathbf{k}_{\perp}\rangle$. We can then simplify the integral

$$\int_{-\infty}^{\infty} dt\hat{H}_I(t) = \int_{-\infty}^{\infty} dt \int d^3\mathbf{r} \int_0^{\infty} d\omega \sum_{\mathbf{k},\mathbf{q}} \frac{ev}{L^3} e^{i\mathbf{q}\cdot(\mathbf{r}-\mathbf{v}t)}\hat{c}^{\dagger}_{\mathbf{k}}\hat{c}_{\mathbf{k}+\mathbf{q}}\hat{A}_z(\mathbf{r},\omega)e^{-i\omega t} + \text{H.c.} =$$

$$\int_0^{\infty} d\omega \int d^3\mathbf{r} e^{-i\omega z/v}\hat{A}_z(\mathbf{r},\omega)\left(\sum_{\mathbf{k}_{\perp},\mathbf{q}_{\perp}} \frac{e}{L^2} e^{i\mathbf{q}_{\perp}\cdot\mathbf{R}}\hat{c}^{\dagger}_{\mathbf{k}_{\perp}}\hat{c}_{\mathbf{k}_{\perp}+\mathbf{q}_{\perp}}\right)\left(\sum_{k_z}\hat{c}^{\dagger}_{k_z}\hat{c}_{k_z-\frac{\omega}{v}}\right) + \text{H.c.} =$$

$$\int_0^{\infty} d\omega\, \hat{b}^{\dagger}(\omega)\int d^3\mathbf{r} e^{-i\omega z/v}\hat{A}_z(\mathbf{r},\omega)\hat{j}_{\perp}(\mathbf{R}) + \text{H.c.}\,,$$

where the transition from the first to the second line was done by separating $\hat{c}_{\mathbf{k}}$ and carrying out the time integration resulting in $L/v\,\delta_{q_z,-\omega/v}$. We then also denoted

$$\hat{b}^{\dagger}(\omega) = \sum_{k_z}\hat{c}^{\dagger}_{k_z}\hat{c}_{k_z-\frac{\omega}{v}}\,, \quad \hat{j}_{\perp}(\mathbf{R}) = \sum_{\mathbf{k}_{\perp},\mathbf{q}_{\perp}} \frac{e}{L^2} e^{i\mathbf{q}_{\perp}\cdot\mathbf{R}}\hat{c}^{\dagger}_{\mathbf{k}_{\perp}}\hat{c}_{\mathbf{k}_{\perp}+\mathbf{q}_{\perp}}\,. \tag{2.41}$$

An effective way to deal with the acting of $\hat{j}_{\perp}(\mathbf{R})$ is to approximate it with its average over the perpendicular degrees of freedom and subsequently omit them from the density operator. We can therefore calculate

$$\langle\phi_{\perp}|\hat{j}_{\perp}(\mathbf{R})|\phi_{\perp}\rangle = \sum_{\mathbf{k}_{\perp},\mathbf{q}_{\perp}} \frac{e}{L^2} e^{i\mathbf{q}_{\perp}\cdot\mathbf{R}}\alpha^*_{\mathbf{k}_{\perp}}\alpha_{\mathbf{k}_{\perp}+\mathbf{q}_{\perp}} =$$

$$\sum_{\mathbf{k}_{\perp},\mathbf{q}_{\perp}} \frac{e}{L^2} e^{i\mathbf{q}_{\perp}\cdot\mathbf{R}}\int d^2\boldsymbol{\lambda}_1 \int d^2\boldsymbol{\lambda}_2 \frac{1}{L^2}\phi^*_{\perp}(\boldsymbol{\lambda}_1)\phi_{\perp}(\boldsymbol{\lambda}_2)e^{i\mathbf{k}_{\perp}\cdot\boldsymbol{\lambda}_1}e^{-i(\mathbf{k}_{\perp}+\mathbf{q}_{\perp})\cdot\boldsymbol{\lambda}_2} =$$

$$e\int d^2\boldsymbol{\lambda}_1 \int d^2\boldsymbol{\lambda}_2\phi^*_{\perp}(\boldsymbol{\lambda}_1)\phi_{\perp}(\boldsymbol{\lambda}_2)\langle\boldsymbol{\lambda}_1|\left(\sum_{\mathbf{k}_{\perp}}|\mathbf{k}_{\perp}\rangle\langle\mathbf{k}_{\perp}|\right)|\boldsymbol{\lambda}_2\rangle\langle\mathbf{R}|\left(\sum_{\mathbf{q}_{\perp}}|\mathbf{q}_{\perp}\rangle\langle\mathbf{q}_{\perp}|\right)|\boldsymbol{\lambda}_2\rangle =$$

$$e\int d^2\boldsymbol{\lambda}_1 \int d^2\boldsymbol{\lambda}_2\phi^*_{\perp}(\boldsymbol{\lambda}_1)\phi_{\perp}(\boldsymbol{\lambda}_2)\delta^{(2)}(\boldsymbol{\lambda}_1-\boldsymbol{\lambda}_2)\delta^{(2)}(\mathbf{R}-\boldsymbol{\lambda}_2) = e|\phi_{\perp}(\mathbf{R})|^2\,,$$

where we only utilized the completeness of perpendicular wavevector and perpendicual coordinate bases. By further defining

$$\hat{\mathcal{A}}\,(\omega) = \frac{-ie}{\hbar}\int d^3\mathbf{r}|\phi_{\perp}(\mathbf{R})|^2 e^{-i\frac{\omega z}{v}}\hat{A}_z(\mathbf{r},\omega)\,, \tag{2.42}$$

[12]Which is a direct consequence of the fact that the commutator of two Hemitian operators is anti-Hermitian and we then multiply it by i.

we can rewrite

$$-\frac{i}{\hbar}\int_{-\infty}^{\infty} dt\hat{H}_I(t) = \int_0^{\infty} d\omega \left[\hat{b}^\dagger(\omega)\hat{\mathcal{A}}\,(\omega) - \hat{b}(\omega)\hat{\mathcal{A}}^{\,\dagger}(\omega)\right] .$$

The algebraic properties of $\hat{b}$, $\hat{\mathcal{A}}$ can be derived by the same methods that were used to determine $\left[\hat{\mathbf{j}}(\mathbf{r},t),\hat{\mathbf{j}}(\mathbf{r}',t')\right] = 0$ and (2.36), the results of which are

$$\begin{aligned}
&\left[\hat{b}(\omega),\hat{b}(\omega')\right] = \left[\hat{b}^\dagger(\omega),\hat{b}^\dagger(\omega')\right] = \left[\hat{b}(\omega),\hat{b}^\dagger(\omega')\right] = 0\,,\\
&\left[\hat{\mathcal{A}}\,(\omega),\hat{\mathcal{A}}\,(\omega')\right] = \left[\hat{\mathcal{A}}^{\,\dagger}(\omega),\hat{\mathcal{A}}^{\,\dagger}(\omega')\right] = 0\,,\\
&\left[\hat{\mathcal{A}}\,(\omega),\hat{\mathcal{A}}^{\,\dagger}(\omega')\right] = \delta(\omega-\omega')\frac{4\alpha}{c}\int d^2\mathbf{R}\int d^2\mathbf{R}'|\phi_\perp(\mathbf{R})|^2|\phi_\perp(\mathbf{R}')|^2\\
&\qquad\qquad \int dz\int dz'\Im\left\{G_{zz}(\mathbf{R},z,\mathbf{R}',z',\omega)\right\}\cos\left[\frac{\omega}{v}(z-z')\right] .
\end{aligned} \tag{2.43}$$

The only non-zero commutator is very familiar and by comparing it with (1.37), we can realize its connection to the semi-classical EELS probability. The usual procedure at this point involves the assumption $|\phi_\perp(\mathbf{R})|^2 \approx \delta^{(2)}(\mathbf{R}-\mathbf{R}_0)$, which reduces the commutator exactly to $\Gamma_{\mathrm{EELS}}(\mathbf{R}_0,\omega)$. However, we wish to incorporate at least the first-order correction stemming from a finite width of $|\phi_\perp(\mathbf{R})|^2$, which can be achieved by assuming a non-zero contribution only at $\mathbf{R}=\mathbf{R}'$ and therefore $|\phi_\perp(\mathbf{R})|^2|\phi_\perp(\mathbf{R}')|^2 \approx |\phi_\perp(\mathbf{R})|^2\delta^{(2)}(\mathbf{R}-\mathbf{R}')$, which is valid only for very narrow distributions and subsequently yields exactly the averaged semi-classical probability (1.38). If we then define the square-root of this probability $\gamma(\omega) \equiv \sqrt{\Gamma_{\mathrm{EELS}}(\omega)}$, we can renormalize $\hat{a}(\omega) = \hat{\mathcal{A}}\,(\omega)/\gamma(\omega)$, which then leads to the bosonic commutator

$$\left[\hat{a}(\omega),\hat{a}^\dagger(\omega)\right] = \delta(\omega-\omega')\,. \tag{2.44}$$

The final result for $\hat{U}(\infty,-\infty)$ is then

$$\hat{U}(\infty,-\infty) = \exp\left(\int_0^{\infty} d\omega\,\gamma(\omega)\left[\hat{b}^\dagger(\omega)\hat{a}(\omega) - \hat{b}(\omega)\hat{a}^\dagger(\omega)\right]\right) . \tag{2.45}$$

This result has a very clear interpretation. Operators $\hat{a}(\omega)$, $\hat{a}^\dagger(\omega)$ annihilate and create scalar (unlike $\hat{\mathbf{f}}$, $\hat{\mathbf{f}}^\dagger$) bosonic excitations within the medium-assisted EM field and they are paired with operators $\hat{b}^\dagger(\omega)$ and $\hat{b}(\omega)$, respectively. By looking at (2.41), we can see that $\hat{b}^\dagger(\omega)$ increases the electron's longitudinal momentum by $\hbar\omega/v$ and its Hermitian conjugate does the opposite. Operator (2.45) then includes annihilation of an excitation followed by an increase in the electron's momentum and the inverse process as well. The coupling strength between $\hat{b}^\dagger(\omega)$, $\hat{a}(\omega)$ is then represented through $\sqrt{\Gamma_{\mathrm{EELS}}(\omega)}$, which we semi-classically determined to be the probability amplitude of an electron exchanging a photon with the sample.

2.3.3 Photon statistics

Now that we are equipped with all the tools required for evaluating averages (2.40), we will determine some of the fundamental properties of the EM field

after interaction. In the interest of clarity, we will further abbreviate the following notation

$$\hat{\rho} \equiv \hat{\rho}_{e-f}(-\infty)\,, \quad \hat{U} \equiv \hat{U}(\infty, -\infty)\,.$$

The results derived in this subsection will be then visualized for specific physical parameters in the following subsection.

The simplest quantity of interest is the mean number of photons at a given frequency present in the field after the interaction has taken place. We therefore want to calculate

$$n(\omega) = \langle \hat{a}^\dagger(\omega)\hat{a}(\omega)\rangle = \mathrm{Tr}\left[\hat{\rho}\,\hat{U}^\dagger\hat{a}^\dagger(\omega)\hat{U}\hat{U}^\dagger\hat{a}(\omega)\hat{U}\right]\,, \tag{2.46}$$

where the insertion of $\hat{\mathbb{1}} \equiv \hat{U}\hat{U}^\dagger$ between the field operators simplifies the subsequent calculation. It is of great importance to recall the BCH-formula in the form

$$e^{\hat{X}}\hat{Y}e^{-\hat{X}} = \hat{Y} + \left[\hat{X}, \hat{Y}\right]\,, \tag{2.47}$$

which is valid if $\left[\hat{X}, \left[\hat{X}, \hat{Y}\right]\right] = \left[\hat{Y}, \left[\hat{X}, \hat{Y}\right]\right] = 0$. By remembering the zero commutators held by $\hat{b}$, $\hat{b}^\dagger$ (see (2.43)) and evaluating

$$\int_0^\infty d\omega'\gamma(\omega')\left[\hat{b}(\omega')\hat{a}^\dagger(\omega') - \hat{b}^\dagger(\omega')\hat{a}(\omega'), \hat{a}(\omega)\right] = -\gamma(\omega)\hat{b}(\omega)\,,$$

where we only made use of (2.44), we can see that the conditions needed for (2.47) are indeed satisfied. We are then able to simplify

$$n(\omega) = \mathrm{Tr}\left[\left(\hat{a}(\omega) - \gamma(\omega)\hat{b}(\omega)\right)\hat{\rho}\left(\hat{a}^\dagger(\omega) - \gamma(\omega)\hat{b}^\dagger(\omega)\right)\right]\,.$$

Operators $\hat{a}$, $\hat{a}^\dagger$ ultimately vanish from this expression, since $\hat{\rho}$ contains only the initial electromagnetic vacuum apart from the electron's longitudinal degrees of freedom. Furthermore, the action of $\hat{b}^\dagger(\omega)\hat{b}(\omega)$ on any single electron z-component wavevector basis state $|q_z\rangle$ retains it, because

$$\hat{b}^\dagger(\omega)\hat{b}(\omega)|q_z\rangle = \sum_{k_z,k_z'}\hat{c}^\dagger_{k_z}\left(\delta_{k_z,k_z'} - \hat{c}^\dagger_{k_z'-\omega/v}\hat{c}_{k_z-\omega/v}\right)\hat{c}_{k_z'}|q_z\rangle = \sum_{k_z}\hat{c}^\dagger_{k_z}\hat{c}_{k_z}|q_z\rangle = |q_z\rangle\,.$$

We may therefore conclude the important result

$$n(\omega) = \gamma^2(\omega)\,\mathrm{Tr}\,\hat{\rho} = \gamma^2(\omega) = \Gamma_{\mathrm{EELS}}(\omega)\,. \tag{2.48}$$

Equation (2.48) implies that the post-interaction average number of specific frequency photons contained within the field is completely unaffected by the given mixture of states present within $\hat{\rho}$ and moreover, it is expressed by the semi-classically determined EELS probability. The total number of photons can be then calculated by integrating over all frequencies. We can also further derive the variance

$$\sigma_n^2(\omega) = \left\langle\left(\hat{a}^\dagger(\omega)\hat{a}(\omega)\right)^2\right\rangle - n^2(\omega) = \left[\gamma^4(\omega) + \gamma^2(\omega)\right] - \gamma^4(\omega) = \Gamma_{\mathrm{EELS}}(\omega)\,, \tag{2.49}$$

where the result $\left\langle\left(\hat{a}^\dagger(\omega)\hat{a}(\omega)\right)^2\right\rangle = \gamma^4(\omega) + \gamma^2(\omega)$ was obtained by the same techniques leading to (2.48).

Having estabilished the post-interaction number of photons, we shall now turn to the analysis of their coherence properties. First, we will remark that any averages of time-dependent field quantities $\langle \hat{F}(t) \rangle$ are going to be evaluated at large t with respect to the time scale of electron-sample interaction, which therefore permits the approximation $\hat{S}(t, -\infty) \approx \hat{S}(\infty, -\infty)$ within the trace. For the purpose of subsequent calculations, we also adapt the specific notation

$$\begin{aligned} \hat{\rho} &= \sum_{l,l'} \rho_{ll'} |k_l, 0\rangle\langle k_{l'}, 0| \,, \quad \text{with} \\ \rho_{ll'} &\equiv \sum_{n=0}^{\infty} f_l^n (f_{l'}^n)^* \exp\left[2\pi i (l'^2 - l^2) \frac{d}{z_T}\right] \,, \; |k_l, 0\rangle \equiv |k_0 + l\omega_0/v\rangle \otimes |0\rangle_f \,. \end{aligned} \tag{2.50}$$

In order to find a simple way to quantify coherence of the resulting EM field, at first without explicitly using any external reference field, we need to realize that the post-interaction fields themselves are created sequentially through the sample coupling to incoming energy sidebands. Every individual element in the electron state mixture therefore induces a part of each final field frequency component in a particular phase. If these phases were to be entirely random, we would get the vanishing field average over electron statistical ensemble, $\left\langle \hat{E}_i(\mathbf{r}, \omega) e^{-i\omega t} \right\rangle = 0$ and the resulting field could not exhibit any coherence. This elementary idea motivates the following definition of a simple approach towards quantifying coherence of the field by the normalized frequency dependent degree of coherence

$$\mathcal{D}(\omega) = \frac{\left\langle \hat{E}_i^\dagger(\mathbf{r}, \omega) \right\rangle \left\langle \hat{E}_i(\mathbf{r}, \omega) \right\rangle}{\left\langle \hat{E}_i^\dagger(\mathbf{r}, \omega) \hat{E}_i(\mathbf{r}, \omega) \right\rangle} \,, \tag{2.51}$$

where the time-dependence stemming from evaluations in the interaction picture automatically vanishes and as will be evident from the following calculations, the dependence on polarization and spatial profile will also be canceled out. We can see from (2.51) (and even more clearly from the derived version (2.56)) that if all the phases, in which the frequency components are created by an element of the electron's statistical ensemble, were to be identical, they would cancel in the numerator as well and we would get $\mathcal{D}(\omega) = 1$. In the opposite case of zero correlation, the expected values of particular frequency components would be averaged out, therefore resulting in only a randomly fluctuating field and $\mathcal{D}(\omega) = 0$.

Before proceeding to the calculation of $\mathcal{D}(\omega)$, we will recall

$$\begin{aligned} \hat{E}_i(\mathbf{r}, \omega) &= i\sqrt{\frac{\hbar}{\pi\varepsilon_0}} \frac{\omega^2}{c^2} \int d^3\mathbf{r}' \sqrt{\Im\{\varepsilon(\mathbf{r}', \omega)\}} \sum_{j=1}^{3} G_{ij}(\mathbf{r}, \mathbf{r}', \omega) \hat{f}_j(\mathbf{r}', \omega) \,, \\ \hat{a}(\omega) &= -\frac{ie\omega}{c^2 \gamma(\omega) \sqrt{\pi\hbar\varepsilon_0}} \int d^3\mathbf{r} |\phi_\perp(\mathbf{R})|^2 e^{-i\frac{\omega z}{v}} \int d^3\mathbf{r}' \sqrt{\Im\{\varepsilon(\mathbf{r}', \omega)\}} \\ &\qquad \sum_{j=1}^{3} G_{zj}(\mathbf{r}, \mathbf{r}', \omega) \hat{f}_j(\mathbf{r}', \omega) \,. \end{aligned}$$

Since both of these quantities are linear in $\hat{\mathbf{f}}$, we can use the same methods as before to derive

$$\left[\hat{E}_i(\mathbf{r}, \omega), \hat{a}^\dagger(\omega')\right] = -\delta(\omega - \omega') \frac{e\omega g_i(\mathbf{r}, \omega)}{\pi\varepsilon_0 \gamma(\omega) c^2} \,, \tag{2.52}$$

where we denoted

$$g_i(\mathbf{r},\omega) \equiv \int d^3\mathbf{r}' |\phi_\perp(\mathbf{R}')|^2 e^{i\frac{\omega z'}{v}} \Im\{G_{iz}(\mathbf{r},\mathbf{r}',\omega)\}\,. \tag{2.53}$$

Equation (2.52) validates the use of (2.47) to calculate

$$\langle \hat{E}_i(\mathbf{r},\omega)\rangle = \mathrm{Tr}\left\{\hat{\rho}\left(\hat{E}_i(\mathbf{r},\omega) - \int_0^\infty d\omega' \gamma(\omega')\hat{b}(\omega')\left[\hat{E}_i(\mathbf{r},\omega), \hat{a}^\dagger(\omega')\right]\right)\right\}$$

and since the acting of $\hat{E}_i(\mathbf{r},\omega)$ on electromagnetic vacuum results in zero, we get

$$\langle \hat{E}_i(\mathbf{r},\omega)\rangle = \frac{e\omega g_i(\mathbf{r},\omega)}{\pi\varepsilon_0 c^2}\langle \hat{b}(\omega)\rangle\,. \tag{2.54}$$

Interestingly, we can also evaluate

$$\langle \hat{a}(\omega)\rangle = -\gamma(\omega)\langle \hat{b}(\omega)\rangle$$

and estabilish the important proportionality

$$\langle \hat{E}_i(\mathbf{r},\omega)\rangle \propto \langle \hat{a}(\omega)\rangle\,. \tag{2.55}$$

By utilizing the same techniques that were applied in order to evaluate (2.46), we can determine

$$\left\langle \hat{E}_i^\dagger(\mathbf{r},\omega)\hat{E}_i(\mathbf{r},\omega)\right\rangle = \left(\frac{e\omega}{\pi\varepsilon_0 c^2}\right)^2 |g_i(\mathbf{r},\omega)|^2$$

and we can see that (2.51) simplifies to

$$\mathcal{D}(\omega) = \frac{\left\langle \hat{a}^\dagger(\omega)\right\rangle \langle \hat{a}(\omega)\rangle}{\left\langle \hat{a}^\dagger(\omega)\hat{a}(\omega)\right\rangle} = \left\langle \hat{b}^\dagger(\omega)\right\rangle \left\langle \hat{b}(\omega)\right\rangle\,, \tag{2.56}$$

where it becomes clear that both specific polarization and spatial profile do not affect the locally defined degree of coherence and the second equation also shows that this measure of coherence can be studied solely by examining the initial mixture of electron states. It is then very straightforward to show that

$$\langle \hat{b}(\omega)\rangle = \sum_{q_z}\sum_{l,l'}\sum_{k_z} \rho_{ll'}\langle q_z|k_l\rangle\langle k_{l'}|\hat{c}^\dagger_{k_z-\omega/v}\hat{c}_{k_z}|q_z\rangle = \delta_{\omega,\kappa\omega_0}\sum_l \rho_{l+\kappa,l}\,,$$

where we have only utilized the completeness and orthonormality of the wavevector basis and denoted the harmonic order as $\kappa \equiv \omega/\omega_0 \in \mathbb{N}\cup\{0\}$. The final result then reads

$$\mathcal{D}(\omega) = \delta_{\omega,\kappa\omega_0}\left|\left(\sum_{l=-\infty}^{\infty}\rho_{l+\kappa,l}\right)\right|^2,\ \kappa\in\mathbb{N}\cup\{0\}\,. \tag{2.57}$$

The fact that (2.57) depends only on the post-modulation electron density matrix suggests that $\mathcal{D}(\omega)$ quantifies the transfer of optical coherence that was carried by the electron after the PINEM interaction. Also, despite it being initially defined as a spatially local quantity, we can see that neither the geometry nor the material of our sample appears in the result, which makes it a truly inherent property of the modulated electron probe. The density matrix formalism

that we have adapted throughout the calculations now allows us to look at $\mathcal{D}(\omega)$ for different statistics of the modulating photons. However, there are some general properties of (2.57). The first being that $\mathcal{D}(0) = 1$, since $\hat{\rho}$ is normalized, which will later serve as a valuable tool for verifying the stability of numerical calculations. The second visible property is spatial periodicity in d, the distance travelled by the electron, with a period of $z_T/2\kappa$, which can be seen directly from (2.50).

2.3.4 Numerical results

In order to better understand the theoretical results contained within the previous section, we will now visualize their dependencies on specific physical parameters in various situations.

Regarding the post-interaction average number of photons at frequency ω (2.48), which coincides with the classically determined EELS probability, we are not only interested in the actual shape of $\Gamma_{\mathrm{EELS}}(\omega)$, but also in its alteration stemming from the inclusion of the first-order correction with respect to a finite width of the electron beam in perpendicular direction. We can examine this effect in a specific geometry by recalling the analytically solved case of a single homogeneous sphere from the first chapter, which resulted in (see (1.36))

$$\Gamma_{\mathrm{EELS}}(b,\omega) = \frac{4\pi\alpha}{\omega}\sum_{l=1}^{\infty}\sum_{m=-l}^{l} K_m^2\left(\frac{\omega b}{\gamma v}\right)\left[\Im\{t_l^E\}\left|\xi_{lm}^E\right|^2 + \Im\{t_l^M\}\left|\xi_{lm}^M\right|^2\right] .$$

The sole quantity within this expression which takes into account the impact parameter b of the electron trajectory is the modified Bessel function K_m. We can therefore convert to polar coordinates within the xy-plane and rewrite the averaging (1.38) as

$$\Gamma_{\mathrm{EELS}}(\omega) = \int_0^{\infty} dR\, R \int_{-\pi}^{\pi} d\varphi |\phi_{\perp}(R,\varphi)|^2\, \Gamma_{\mathrm{EELS}}(R,\omega) . \tag{2.58}$$

For the purpose of estimating the consequence of averaging (2.58), we can assume a gaussian perpendicular profile of the electron beam

$$|\phi_{\perp}(\mathbf{R})|^2 = \frac{1}{2\pi\sigma^2} e^{-\frac{|\mathbf{R}-\mathbf{R}_0|^2}{2\sigma^2}} , \tag{2.59}$$

with $\mathbf{R}_0 = (b_0, 0)$. Integrating over the angular coordinate then leaves us with the impact distance distribution

$$\int_{-\pi}^{\pi} d\varphi R|\phi_{\perp}(R,\varphi)|^2 = \frac{R}{\sigma^2} e^{-\frac{R^2+b_0^2}{2\sigma^2}} I_0\left(\frac{b_0 R}{\sigma^2}\right) .$$

Since the perpendicular width of the electron beam is still assumed to be narrow ($\sigma \ll b_0$), we can further approximate [3] $I_0(z) \approx e^z/\sqrt{2\pi z}$ and the averaging (2.58) is then simply done by replacing

$$K_m^2\left(\frac{\omega b_0}{\gamma v}\right) \longrightarrow \int_0^{\infty} \frac{dR}{\sigma}\sqrt{\frac{R}{2\pi b_0}} e^{-\frac{(R-b_0)^2}{2\sigma^2}} K_m^2\left(\frac{\omega R}{\gamma v}\right) . \tag{2.60}$$

In order to comply with the validity of our calculations and at the same time respect the current experimental capabilities, we will assume the width of perpendicular electron beam profile to be quantified by $\sigma \approx a/25$. This means that if we referred back to the case of aluminium, where $c/\omega_p \approx 13.2\,\mathrm{nm}$ and took the radius of the sphere to be around this value, we would get an electron beam focused onto a surface about a nanometer wide. Such a narrow focus is still experimentally obtainable and with this in mind, we have visualized the dependencies of $\Gamma_{\mathrm{EELS}}(b,\omega)$ (dashed lines) and its averaged counterpart (full lines) in figure 2.2.

The first property we can notice, is the overall larger magnitude of $\Gamma_{\mathrm{EELS}}(\omega)$ with respect to $\Gamma_{\mathrm{CL}}(\omega)$ (see figure 1.3), which reaffirms the fact that only a fraction of all photons mediating the interaction contribute to far-field radiation detectable as CL. However, they coincide when the sample is not able to absorb any energy, which we can verify by looking at figures 2.2c and 1.3c, specifically at the graphs with $\eta = 0$. Contrary to the dependence of $\Gamma_{\mathrm{CL}}(\omega)$, where the influence of electron velocity was quite complex, the overall energy losses are rising with declining β, which is expected, since it prolongs the interaction duration. We can also observe that at low electron energies and close incident distances, the change stemming from averaging over the perpendicular electron profile becomes noticable even for the considered narrow gaussian distribution. Averaging also always tends to increase the amount of post-interaction photons, since the contribution of closer incident distances of the electron outweigh the effect of lower central peak in its perpendicular probability distribution. Apart from these specific cases, we can see that applying the standard EELS probability $\Gamma_{\mathrm{EELS}}(b,\omega)$ works well, but one should keep in mind that the described deviations need to be accounted for, when discussing certain modes of the interaction.

We now turn to the analysis of the derived degree of coherence (2.57), which quantifies the transmission of optical coherence imprinted upon and carried by the modulated electron beam. By not applying the usual PINEM limit $|l| \ll n \approx \mu$ (number of photons exchanged assumed to be significantly lesser than the infinitely narrow bosonic mode population), we have obtained a formalism that permits the examination of $\mathcal{D}(\omega)$ also in situations, in which the electron was not modulated coherently, e.g. by scarcely or thermally populated bosonic modes. Since the final result (2.57) is not dependent on sample material or geometry, such an analysis then constitutes an insight into the inherent ability of free electrons to mediate the transfer of optical coherence between two spatially separate fields under various circumstances.

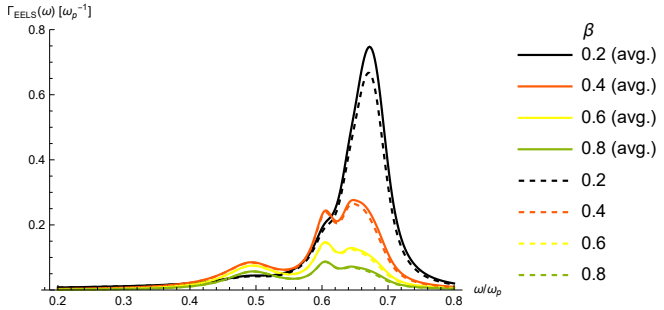

(a)

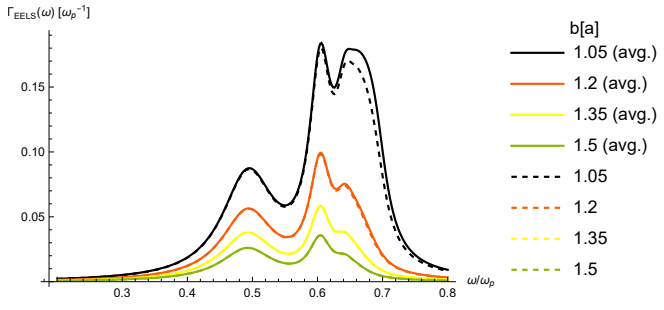

(b)

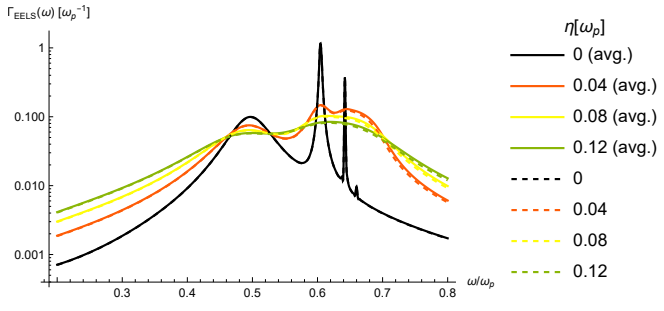

(c)

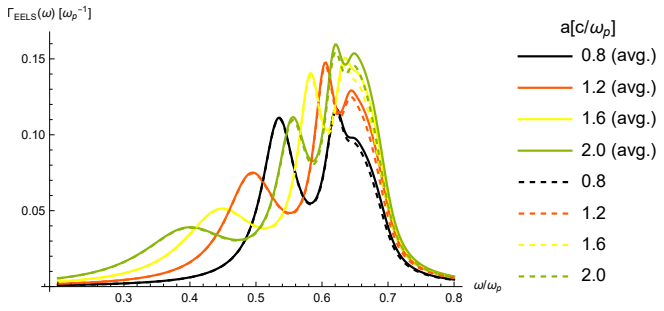

(d)

Figure 2.2: Comparison of the analytical EELS probabilities $\Gamma_{\mathrm{EELS}}(\omega)$ (or post-interaction photon counts per frequency) for a single dielectric sphere given by (1.36) and the same quantity averaged over the narrow gaussian perpendicular electron beam profile (2.60). Dependencies on photon frequency are depicted for different values of (a) the ratio β of electron's velocity to c, (b) the impact parameter b of the trajectory, (c) the electron gas damping frequency η, (d) the dielectric sphere's radius a. Plots (a), (b), (c) consider the sphere's radius $a = 1.2\,c/\omega_p$, plots (a),(b) and (d) are evaluated for $\eta = 0.04\,\omega_p$. Plots (a), (c), (d) represent a situation with impact parameter $b = 1.1a$ and (b), (c), (d) assume $\beta = 0.6$. Width of the perpendicular profile in all graphs is quantified by $\sigma = a/25$.

By recalling (2.8), we can calculate

$$f_{l+\kappa}^{n}(f_{l}^{n})^{*} = (-\beta_0)^{\kappa} e^{-|\beta_0|^2} |\beta_0|^{2l} n!\, \Sigma_{l+\kappa}^{n} \Sigma_{l}^{n}\,, \quad \text{where}$$
$$\Sigma_{l}^{n} \equiv \sqrt{(n+l)!\, p_{n+l}} \sum_{j=\max\{0,-l\}}^{n} \frac{(-|\beta_0|^2)^j}{j!(j+l)!(n-j)!}\,. \tag{2.61}$$

The regime of modulation is described through the probability distribution p_n, which characterizes the population of the single bosonic mode that dominates the modulating process and via the coupling parameter β_0. Combining (2.61) with (2.50) and inserting into (2.57) then yields an expression for the degree of coherence

$$\mathcal{D}(\omega) = \delta_{\omega,\kappa\omega_0} |\beta_0|^{2\kappa} e^{-2|\beta_0|^2} \Big| \sum_{l=-\infty}^{\infty} \sum_{n=0}^{\infty} e^{-4\pi i l \kappa d/z_T} |\beta_0|^{2l} n!\, \Sigma_{l+\kappa}^{n} \Sigma_{l}^{n} \Big|^2\,,\ \kappa \in \mathbb{N} \cup \{0\}\,. \tag{2.62}$$

We can first evaluate (2.62) for the spectra depicted in figure 2.1, where the PINEM mode was assumed to be populated by coherent external illumination, which led to Poissonian distribution characterized by a mean number of excitations μ that was considered to be finite[13]. Figure 2.3 visualizes the dependence of the degree of coherence of the first harmonic frequency $\mathcal{D}(\omega_0)$ on the coupling strength $|\beta_0|$ and the distance d travelled by the electron in correspondence with the figure 2.1.

The first note we need to make is that a realistic coupling strength is severely limited and entirely dependent on the PINEM sample material and geometry, which gives rise to a specific electric-field distribution. One of the stronger couplings have been examined in plasmonic cavities [19], where $|\beta_0| \sim 0.1$ for mode energies $\hbar\omega_0 \sim 1\,\mathrm{eV}$, which needs to be taken into account when we wish to understand the plots from a practical viewpoint. We can however still make some interesting theoretical observations by looking at the entire 2D maps.

We notice that all the plots in figure 2.3 possess a common feature, which is the main arch peak that repeats with a period of $d/(2z_T)$. The width of this peak scales as $\sqrt{\mu}|\beta_0|$, but its height appears to be bound by a specific value. The presence of the peak even in the 2D map with $\mu = 2$, corresponding to the case of very weak modulation, suggests that its predicted appearance should not be affected by the specific statistics p_n in the small μ limit. This simple hypothesis was numerically verified by examining the contrast between excitations resulting from coherent illumination and chaotic illumination (thermal excitations) for μ approaching zero. The specific form of p_n then primarily affects the limiting height and sharpness of the main peak for large μ as well as the formation of sidepeaks visible in figure 2.3, which will be associated with the imprinted coherence.

By comparing figures 2.3a and 2.3b, we can then see that adding only a few more excitations in the case of coherent illumination raises the main peak dramatically (more than two thirds of the remaining distance to the limiting value) and in the second plot, much of the main peak now lies in a regime, which is already reachable via realistic strong coupling. One can also observe the formation of the first two sidepeaks, which do not occur in the case of incoherent

[13]Such a regime could in theory be achieved by a low intensity coherent illumination of the PINEM sample.

PINEM mode population. The transition between figures 2.3c and 2.3d then emphasizes that any substantial increase in μ does not heighten the main peak, but rather increases the number and magnitude of the subsequent coherent peaks.

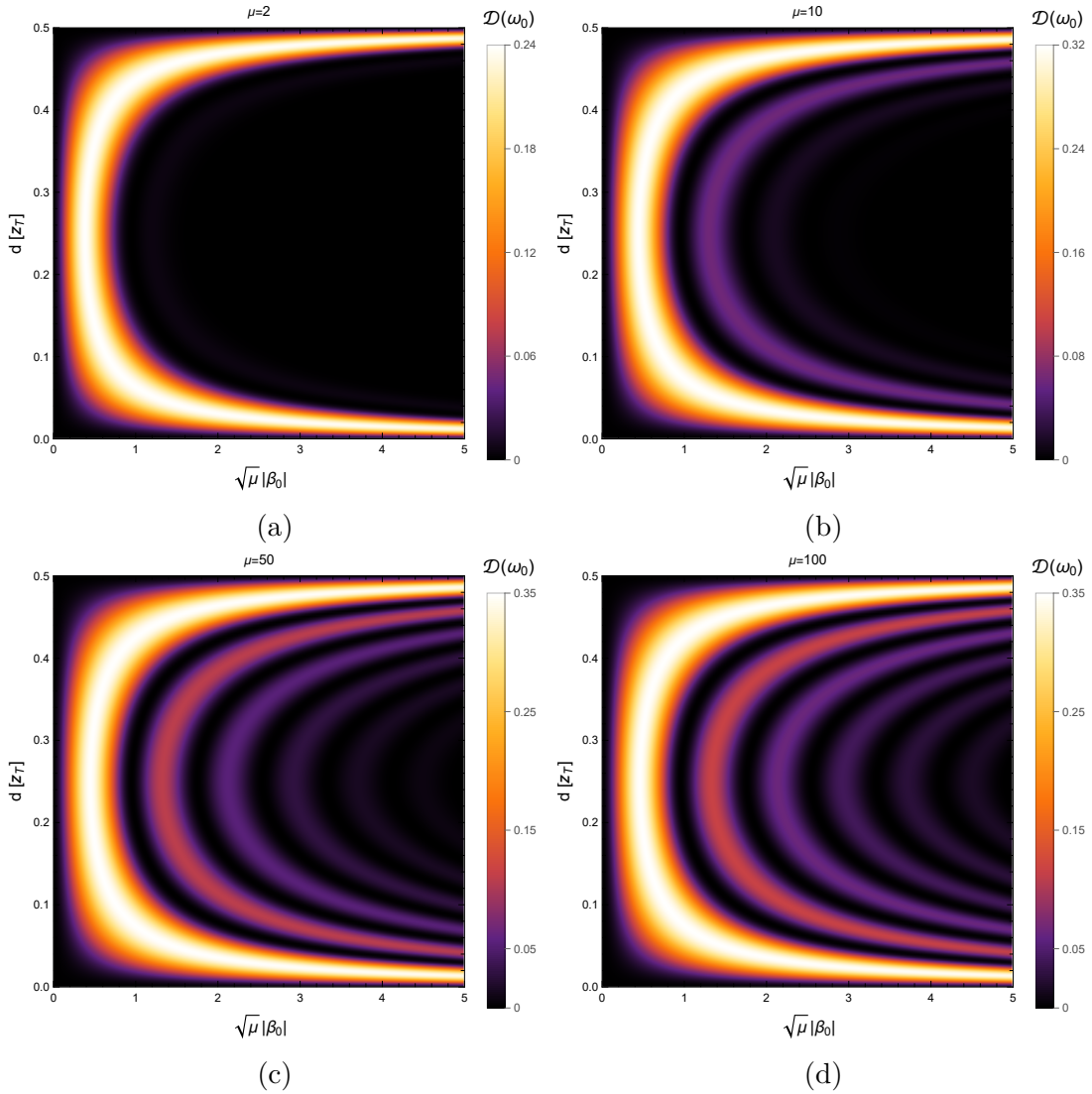

Figure 2.3: Dependence of the degree of coherence (2.62), corresponding to the first harmonic frequency ($\kappa = 1$), on the distance travelled by the electron d and coupling strength $|\beta_0|$ of the modulating bosonic optical mode. Individual 2D maps contain one spatial period $\Lambda = z_T/2$ and they each consider a specific average number of excitations μ, which were populated by coherent illumination and correspond exactly to the post-PINEM spectra depicted in figure 2.1. Heights of the main peaks $\mathcal{D}^{(\mu)}_{\max}$ were numerically determined as (a) $\mathcal{D}^{(2)}_{\max} \doteq 0.236$, (b) $\mathcal{D}^{(10)}_{\max} \doteq 0.312$, (c) $\mathcal{D}^{(50)}_{\max} \doteq 0.333$ and (d) $\mathcal{D}^{(100)}_{\max} \doteq 0.336$.

We can further use the derived general formalism to assess the two easily accessible extreme cases of modulating bosonic populations. The first one is the widely used PINEM limit, which considers an infinitely narrow statistics with a very large average number of excitations $\mu \gg 1$ and a comparatively small number of exchanged photons $|l| \ll \mu$. These assumptions are then used[14] to approximate $p_{n+l} \approx p_n \approx \delta_{n\mu}$, effectively leading to a Fock state and a result that matches the description of PINEM modulation via illumination with classical light fields. The opposite limit of incoherently created bosonic mode population can be modelled by thermal excitations that are inducible by chaotic illumination, resulting in the Bose-Einstein statistics $p_n = (1 - e^{-\vartheta})e^{-n\vartheta}$, with $\vartheta = \hbar\omega_0/(k_B T)$. The average occupation number then obeys the relation $\mu = 1/(e^{\vartheta} - 1)$. In order to determine a realistic maximal μ for the case of thermal excitations, we can consider low energy modes $\hbar\omega_0 \sim 10\,\mathrm{meV}$ and calculate the corresponding sample temperature $T \approx \mu\hbar\omega_0/k_B \sim \mu \times 100\,\mathrm{K}$. A large number of excitations therefore requires considerably high temperatures, but there are structures which can withstand such conditions. An example we could refer to are plasmonic modes in graphene [19] which has a vacuum melting point of at least 4000 K and we can therefore justify values of μ around $10 - 50$.

Comparison of the two discussed extreme cases is shown in figure 2.4. The qualitative difference between the two plots is clear, we see that the thermal excitations do not give rise to any of the sidepeaks associated with coherent modulation and the thermal main peak is noticably lower and wider (towards the center of the plot) than in the case of modulation by a Fock state with a large number of excitations. Accurately calculating the height of the main peak in the case of Bose-Einstein statistics $\mathcal{D}_{\max}^{(\mu_t)}$ can prove numerically quite challenging for larger μ_t, because the upper bound N of the sum over n in the expression (2.62) has to be linearly increased to achieve the same precision, which causes significant extension[15] of the required computation time. A reasonable assumption for the limiting height of the main peak in the $\mu_t \gg 1$ case can still be made however, based on the values obtained for manageably large μ_t. Conducted numerical simulations on the realistic interval $\mu_t \in \langle 10,\, 40\rangle$ have shown a convergence rate similar to Poissonian statistics and the resulting estimated maximum height has been determined as $\mathcal{D}_{\max}^{(\infty_t)} \doteq 0.199$. On the other hand, the PINEM limit main peak height converges already around $\mu_f \approx 600$ to the value $\mathcal{D}_{\max}^{(\infty_f)} \doteq 0.3386$ and the relative heights of subsequent coherent peaks also no longer change.

[14] Mathematical details can be seen in [15], [19].

[15] From expressions (2.61) and (2.62), one can see that time complexity rises at least quadratically with N.

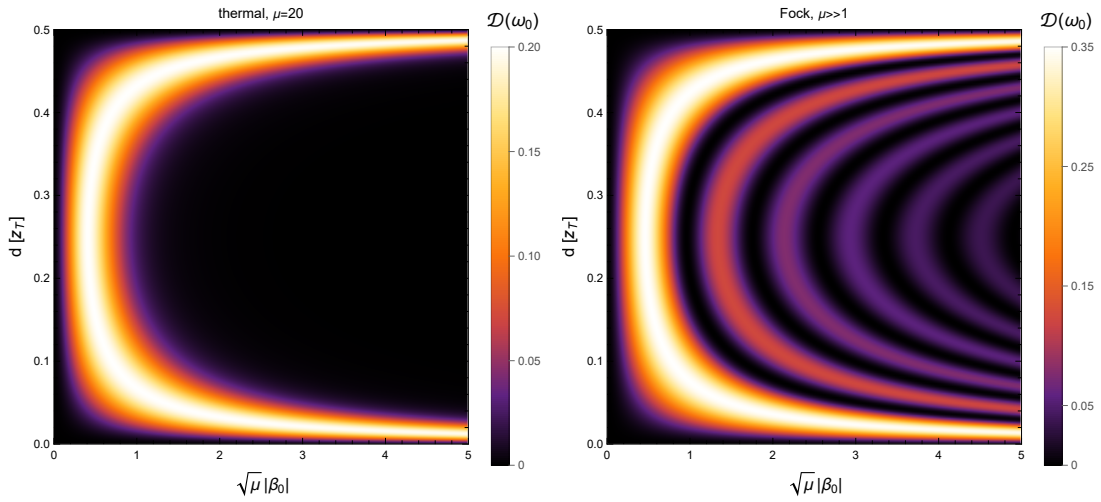

(a) (b)

Figure 2.4: Comparison between the degrees of coherence (2.62) of the first harmonic frequencies ($\kappa = 1$), corresponding to situations in which an electron beam was modulated by (a) a thermally populated bosonic mode (practically feasible by chaotic illumination) with an average number of excitations $\mu_t = 20$ and (b) an optical bosonic mode populated by a strong coherent illumination, effectively resulting in a Fock state with $\mu \gg 1$, which constitutes the usual PINEM limit. Heights of the main arch peaks were numerically determined as (a) $\mathcal{D}_{\max}^{(20_t)} \doteq 0.198$ and (b) $\mathcal{D}_{\max}^{(\infty_f)} \doteq 0.3386$.

The remaining unexplored property is the magnitude of $\mathcal{D}(\omega)$ for higher harmonics ($\kappa > 1$). We already know that $\mathcal{D}(\kappa\omega_0)$ is periodical in d with a spatial period $\Lambda = z_T/(2\kappa)$ and also even with respect to its center $z_T/(4\kappa)$ (as can be verified from the presented 2D maps). We have therefore taken slices of the higher harmonics 2D maps corresponding to obtainable fixed values of $|\beta_0|$ and visualized the dependence of $\mathcal{D}(\omega)$ on d and harmonic order in figure 2.5.

By looking at 2.5a and 2.5c, we can see that both weak and incoherent modulation do not allow for the defined degree of coherence to extend over a larger number of harmonics and substantial values are present only for $\kappa \in \{1, 2, 3\}$. The plot 2.5b, which corresponds to coherent modulation with $\sqrt{\mu_c}|\beta_0| = 2$, already captures the slice from 2.3d where 2 coherent sidepeaks are present in the first harmonic, which gives rise to a more interesting pattern of $\mathcal{D}(\omega)$ that extends up to $\kappa \approx 9$. The most complex behaviour by far is then shown on figure 2.5d, which depicts the limit of strong coherent modulation by a Fock state with large number of excitations μ_f. The resulting pattern then reaches up to $\kappa \approx 21$ harmonic orders and the narrow profile of individual peaks in the $\sqrt{\mu_f}|\beta_0| = 5$ region (see figure 2.4b) makes for a diverse dependence on d and harmonic order. Two particular propagation distances were then selected from this plot and the resulting distributions of $\mathcal{D}(\omega)$ across harmonic orders can be seen in figures 2.5e and 2.5f. Their comparison then shows that depending on d, the magnitude of imprinted coherence can either exhibit an overall declining trend with the rising harmonic order or we might see an effective suppression of optical coherence at certain frequencies of the observed spectrum. The presented theoretical results for $\mathcal{D}(\omega)$ are however considerably impacted by the assumption of an infinite co-

herence length of the electron beam. One could expect that by taking an electron pulse of a finite duration, the individual peaks present in patterns shown in figure 2.5 would appear distorted (increasingly with shorter beams) and would fade quicker with rising harmonic order. Such an effect has been commented upon in [2] and could be incorporated in the future through numerical simulations.

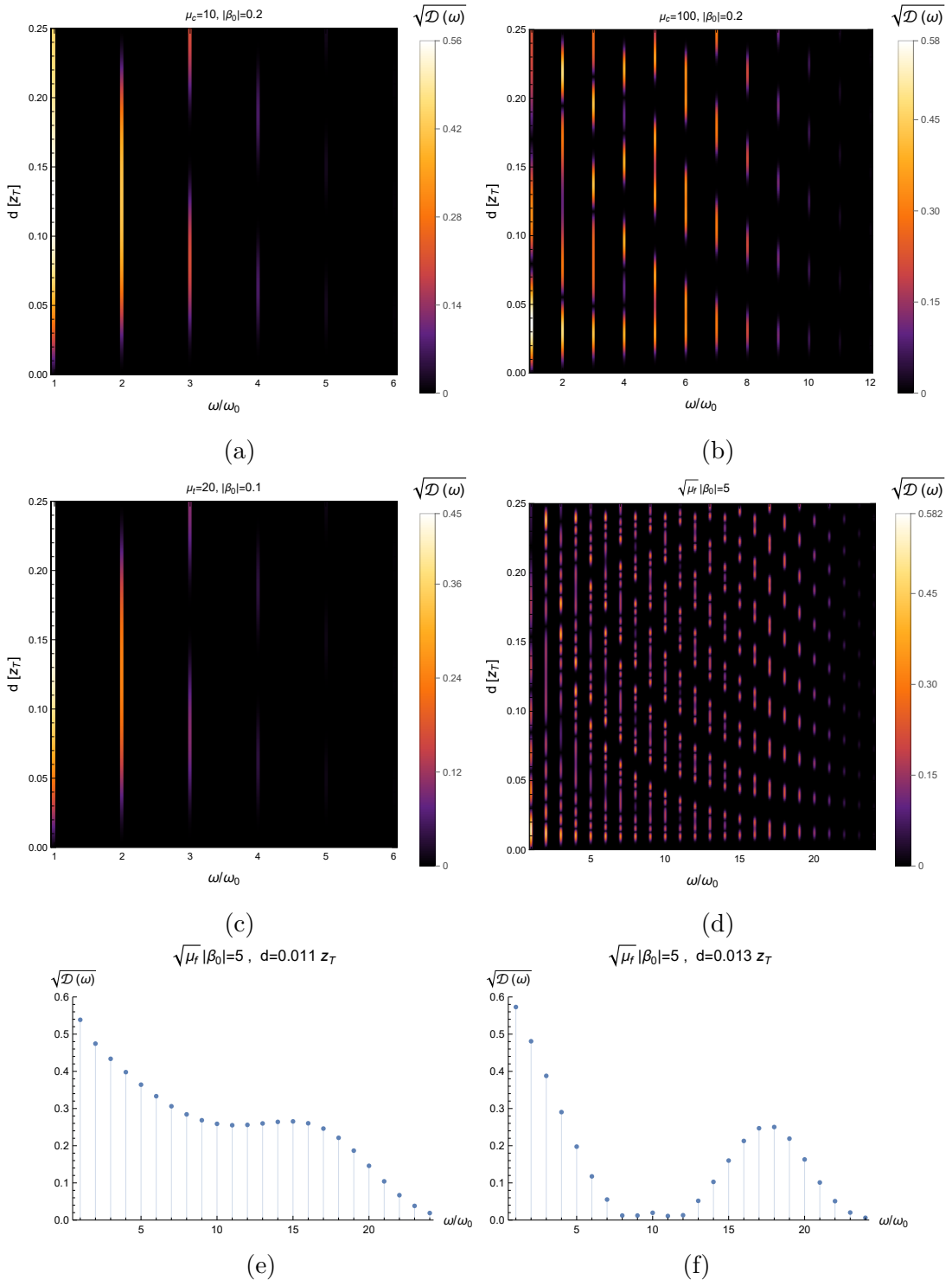

Figure 2.5: Dependence of the degree of coherence (2.62) on frequency ω and electron beam propagation distance d in case of PINEM modulation by (a) a coherently populated bosonic mode with average number of excitations $\mu_c = 10$ and coupling strength $|\beta_0| = 0.2$, (b) the same setup with a larger average population $\mu_c = 100$, (c) thermal bosonic excitations (incoherently populated mode) with $\mu_t = 20$ and coupling parameter $|\beta_0| = 0.1$, (d) an optical bosonic mode populated by a strong coherent illumination (effectively resulting in a Fock state) with $\mu_f \gg 1$ and $|\beta_0|$ satisfying $\sqrt{\mu_f}|\beta_0| = 5$. Plots (e) and (f) then constitute the isolated frequency dependence of $\mathcal{D}(\omega)$ obtained from the case (d) by choosing two specific distances $d = 0.011\, z_T$ and $d = 0.013\, z_T$, respectively.

Conclusion

In this thesis, we have theoretically studied the interaction of a modulated electron beam with optical modes sustained by a nanoscopic sample. To gain a better understanding of this problem, we have dedicated the first chapter to describing the energy losses experienced by a charged point-particle undergoing an interaction with a polarizable dielectric sample, described by a causal homogeneous dielectric function, all within the formalism of classical electrodynamics. This discussion has been considerably simplified by limiting ourselves to the case of swift electrons interacting with sample modes of low excitation energies, which allowed us to adapt the widely used non-recoil approximation that assumes an electron with constant velocity. Within this approximation, we have described the semi-classical probability for the occurance of a general electron energy-loss event. Among all such events, we have identified an interesting subset, which encompasses energy transfers from the electron to radiative modes, consequently contributing to non-vanishing asymptotic EM field upon decaying. These probabilities are very difficult to determine analytically for complex geometries with the inclusion of all relativistic effects, which are neccessary to account for when one considers high-energy electrons. We have therefore derived the EELS and CL probabilities only for the case of a single dielectric sphere and went through the underlying calculations and concepts in great detail. These efforts have not been self-serving, since as we then discussed, the defined semi-classical EELS probabilities also play a crucial role as coupling coefficients in the interaction of electron states with a quantized EM field in the quantum picture.

In the second chapter, we first examined the process of modulation of the incident electron wavepacket by photons contained within a specifically prepared electromagnetic near-field, resulting from light scattering off the surface of a nanostructure. This so-called PINEM approach was chosen mainly because of its reciprocity with respect to the subsequent interaction of the modulated electron with radiative sample modes. We have worked with a simplification, in which the modulating process is dominated by a single optical bosonic mode that could, however, have been populated by various forms of external illumination. In order to work with a general bosonic mode population and not just the usual limit of its narrow statistics with a very large average number of excitations, we have allowed the post-modulation electron state to be described by a density operator. The specific regime of modulation was consequently imprinted upon the mixture of states through the bosonic mode initial statistics and its coupling strength parameter. To describe the interaction of the modulated electron with an EM field in the presence of a dielectric sample, we then required the procedure of medium-assisted field quantization, the overview of which was covered along its vacuum counterpart, with particular emphasis being placed on their main conceptual differences. Once we obtained the neccessary formalism, we formulated the Hamiltonian of our system through the minimal coupling approach and analytically solved its evolution in the interaction picture.

By acquiring the evolved density operator of the electron-field system, we have paved the way for examining the post-interaction statistical properties of CL photons. The first quantity that we determined, was the number of photons at specific

frequencies contained within the medium-assisted EM field, which turned out to be independent of the modulated electron state and coincided with the semi-classical EELS probability. Our approach towards the S-operator derivation also included the first-order correction with respect to a finite width of the electron beam in perpendicular direction, the impact of which we then assessed via numerical simulations for the analytically solved case of a single dielectric sphere. The main result however, was the normalized degree of coherence, defined as a simple spatially local correlation function of the post-interaction electric field frequency components. This quantity turned out to be dependent only on the post-modulation electron density matrix, therefore implying its meaning as an inherent ability of the modulated electron probe to mediate the transfer of optical coherence. The extension of existing formalism for its calculation allowed us to examine various regimes of electron beam modulation and their impact on the measure of optical coherence passed on to the medium-assisted EM field, which we subsequently analyzed in simple numerical simulations.

Moreover, the presented theoretical framework can now be utilized in calculations of practically measurable quantities, such as intensity correlations in interferometric experiments, where one could experimentally observe the transfer of optical coherence from interference patterns created by the emitted CL and modulating laser pulse as a reference field. The general density operator formalism then enables the study of different approaches towards electron beam modulation and with suitable numerical methods, we could study its effect in a vast range of sample geometries.

Bibliography

[1] Ofer Kfir, Valerio Di Giulio, F Javier García de Abajo, and Claus Ropers. Optical coherence transfer mediated by free electrons. *Science Advances*, 7(18):eabf6380, 2021.

[2] Valerio Di Giulio, Ofer Kfir, Claus Ropers, and F Javier Garcia de Abajo. Modulation of cathodoluminescence emission by interference with external light. *ACS nano*, 15(4):7290–7304, 2021.

[3] Frank WJ Olver. *NIST handbook of mathematical functions hardback and CD-ROM*. Cambridge university press, 2010.

[4] FJ García De Abajo. Optical excitations in electron microscopy. *Reviews of modern physics*, 82(1):209, 2010.

[5] F Javier Garcia de Abajo and Valerio Di Giulio. Optical excitations with electron beams: Challenges and opportunities. *ACS photonics*, 8(4):945–974, 2021.

[6] AV Andrade-Neto. Dielectric function for free electron gas: comparison between drude and lindhard models. *Revista Brasileira de Ensino de Física*, 39, 2016.

[7] Hartmut Haug and Stephan W Koch. *Quantum theory of the optical and electronic properties of semiconductors*. World Scientific Publishing Company, 2009.

[8] N David Mermin. Lindhard dielectric function in the relaxation-time approximation. *Physical Review B*, 1(5):2362, 1970.

[9] John David Jackson. Classical electrodynamics, 1999.

[10] FJ García de Abajo. Relativistic energy loss and induced photon emission in the interaction of a dielectric sphere with an external electron beam. *Physical Review B*, 59(4):3095, 1999.

[11] Francis E Low. *Classical field theory: electromagnetism and gravitation*. John Wiley & Sons, 2008.

[12] Julius Adams Stratton. *Electromagnetic theory*, volume 33. John Wiley & Sons, 2007.

[13] Izrail Solomonovich Gradshteyn and Iosif Moiseevich Ryzhik. *Table of integrals, series, and products*. Academic press, 2014.

[14] EL Hill. The theory of vector spherical harmonics. *American Journal of Physics*, 22(4):211–214, 1954.

[15] Sang Tae Park, Milo Lin, and Ahmed H Zewail. Photon-induced near-field electron microscopy (pinem): theoretical and experimental. *New Journal of Physics*, 12(12):123028, 2010.

[16] RH Ritchie and A Howie. Inelastic scattering probabilities in scanning transmission electron microscopy. *Philosophical Magazine A*, 58(5):753–767, 1988.

[17] FJ García de Abajo and M Kociak. Electron energy-gain spectroscopy. *New Journal of Physics*, 10(7):073035, 2008.

[18] Valerio Di Giulio and F Javier García de Abajo. Free-electron shaping using quantum light. *Optica*, 7(12):1820–1830, 2020.

[19] Valerio Di Giulio, Mathieu Kociak, and F Javier García de Abajo. Probing quantum optical excitations with fast electrons. *Optica*, 6(12):1524–1534, 2019.

[20] Pierre Meystre and Marlan O Scully. *Quantum optics*. Springer, 2021.

[21] Roy J Glauber. Coherent and incoherent states of the radiation field. *Physical Review*, 131(6):2766, 1963.

[22] Christian Raabe. Macroscopic qed in linearly responding media and a lorentz-force approach to dispersion forces. 2008.

[23] Stefan Scheel and Stefan Yoshi Buhmann. Macroscopic qed-concepts and applications. *arXiv preprint arXiv:0902.3586*, 2009.

[24] Claude Itzykson and Jean-Bernard Zuber. *Quantum field theory*. Courier Corporation, 2006.

List of Figures